UNIVERSITY OF OKLAHOMA

GRADUATE COLLEGE

# CHEMOSTRATIGRAPHY, MINERAL DISTRIBUTIONS AND WATER CHEMISTRY ANALYSIS OF THE GREEN RIVER FORMATION, PICEANCE BASIN, NORTHWESTERN COLORADO

A DISSERTATION

SUBMITTED TO THE GRADUATE FACULTY

in partial fulfillment of the requirements for the

Degree of

DOCTOR OF PHILOSOPHY

By

TENGFEI WU

Norman, Oklahoma

2021

Downloaded from SHAREOK. Persistent Handle URL: https://hdl.handle.net/11244/329583

# CHEMOSTRATIGRAPHY, MINERAL DISTRIBUTIONS AND WATER CHEMISTRY ANALYSIS OF THE GREEN RIVER FORMATION, PICEANCE BASIN, NORTHWESTERN COLORADO

A DISSERTATION APPROVED FOR THE

SCHOOL OF GEOSCIENCES

BY THE COMMITTEE CONSISTING OF

Dr. Andrew S. Elwood Madden, Chair

Dr. Deepak Devegowda

Dr. Jeremy Boak

Dr. Xiaolei Liu

Dr. Michael Soreghan

© Copyright by TENGFEI WU 2021
All Rights Reserved.

This dissertation is for my family, without their endless Love and Support, I would never have made it.

## Acknowledgements

There are so many people in my life that help me get through the ups and downs during my journey in pursuing my Ph.D degree in geology. I would like to express my thanks to my major advisor, Dr. Jeremy Boak, who brought me to Colorado School of Mines when he was a research professor there. Without him, I wouldn't have been able to pursue my Ph.D program in the Green River oil shale at Mines. Also, because of him, I transferred to University of Oklahoma to continue my research on the same topic. We had been through many hard times to get the funding to support me and eventually, it worked out. I give my thank you to Dr. Boak who helped me a lot in my research and always encouraged me to not give up even though I made a very slow progress in my research. Thanks for everything you have done for me.

I would also like to thank my committee chair, Dr. Andrew Elwood Madden for the time you spent with me on the discussion and revision of my thesis. Whenever I need to talk with you, you are always ready to help. The passion and energy you devote to your research and teaching inspired me and I learnt a lot from you.

I would also like to express my thanks to another 3 committee members: Dr. Deepak Devegowda, Dr. Michael Soreghan and Dr. Xiaolei Liu for the time you contributed to my research. Your comments and suggestions on my thesis really helped me to improve the quality of my research. Besides, I want to show my gratitude to Dr. David London, and Dr. Roger Slatt, who had spent lots of time on reviewing the draft of my research. Dr. Slatt, rest in peace, and you will be remembered for ever. In addition, special thanks go to Dr. Justin Birdwell and Ronald Johnson, from the U.S. Geological Survey. My research could have never been completed without the financial support for the data analysis from the survey. Last, I also want to express my thanks

to Oklahoma Geological Survey, Dean Mike Stice, and School of Geosciences for all the financial support I got. Without these selfless support, my research would never have been possible.

I want to thank all my friends at OU and Mines, who helped me to spend the lonely life abroad. Without you guys around, my life would be less colorful. These guys include but not limited to Suriamin, Jianjun Li, Chenxi Xu, Pengfei Hou, Jingqi Xu, Henry, Daniela, Nanya and so on. I would like to thank Rebecca, Joyce, Shanika, David Brown, Richard and other staff members at OU for everything you have done for me. Without your help, my study wouldn't have been so smooth.

Without the selfless support and courage I gained from my families, I would never have travelled this far in my life. I would like to thank my parents first who always encouraged me to pursue my goals regardless of the obstacles that I encountered along the way, even though they didn't understand what I was doing in geology and why I haven't graduated after having been studying in the U.S for such a long time. Without their love and sacrifice for me, I wouldn't have the chance to become who I am now. I would also like to thank my brother and sister, who are contributing what they can to our big family. It's them who spent time with my parents when I'm not around.

Finally, I give my thanks and gratitude to my fiancée, Xin Miao for everything she has done for me. Without her around me, I would never be able to make it. She always has faith on me and gives me confidence. She always encourages me and says I can do it no matter what happens. She is my soulmate. She also gave me the most precious gift I could have ever imaged, our daughter, Aurora. They are the backbone of my life and they are the incentives I should be good and motivated. My life has been lit up since they came to my world. I would try my best to be a qualified husband and dad.

Table of Contents

Acknowledgements ..... v

Table of Contents ..... vii

List of Tables ..... xi

List of Figures ..... xii

Abstract ..... xvi

Chapter 1: Introduction ..... 1

Research Objectives ..... 3

Chapter 2: Investigation of sedimentary processes in the Green River Formation: geochemical signals extracted from the Piceance Basin, Colorado ..... 4

Abstract ..... 4

Introduction ..... 6

Geologic setting ..... 8

Piceance Basin (PB) ..... 8

Eocene Stratigraphy of the GRF in PB ..... 9

Dataset and Methods ..... 14

Results ..... 17

Indicators of Terrestrial Input ..... 17

Indicators of Carbonate Deposition ..... 19

Salinity Indicators ..... 20

Organic Carbon Content ..... 21

Productivity Indicator ..... 22

Redox Indicators ..... 27
Discussion ..... 36
Climatic control on the clastic influx and carbonate deposition ..... 36
Iron deficiency ..... 41
Redox conditions ..... 44
Productivity and TOC Deposition ..... 47
Variations in Salinity ..... 52
Conclusions ..... 58
Acknowledgements ..... 59
References ..... 59
Chapter 3: Quantitative Analysis of the Green River Formation, Piceance Basin, Northwest Colorado ..... 67
Abstract ..... 67
Introduction ..... 68
Stratigraphy and Geologic Setting ..... 71
Materials and Methods ..... 73
Sample Information ..... 73
Geochemical Analyses ..... 74
Data Analysis Methods ..... 75
Results ..... 79
Chemofacies derived from the integration of DP, JS and Shell ..... 79
Chemofacies in the Basin Margin ..... 84
Chemofacies in the Basin Center ..... 88

Discussion ..... 94
Chemofacies of the combined dataset ..... 94
Chemofacies of the Basin Margin ..... 94
Chemofacies of the Basin Center ..... 97
Conclusion ..... 101
Acknowledgements ..... 102
References ..... 102
Chapter 4: Variations in Water Chemistry of Eocene Lake Uinta derived from mineral assemblages in the Green River Formation, Piceance Basin, Colorado ..... 107
Abstract: ..... 107
Introduction: ..... 109
Geologic Setting ..... 112
History of Lake Uinta ..... 112
Stratigraphy of the GRF ..... 115
Summary of Mineral Distributions ..... 116
Methods ..... 118
Results and Discussion ..... 119
The initial parameters in the system ..... 119
Origin of Analcime ..... 121
Lower Mineralogic Unit (LMU) water chemistry ..... 125
Middle Mineralogic Unit (MMU) water chemistry ..... 126
Upper Mineralogic Unit (UMU) water chemistry ..... 127
The $CO_2$ concentration in the Eocene paleolake ..... 129

The Significance of the Mineral Stability Diagrams for GRF water chemistry 130

Conclusion ..... 132

Acknowledgements ..... 133

References ..... 133

Chapter 5: Future Work ..... 139

# List of Tables

Table 2.1 Average Chemical Composition of Lake Stages in Three Stratigraphic Sections of the Green River Formation. ..... 26

Table 3.1 Matrix of average elemental enrichment ratios (ER) by cluster in the combined dataset. . ..... 81

Table 3.2 Key chemical features of combined dataset from chemofacies of DP, Shell, and JS ……..83

Table 3.3 Matrix of average elemental enrichment ratios (ER) by cluster in Douglas Pass.. ..... 86

Table 3.4 Key chemical features of chemofacies of Douglas Pass …… 87

Table 3.5 Matrix of average elemental enrichment ratios (ER) by cluster in Shell 23X-2 well. . ..... 89

Table 3.6 Key chemical features of chemofacies of Shell 23X-2 well.. ……90

Table 3.7 Matrix of average elemental enrichment ratios (ER) by cluster in John Savage...92

Table 3.8 Key chemical features of chemofacies of John Savage well…….....93

Table 4.1 Stratigraphy of the Eocene Green River Formation, rich and lean oil shale zones…116

# List of Figures

Figure 1.1 Illustrative depositional model of the Green River Piceance Creek lake basin2

Figure 2.1 Stratigraphy of the Eocene Green River Formation, rich and lean oil shale zones…… 10

Figure 2.2 Location of the Piceance Basin and surrounding uplifts ..... 13

Figure 2.3 Correlation between Eocene climate curve, evolutionary lake stages (Stages 1 to 6), rich and lean zones (R/L), basin stratigraphy, lake types (L.T.)..... 13

Figure 2.4 Map of Piceance Creek Basin with outcrop and well locations. ..... 16

Figure 2.5 The distribution of typical geochemistry proxies derived from ICP-OES in Douglas Pass area..... 23

Figure 2.6 The Distribution of typical geochemistry proxies derived from ICP-OES in John Savage 24-1..... 24

Figure 2.7 The Distribution of typical geochemistry proxies derived from ICP-OES in Shell 23X-2..... 25

Figure 2.8 The average concentration of selective major elements in DP, JS and Shell 30

Figure 2.9 The average values of redox proxies and TOC from DP, JS and Shell, respectively ..... 31

Figure 2.10 U-EF vs. Mo-EF for Douglas Pass area ..... 32

Figure 2.11 U-EF vs. Mo-EF for core John Savage 24-1 ..... 33

Figure 2.12 U-EF vs. Mo-EF for core Shell 23X-2 ..... 34

Figure 2.13 Plot of Fe vs S showing degree of pyritization (DOP) for basin margin samples and basin center samples ..... 35

Figure 2.14 The average values of detrital input, carbonate proxies, salinity and TOC from basin margin (DP) to center (Shell, JS). ..... 39
Figure 2.15 The ratio of detrital elements to detrital plus carbonate elements (Si+Al+Ti+K)/ (Si+Al+Ti+K+Ca+Mg+Mn) in Douglas Pass, John Savage 24-1, and Shell 23-X2 sections ..... 40
Figure 2.16 Crossplot of Al vs Fe from basin margin(DP) to center (Shell, JS) ..... 42
Figure 2.17 The Average Shale-normalized concentration of trace elements ..... 43
Figure 2.18 Uranium and molybdenum enrichment factor values for Douglas Pass area, John Savage 24-1 core, and Shell 23X-2 core. ..... 47
Figure 2.19 . Plot of phosphorus and total organic carbon content of samples from all three sections. ..... 51
Figure 2.20 Molybdenum enrichment factor (EF Mo) vs . TOC for samples from the basin center(JS and Shell) and basin margin(DP) ..... 52
Figure 2.21 Crossplot of Sodium vs.Rb/K* for samples from the basin margin (DP) ... 56
Figure 2.22 Crossplot of Na vs B/Ga, Na vs Rb/K* and B/Ga vs Rb/K* for samples from JS and Shell ..... 57
Figure 3.1 Stratigraphy of the Eocene Green River Formation, rich and lean oil shale zones ..... 73
Figure 3.2 Map of Piceance Creek Basin with outcrop and well locations. ..... 77
Figure 3.3 Difference Between Euclidean Distances and Manhattan Distances. ..... 78
Figure 3.4 Schematic Illustrating Distances Using Ward's Method..... 78
Figure 3.5 The individual chemofacies logs generated from the integrated logs ..... 82

Figure 3.6 Crossplot of the sum of siliciclastic index elements and the sum of carbonate index elements of average values for chemofacies defined from the integrated DP, JS and Shell datasets. ..... 84
Figure 3.7 Computed Chemofacies of Douglas Pass area, with 5 facies identified ..... 86
Figure 3.8 Crossplot of the sum of siliciclastic index elements and the sum of carbonate index elements of average values for chemofacies defined from the integrated DP, JS and Shell datasets, and from the DP dataset alone..... 87
Figure 3.9 Computed Chemofacies of Shell 23X-2, with 5 facies identified. ..... 89
Figure 3.10 Crossplot of the sum of siliciclastic index elements and the sum of carbonate index elements of average values for chemofacies defined from the integrated DP, JS and Shell datasets, and from the Shell dataset alone. ..... 90
Figure 3.11 Computed Chemofacies of John Savage 24-1, with 5 facies identified ..... 92
Figure 3.12 Crossplot of the sum of siliciclastic index elements and the sum of carbonate index elements of average values for chemofacies defined from the integrated DP, JS and Shell datasets, and from the JS dataset alone. ..... 93
Figure 4.1 Map of the central Rocky Mountain region ..... 114
Figure 4.2 North-South cross-section showing the transition in indicator mineral occurrences and oil shale thickness for the Green River Formation across the Piceance Basin ..... 118
Figure 4.3 Ratios of silicon to aluminum and silicon to aluminum plus sodium in analcime from 91 samples with and without dawsonite, Parachute Member. ..... 122
Figure 4.4 Activity-activity diagram representing the mineral assemblage of the basin margin in the Douglas Pass area..... 124

Figure 4.5 Activity-activity diagram representing the mineral assemblage for the Lower Mineralogic Unit ..... 125
Figure 4.6 Activity-activity diagram representing the mineral assemblage for the Middle Mineral Unit(MMU) ..... 127
Figure 4.7 Activity-activity diagram representing the mineral assemblage for the Upper Mineral Unit(UMU) ..... 129

# Abstract

The Eocene Green River Formation (GRF) in the Piceance Basin of Colorado is estimated to contain the largest oil shale deposits in the world and is a well-documented example of a lacustrine depositional system. In addition, the quantities of mineral resources in the oil shale, like nahcolite ($NaHCO_3$) and dawsonite ($NaAl(CO_3)(OH)_2$) deposits, are of potential economic value. Detailed geochemical and mineralogical analysis across the basin can be critical to understanding the depositional environment, sedimentary processes and water-chemistry evolution in the basin. Quantitative geochemical data for the GRF were collected by Inductively Coupled Plasma Optical Emission Spectroscopy and Mass Spectrometry (ICP-OES-MS) as part of this study. The basin margin was represented by samples from the Douglas Pass area and the basin center area was characterized by samples of cores from the Shell 23X-2 and John Savage 24-1 wells at the U.S. Geological Survey Core Research Center. Outcrop and core samples were taken based on observed changes of sedimentary structures and lithofacies from the full stratigraphic sections.

Major elements and element groups, (Si, Al, K, Ti), (Ca, Mg), Na, and P were used as proxies for clastic influx, carbonate precipitation, salinity and paleo-productivity, respectively. Trace metal elements (As, Mo, U, Cu, Zn) were used primarily to characterize the redox conditions of Lake Uinta. The changes of these major & trace elements in different lake stages, indicate the variations of the sedimentary components and processes in the lake development. The distinctions between the basin margin and the basin center, in terms of clastic input, salinity, carbonate, paleo-productivity, redox condition and total organic carbon (TOC), support the model of a permanently stratified lake through most of the depositional interval. The detailed geochemistry from this study indicates that Na became elevated earlier in portions of the basin margin than in the deeper basin. During the early stage of lake expansion, the salinity may have been elevated first in the shallow

basin margin, because of more efficient evaporation, which then elevated salinity in the basin center through transport of saline density currents. Period IV transition metal elements show only local occurrence of high enrichment, but analysis of Fe/Al ratios suggests that the low enrichments may be related to source rocks depleted in mafic constituents.

Hierarchical clustering analysis (HCA) on these major & trace elements generated 5 chemofacies when integrating all datasets, which represent 1) carbonate facies (high Ca, Mg, Sr and Mn); 2) siliciclastic facies (high Si, Al, K, Ti, Zr, Nb, and P); 3) high TOC with high redox proxies (S, As, Mo, and Cu, etc); 4) saline facies (high Na); 5) mixed carbonate and siliciclastic facies (moderate-high in Ca, Mg, Sr, Mn and Si, K). The chemofacies derived from geochemical data further clarify the depositional environment and sedimentary processes across the basin and provide new perspective on the evolutionary history of the lake. The general coherency of period IV transition metal enrichments/depletions in most chemofacies suggests that, despite lower overall abundances, these elements do reflect the influence of redox conditions in the basin center and the basin margin.

In addition, the distributions of key minerals in the GRF of the Piceance Basin reflect spatial and temporal variations in water chemistry in the paleolake. Mineral stability diagrams generated by thermodynamic modeling constrain the water chemistry under which those minerals were formed. The important minerals identified in the system include analcime, illite, dawsonite, nahcolite and albite/K-feldspar. Based on the mineral stability diagrams, the water chemistry can be defined in terms of silica activity, alkalinity, salinity and $CO_2$ concentration. The Na concentration from the dawsonite and nahcolite stability field can reach 58,000 ppm under hypersaline conditions.

# Chapter 1: Introduction

The Green River Formation (GRF) of Colorado in the Piceance Basin has the richest oil shale deposits in the world (Dyni, 2006; Johnson et al., 2010). Its unique mineral resources, especially those saline minerals, like nahcolite ($NaHCO_3$) and dawsonite ($NaAl(CO_3)(OH)_2$), have great economic value, which are good sources for soda ash and aluminum (Hite and Dyni, 1967; Milton, 1971; Brobst and Tucker, 1973; Robb and Smith, 1974; Smith, 1983; Mason, 2007; Johnson et al., 2010a; Feng, 2011; Poole, 2014; Boak and Poole, 2015; Birdwell et al., 2019). The abundant mineral resources and rich organic matter in the Piceance basin make it a "sweet-spot" for exploration and research into production and exploitation of oil shale resources (Dyni, 2006; Johnson et al., 2010a; Poole, 2014). The GRF comprises one of the best documented deposits formed in ancient lakes and is a classic example of a lacustrine depositional system (Bradley, 1931; Cole and Picard, 1978; Dyni and Hawkins, 1981; Grabowski Jr and Pevear, 1985; Hasiotis and Honey, 2000; Katz, 1988; Tänavsuu-Milkeviciene and Sarg, 2012). At present, a stratified lake model is commonly accepted among geologists for the origin of oil shale of the Green River Formation (Desborough, 1978; Johnson, 1985; Poole, 2014; Tänavsuu-Milkeviciene and Sarg, 2012). Tänavsuu-Milkeviciene & Sarg (2012) established a detailed stratigraphic architecture based on facies association analysis, depositional trends, and gamma ray and Fischer assay data (Fig.1.1). The model illustrates how the facies change from the proximal part of the basin margin to the distant area of the basin center, indicating the distinctions of depositional environment. In our study, we are trying to figure out whether detailed high-resolution geochemical and mineral data can unveil the depositional processes of the lacustrine system, in terms of its siliciclastic input, salinity, carbonate, reducing condition and TOC preservation. The occurrence and distribution of large amounts of saline minerals in the basin center indicate the water chemistry is key to

determining which mineral assemblage should be present. To evaluate the water chemistry based on the mineral stability in the basin center, is a direct and effective way to understanding the lake evolution, in terms of silica activity, salinity, alkalinity, and $CO_2$ concentration.

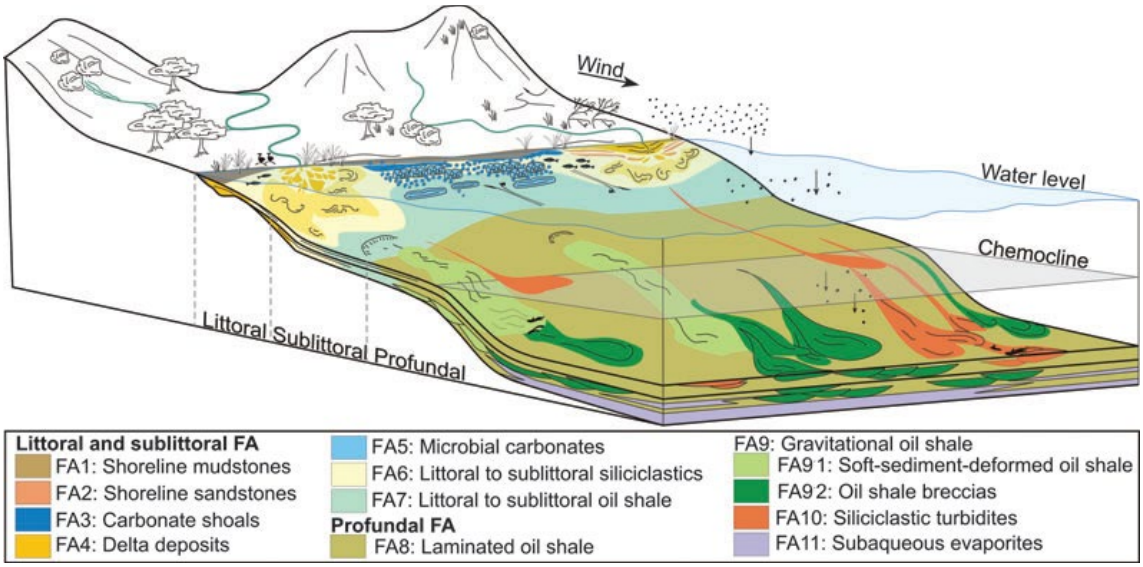



Fig. 1.1. Illustrative depositional model of the Green River Piceance Creek lake basin. Note wave-dominated (right) and fluvial-dominated (left) deposits along the basin margin in the littoral zone, and evaporite deposits within oil shale deposits in the profundal zone. Figure from Tänavsuu-Milkeviciene & Sarg (2012).

## Research Objectives

This study sought to achieve three main goals based on high-resolution geochemistry and mineral datasets:

(1) to refine the understanding of the sedimentary processes of the lacustrine system in the Eocene Epoch based on major element proxies and figure out the depositional environment based on the trace metal redox proxies;

This is addressed in Chapter 2: Investigation of sedimentary processes in the Green River Formation: geochemical signals extracted from the Piceance Basin, Colorado.

(2) to establish appropriate chemofacies for both the basin margin and the basin center, which could represent the "facies" variations throughout the sections and then to explore whether chemofacies reveal hidden features which could not be easily identified just based on major & trace element data;

This is addressed in Chapter 3: Quantitative Analysis of the Green River Formation, Piceance Basin, Northwest Colorado.

(3) to constrain the water chemistry more quantitatively in terms of silica activity, pH, salinity, and $CO_2$ concentration, mainly based on the mineral assemblages in different mineralogic units of the basin, which represent the most significant changes of the water chemistry.

This goal is addressed in Chapter 4: Variations in Water Chemistry of Eocene Lake Uinta derived from mineral assemblages in the Green River Formation, Piceance Basin, Colorado.

# Chapter 2: Investigation of sedimentary processes in the Green River Formation: geochemical signals extracted from the Piceance Basin, Colorado

Tengfei Wu[1], Jeremy Boak[2], Justin Birdwell[3]

1. School of Geosciences, University of Oklahoma

2. Hurricane Peak Geosciences, Littleton, CO

3. U.S. Geological Survey, Denver

## Abstract

The Eocene Green River Formation (GRF) in the Piceance Basin (PB) of Colorado is estimated to contain the largest oil shale deposits in the world and is a well-documented example of a lacustrine depositional system. Detailed geochemical analysis across the basin can be critical to understanding the depositional environment and sedimentary processes in the basin. Sampling in the Douglass Pass area represents the basin margin and the basin center area is characterized by sampling of cores from the Shell 23X-2 and John Savage 24-1 wells, sampled at the U.S. Geological Survey (U.S.G.S) Core Research Center. Quantitative geochemical data for the GRF were collected by Inductively Coupled Plasma Optical Emission Spectroscopy-Mass Spectrometry (ICP-OES-MS). Outcrop and core samples were taken based on observed changes of sedimentary structures and lithofacies selected from the full stratigraphic sections.

Major elements, (Si, Al, K, Ti), (Ca, Mg), P, Na are used as proxies for clastic influx, carbonate deposition, paleo-productivity, and salinity, respectively. Major elements define the variations of these significant components across the basin and through six different lake stages defined by Tänavsuu-Milkeviciene and Sarg (2012) that are closely related to the Early Eocene

Climate Optimum (EECO) event. The average siliciclastic and carbonate fractions are larger in the basin margin than in the basin center, whereas the average values of paleoproductivity and salinity are much lower in the basin margin than in the basin center. All are closely related to the trend in climate change. Trace elements, especially trace metal elements (Mo, U, As, Cu, Zn) are used primarily to characterize the redox conditions of Lake Uinta, with the average values of these trace metals in the basin margin much lower than in the basin center, implying more reducing conditions in the basin center. The degree of pyritization (DOP) also reflects the redox conditions of the paleolake, with relatively higher values of DOP in the basin center. However, among those reducing indicators, only Mo, U, As are enriched, whereas other enrichment factors of Cr, Ni, V, Cu and Zn are relatively depleted compared to average shale in general, which may indicate low mafic constituent input from source areas. The accumulation and preservation of organic matter is controlled by bioproductivity, redox conditions, and dilution by detrital, organic, and carbonate contributions, all of which were directly affected by Eocene climate changes. The relatively good linear relationship between Mo enrichment and total organic carbon (TOC) in the basin suggests that redox conditions exerted a major control over organic matter accumulation and preservation. The salinity of the lake, which is mediated by the balance of precipitation and evaporation in different stages of the lake development and is directly controlled by climate change, can be characterized by Na, B/Ga and Rb/K. The novel discovery that higher salinity, as indicated by elevated Na (this work) and the presence of analcime (Poole, 2014, Boak and Poole, 2015) occurs first in the basin margin and later in the basin center indicates that elevated evaporation and decreased water supply caused rising salinity in the margin that was then swept into the basin center, potentially due to density flows. The opportunity for drying and redissolution of salts at the margin (Remy and Farrell, 1989) could have enhanced this effect.

Detailed inorganic geochemistry analysis provides insight into the sedimentary processes in the Piceance Basin, which further supports the model of a stratified lake, based on the distributions and variations of clastic input, carbonate precipitation, paleosalinity, redox conditions and TOC in the basin margin and the basin center.

## Introduction

The Eocene Green River Formation (GRF) of Colorado in the Piceance Basin (PB) is estimated to have the richest oil shale deposits in the world (Dyni, 2006; Johnson et al.,2010). Its unique economic mineral resources have been studied for over 75 years, especially in the depositional center where the strata show the richest organic content (Bradley, 1928; Smith and Milton, 1966; Surdam and Parker, 1972; Cole and Picard, 1978; Dean et al., 1981; Remy and Ferrell, 1989; Dyni, 1996; Pitman, 1996; Mason, 2007; Tuttle, 2009; Jagniecki and Lowenstein, 2015). The GRF comprises one of the best documented deposits formed in ancient lakes and is a classic example of a lacustrine depositional system (Bradley, 1931; Cole and Picard, 1978; Dyni and Hawkins, 1981; Grabowski Jr and Pevear, 1985; Hasiotis and Honey, 2000; Katz, 1988; Tänavsuu-Milkeviciene and Sarg, 2012). At present, a stratified lake model is commonly accepted among geologists for the origin of oil shale of the Green River Formation (Desborough, 1978; Johnson, 1985; Poole, 2014; Tänavsuu-Milkeviciene and Sarg, 2012). Tänavsuu-Milkeviciene & Sarg (2012) established a detailed stratigraphic architecture based on facies association analysis, depositional trends, and gamma ray and Fischer assay data. They proposed a model comprising six lake-stages, which were similar to the 5 time-stratigraphic periods or lake stages defined by Johnson et al. (2010). Based on the mineral distribution variations across the basin, (Boak et al., 2013) defined three mineralogic units that are strongly related to the six lake stages (Fig. 2.1). Poole (2014) further studied the mineral distribution and rock types of the GRF in the margin and

center of the PB, mainly based on quantitative mineral analyses, by X-Ray Diffraction (XRD) and provided additional information about the depositional environment of the GRF in PB and the water chemistry of the paleolake in which those minerals were formed.

Dean et al. (1981) summarized geochemical and mineralogical analysis on core from the Oil-Shale Core Hole CR-2 without interpretation of the depositional processes implied by those data; Feng (2011) characterized the Green River Formation in the Piceance Basin, by integrating sequence stratigraphy, Rock-Eval pyrolysis and inorganic geochemistry data from core USBM01-A to define trends in the occurrence, quality and distribution of source rock. She concluded that the organic deposition of the Green River oil shale is controlled mainly by three processes: production, destruction and dilution (Feng, 2011). Tuttle (2009) collected and published chemical, mineralogical and stable isotopic data from cores in Colorado, Utah, and Wyoming, concluding that geochemical data can be traced within an oil shale basin and similar depositional conditions prevailed across large areal extents, but no further analysis and interpretation about the difference of the three basins was elaborated.

Inorganic geochemistry data on the GRF of the Piceance Basin are limited. The objective of our study of these outcrop and core cross sections of the GRF was to refine our understanding of the chemical variations throughout the depositional history of the lake beyond the reconnaissance conducted previously (Feng, 2011; Boak, et al. 2013; Poole, 2014).

We chose to conduct our geochemical study by inductively coupled plasma optical emission spectroscopy-mass spectrometry (ICP-OES). Selectively spaced analytical data generated using ICP- OES can provide a quantitative linkage among existing data from core, well-log, Fischer assay, pyrolysis and petrophysical properties at a reasonable resolution and can help to better understand the depositional processes of the lacustrine system in the Eocene era. The

main objective of the paper is to understand depositional trends for the GRF in the PB from the inorganic geochemistry data and relate it to the balance of clastic and carbonate inputs, redox conditions, paleoproductivity and salinity. Specifically, we wish to evaluate how the variations of clastic flux across the basin are affected by climate changes in the Eocene, to identify the most representative trace metal elements for characterizing the redox conditions of the paleolake, and to define how clastic input, redox conditions and paleoproductivity affect the accumulation and preservation of organic matter in the lacustrine system. This study will help to refine our understanding of chemical variations throughout the depositional history of the lake.

## Geologic setting

### Piceance Basin (PB)

The Piceance basin (PB) is a northwest-southeast elongated structural feature ~100 mi long, averaging ~60 mi wide encompassing an area of around 6,000 sq mi in northwestern Colorado (Young, 1995a). The Green River Formation (GRF) of Colorado, Wyoming, and Utah was deposited in a group of continental basins occupying a broken foreland province east of the Cordilleran fold and thrust belt (Smith et al., 2008). The PB is bounded by the Uinta Mountains on the north, by the White River uplift on the east, by the Uncompahgre uplift on the south, and by the Douglas Creek Arch on the west (Figure 2.2).

Subsidence in the PB began synchronously with the rise of the Uncompahgre uplift and the Douglas Creek arch during the Late Cretaceous-Paleocene Laramide orogeny, about 65 Ma (Young, 1995a). The Laramide orogeny is thought to be the product of west-to-east compressional tectonism that affected and reshaped most of western North America (Young, 1995a). The Laramide deformation progressed from west to east. The next uplifts to form in the vicinity of the

subsiding PB would have been the Axial basin and Gunnison uplifts, followed by the White River uplift and the Elk Mountains (Young, 1995a).

The PB formed in a mid-latitude warm-temperate to subtropical climate (Clementz & Sewall, 2011), and was divided by a number of basement-cored Laramide uplifts (Dickinson et al., 1988). The deposition in lakes was initiated and terminated by tectonic and landscape evolution events, which is also tied closely with Eocene climate changes (Carroll et al., 2006; Bohacs et al., 2007; Chetel et al., 2011; Tänavsuu-Milkeviciene & Sarg, 2012).

During Eocene time, volcanism occurred over broad areas of the northwestern United States and provided both fallout tuff and volcaniclastic sediment to the Green River Formation lake basins (Surdam and Stanley, 1980; Smith et al., 2008).

Eocene Stratigraphy of the GRF in PB

The lacustrine strata in the PB record a progression from open to closed and return to open hydrologic conditions (Smith et al., 2008). Alluvial deposits in the Piceance and Uinta Basin are physically separated from each other by the Douglas Creek Arch, and from strata in the Greater Green River Basin by the Uinta uplift and Axial Basin arch (Smith et al., 2008). The rich oil shale interval in the GRF of the PB was deposited in Eocene Lake Uinta, a large, internally drained lake, which extended across both the Piceance Basin and the Uinta Basin to the west (Johnson et al., 2010). The GRF in the Greater Green River and Washakie Basins was deposited in a separate but largely contemporaneous lake, Lake Gosiute. Lake Uinta began as a fresh or brackish lake, and then became increasingly saline through time. Ultimately, large quantities of the potentially valuable mineral nahcolite (naturally occurring sodium bicarbonate - $NaHCO_3$) as well as halite

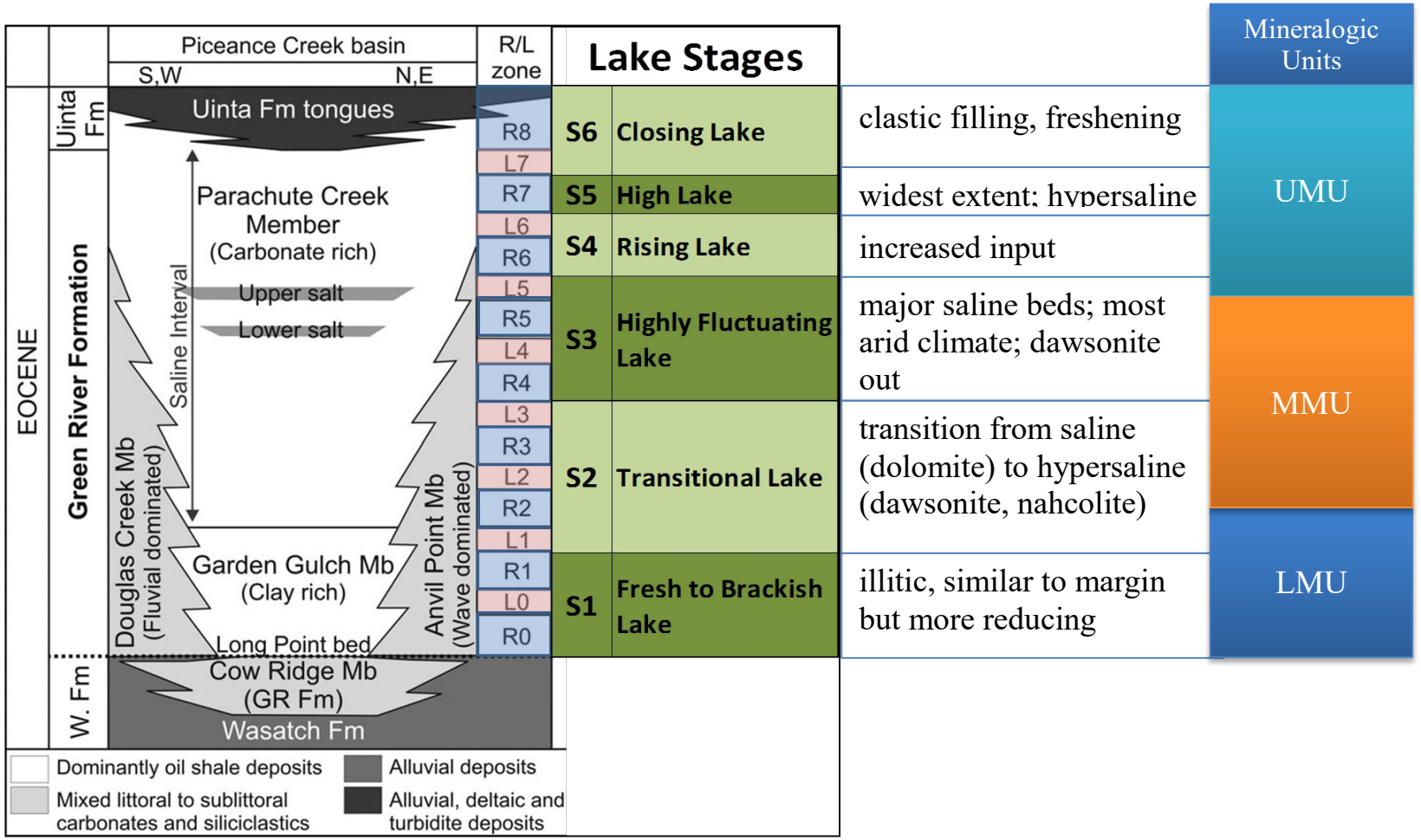



Figure 2.1. Stratigraphy of the Eocene Green River Formation, rich and lean oil shale zones (Cashion and Donnell, 1972, 1974), Lake Stages of Tänavsuu-Milkeviciene and Sarg (2012), and mineralogic units defined in Boak et al. (2013).

were deposited when the lake receded into a comparatively small area in the middle of the Piceance Basin (Johnson et al., 2010). Within the lake basin, oil shale, ostracod-bearing limestone, mollusk-bearing sandstone, and kerogen-rich shale occur interbedded with thin coal and thick siliciclastic deposits formed around the perimeter of the lake (Sarg et al., 2013). In late early to early middle Eocene time, waters of Lake Uinta expanded to cover the entire basin and even transgressed the Douglas Creek Arch to join those of the Uinta Basin in Utah and form a single large lake (Pitman, 1982; Young, 1995b). The Mahogany zone, a thick, widespread organic-rich oil shale, formed at this time (Young, 1995b; Sarg et al., 2013). In middle to late Eocene time, a large delta of volcaniclastic debris (Uinta Formation) began to prograde southward across the basin and eventually obliterated the PB portion of Lake Uinta. The GRF has been divided into four members: the Douglas Creek, Garden Gulch, Anvil Points, and Parachute Creek Members (Fig. 2.1). The Douglas Creek, Garden Gulch and Parachute Creek Members can be found in nearly all outcrop areas of the Green River, but the Anvil Points Member is restricted to the east and southeastern margins of the basin (Young, 1995b).

The name Douglas Creek Member is applied to marginal lacustrine rocks along the west and southwest margins, and Anvil Points Member is applied to marginal lacustrine rocks along the east and southeast margins of the Piceance Basin. The Garden Gulch Member generally comprises illitic oil shale deposited in the early history of Lake Uinta, and the Parachute Creek Member comprises the feldspathic-dolomitic oil shale deposited later (Bradley, 1931; Johnson et al., 2010, Boak et al 2013). The upper part of the Parachute Creek Member interfingers with the alluvial, deltaic and turbidite deposits of the Uinta Formation (Fig. 2.1).

Deposition of the GRF lacustrine sediment spanned a period of ~5 Myr, between *ca* 53 and *ca* 48 Ma (Smith et al., 2008, 2010). Based on kerogen content, The GRF of PB can be subdivided

into 9 rich zones and 8 lean zones (Cashion & Donnell, 1972), as shown in Fig. 2.1. The rich and lean oil shale zones mark time-stratigraphic units and correlate with depositional packages characterizing lake evolution (Fig.2.2). The six lake stages defined by Tänavsuu-Milkeviciene and Sarg (2012) reflect changes in depositional environment and large-scale sedimentological trends of the GRF (Fig. 2.1) and are conformable with the rich and lean zones. The six lake stages are: 1) fresh lake; 2) transitional lake; 3) highly fluctuating lake; 4) rising lake; 5) high lake; 6) closing lake. The evolution of the lake reflects variations in facies association distribution, richness of oil shale, water chemistry, degrees of lake restriction and salinity, and siliciclastic sediment input.

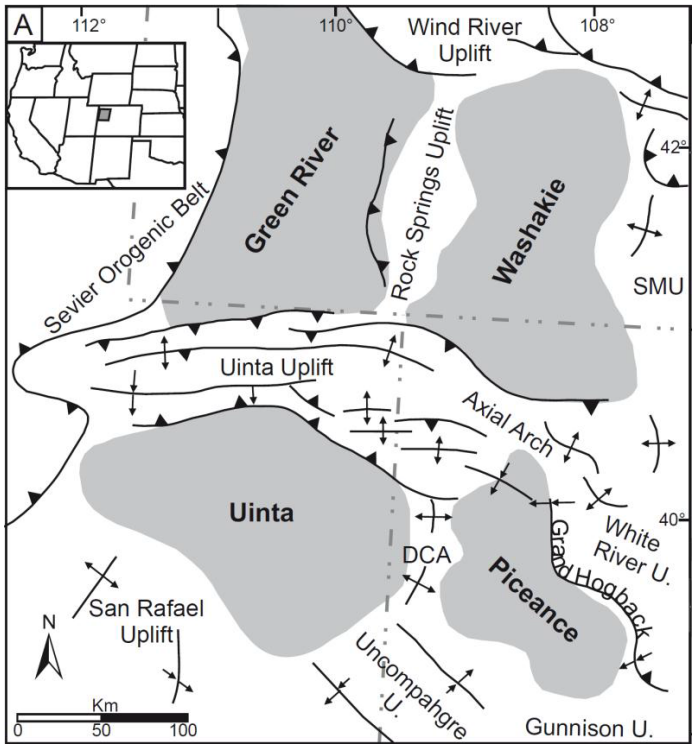



Figure 2.2. Location of the Piceance Basin and surrounding uplifts (modified from Dickinson et al., 1988).

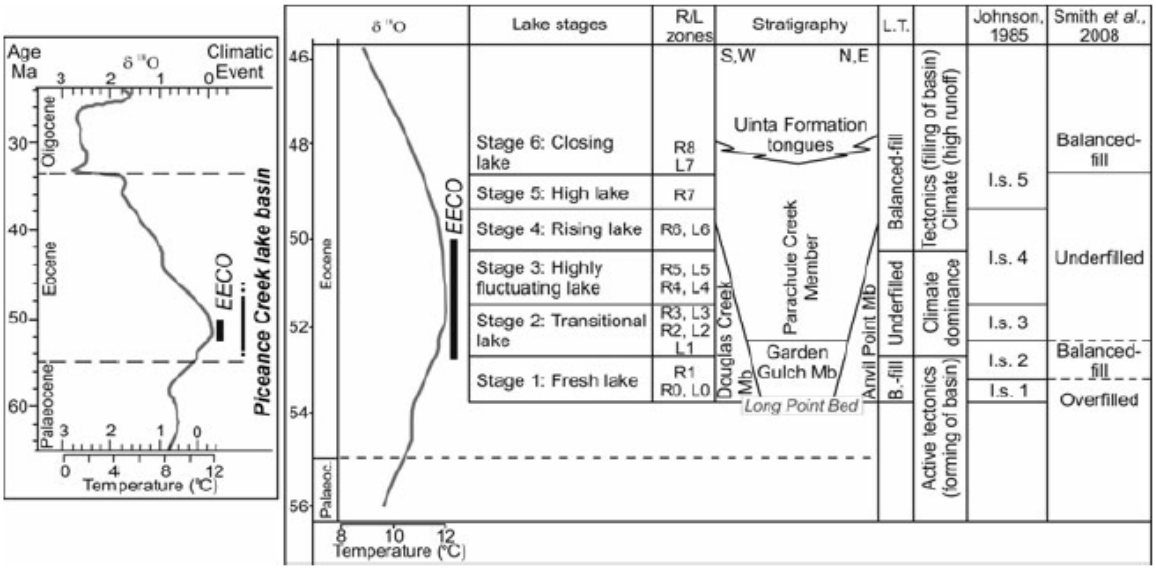



Figure 2.3. Correlation between Eocene climate curve, evolutionary lake stages (Stages 1 to 6), rich and lean zones (R/L), basin stratigraphy, lake types (L.T.), separated in this study, and large-scale basin development model and their relation to the age data. Eocene climate curve modified after Zachos et al. (2001, 2008); age data and correlations after Smith et al. (2008, 2010); rich (R) and lean (L) zones after Cashion & Donnell (1972); stratigraphy after Johnson et al. (2010). The Figure is from Tänavsuu-Milkeviciene & Sarg, 2012.

## Dataset and Methods

Outcrop samples were collected from the Douglas Pass area (DP) on the basin margin, and core samples were obtained from two drilled wells, the Shell 23X-2 (Shell), and the John Savage 24-1 (JS), located in the basin center (Fig. 2.4). The outcrop section recorded the shallower near-shore water depths where lacustrine and fluvial deposits are most likely to reflect changes in lake levels and climatic conditions (Poole, 2014). Douglas Pass is located on the Douglas Creek Arch, at the western margin of the basin, where during high water levels ancient Lake Uinta is proposed to have connected the Piceance Basin to the Uinta Basin (Smith et al., 2008). Samples were collected in two separate sections, representing approximately 680 ft (around 208 m) and located along Highway 139 (from 39°35'54.06"N, 108°49'3.00"W to 39°35'49.44"N, 108°48'22.14"W). 186 samples were collected from the DP outcrop for the geochemical analysis.

The Shell 23X-2 well is located in the depocenter of the basin. The sampled core interval is 1919ft (584.91m) in thickness, from 780 to 2699 ft ((237.74 to 822.66m) and covers from Stage 1 to Stage 6 in the lake stratigraphy framework. The core was sampled and analyzed where a lithofacies change and sedimentary structures occurred (Tänavsuu-Milkeviciene and Sarg, 2012). The John Savage 24-1 well is located in the depocenter as well, and it has well-preserved saline mineral zones. The sample core interval is 1504 ft (458.42m) in thickness, from 1293 to 2797 ft ((394.11 to 852.53m) and covers from Stage 2 to Stage 6 in the lake stratigraphy. Samples taken from cores located in the basin center did not include the nearly pure halite facies.

186, 100, and 90 samples were selected from DP, JS, and Shell, respectively, for ICP-OES analysis. All samples were analyzed for major, minor and trace elements by inductively coupled plasma mass spectrometry/optical emission spectroscopy (ICP-MS/OES) analysis. Total Carbon (including organic and inorganic) content was analyzed by a LECO$^{TM}$ C744 Carbon Analyzer at

the internal lab of the U.S.G.S, Denver. Sample preparation included pulverizing samples until 85% of the material passed through a 200-mesh screen. One split of the powdered samples was analyzed by ICP-OES for abundances of major oxides and several minor elements. The other split of the powered samples was analyzed by ICP-MS for trace elements, rare earths and refractory elements. Detailed information on the ICP-MS analytical protocols was presented by Harris et al. (2013) and Dong et al. (2015). The international standards, SCO-1, SGR-1, SBC-1 and ShBOQ-1 were analyzed as blind samples for quality control.

Enrichment factors normalize trace-element concentrations to aluminum content and to the metal/Al ratio of average shale composites (Calvert and Pedersen, 1993; Tribovillard et al., 2006):

$$EF_{\text{element X}} = X/Al_{\text{sample}} / X/Al_{\text{average shale}}$$

For our study, the standard element concentrations of Wedepohl (1971) for shale were used.

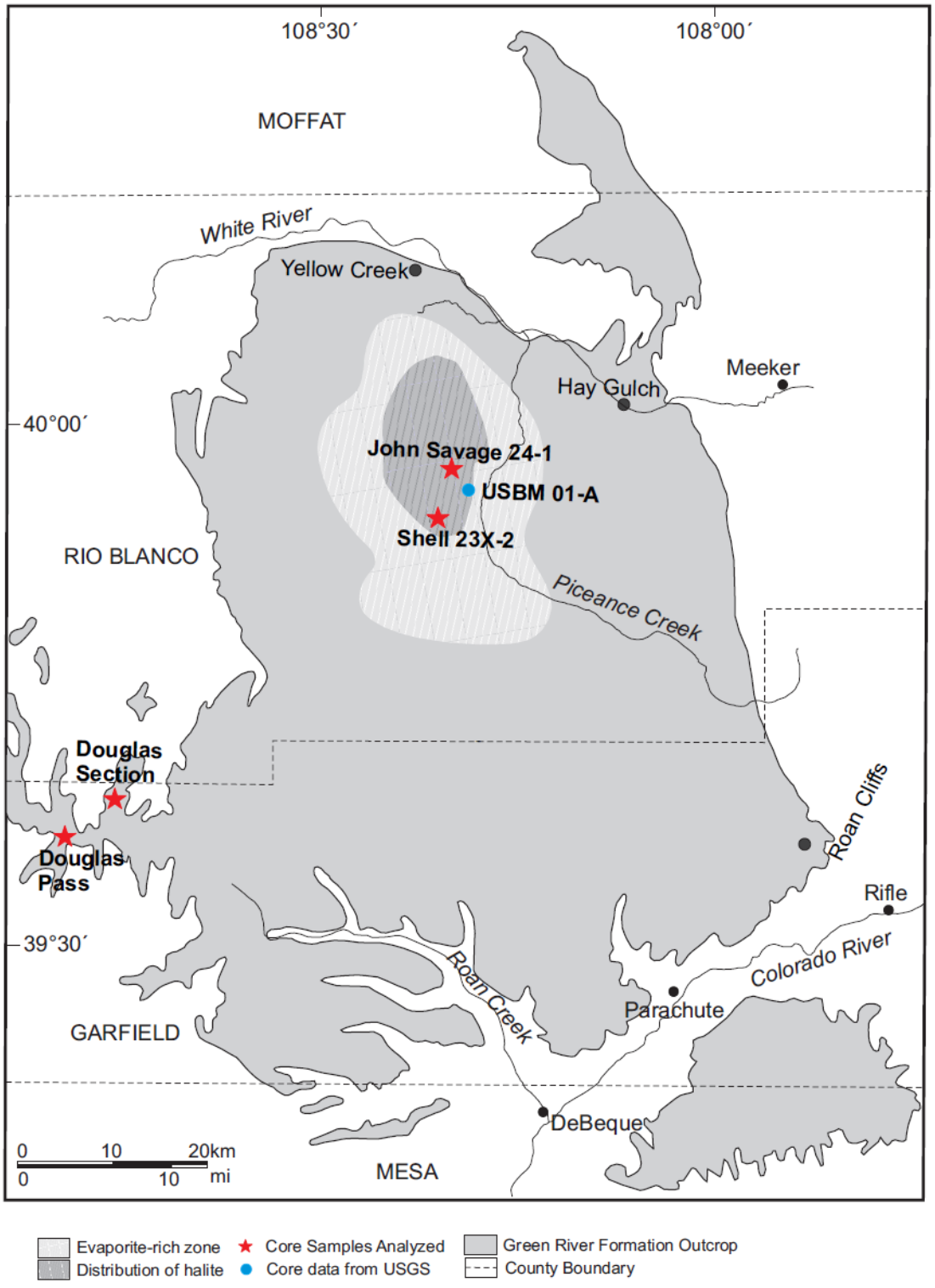



Figure 2.4. Map of Piceance Creek Basin with outcrop and well locations. Shaded area in the northern part of the basin indicates area with bedded evaporite deposits in basin depocenter (modified after Dyni, 1996 and Tänavsuu-Milkeviciene and Sarg, 2012).

## Results

This section summarizes the elemental compositions of the sample suite organized from the perspective of major and trace elements that reflect important depositional components and conditions of the sedimentary sequence. Certain elements can act as proxies for local depositional and environmental conditions during sedimentation (Pearce and Jarvis, 1992; Pearce et al., 1999; Tribovillard et al., 2006; Turner et al.,2016). Representative major and trace elements were selected to characterize the changes in detrital influx, carbonate precipitation, redox condition, salinity, and paleo-productivity in the Piceance Basin (DP, Shell and JS) (Figs.2.5-2.7). Average values by lake stage for each section (DP, Shell, JS) are provided in Table 2.1 for selected element values and calculated parameters. The stages are those defined by Tänavsuu-Milkeviciene and Sarg (2012) for the basin center data, in the JS and Shell cores. However, for the basin margin, the lake stages were not easily constrained and defined. In this study, we used the classification of Johnson et al. (1985) and will discuss the implications of differences in interpretation resulting from the difference in stage boundaries later in this chapter.

### Indicators of Terrestrial Input

Aluminum (Al) and titanium (Ti) are generally immobile during diagenesis (Calvert and Pedersen, 1993; Tribovillard et al., 1994; Sageman and Lyons, 2003; Brumsack, 2006; Tribovillard et al., 2006; Dong et al., 2018). Ti is commonly associated with deposition from a continental source (Pearce and Jarvis, 1992; Pearce et al., 1999) and has a detrital origin, commonly present in minerals such as ilmenite, rutile, and augite in the sand and silt-sized grains; whereas Al is mainly derived from clay and feldspar (Pearce et al., 1999; Tribovillard et al., 2006). Al and Ti have been used as indicators of detrital flux (Caplan and Bustin, 1999; Ver Straeten et al., 2011).

Silicon (Si) can have detrital, biogenic and authigenic origins (Ross and Bustin, 2009). Based on the mineralogy and geochemical data from Poole (2014) and Boak et al. (2016), Si is interpreted to be mainly of detrital origin and present in quartz, feldspar, analcime, and clay minerals, representing detrital and authigenic origins.

Potassium (K) is also associated with clay minerals and alkali feldspars (Pearce et al., 1999; Tribovillard et al., 2006; Turner et al., 2016). Therefore, Si, Al, K, Ti can serve as the proxies for siliciclastic flux. The sum of Si, Al, K, Ti oxides is calculated to represent the detrital flux delivered to the basin via different lake stages.

Stratigraphic profiles of the sum of $SiO_2$, $Al_2O_3$, $K_2O$ and $TiO_2$ concentrations for DP, JS and Shell are presented in Figs. 2.5-2.7. Average abundances of $SiO_2$, $Al_2O_3$, $K_2O$ and $TiO_2$ in each lake stage are displayed in Table 2.1. For the basin margin, the average values of $SiO_2$, $Al_2O_3$, $TiO_2$ in different lake stages show the same trend (Table 2.1), decreasing from S1 to S2, and then increasing from S2 to S3; whereas the average value of $K_2O$ increases upsection from S1 to S3. In the basin center, the Shell core records a complete profile from S1 to S6. S1 has the highest average values of $SiO_2$, $Al_2O_3$, $TiO_2$. S2 and S3 have the lowest average values of $SiO_2$, $Al_2O_3$, $K_2O$ and $TiO_2$, and S4 and S5 have intermediate average values of those detrital elements, which then increases in S6 (Table 2.1). For JS, the chemical profiles for $SiO_2$, $Al_2O_3$, $K_2O$, and $TiO_2$ have similar trends to Shell from S2 to S6 (Table 2.1). Overall, the average values of Si, Al, K, and Ti are higher in the basin margin area (DP) than the basin center (JS, Shell), as shown in Fig.2.8. Integrating $SiO_2$, $Al_2O_3$, $K_2O$ and $TiO_2$ into a single chemical plot representing the detrital flux for DP and JS and Shell (Figs. 2.5-2.7), the siliciclastic input for DP illustrates the highest sediment input in S1, decrease in S2 and then increase in S3. Shell has a similar clastic sediment load to DP in S1, and lowest detrital flux in S2 and S3, with S4 and S5 representing intermediate

sediment supplies, and S6, marking the close of lake expansion in the basin center. The DP section shows a bimodal distribution, with a few very low values of detrital input (the limestone layers) and a larger number of large values. The Shell and JS sections show less distinctly bimodal distribution.

Indicators of Carbonate Deposition

Ca is mainly associated with carbonate and phosphate (Banner 1995; Tribovillard et al. 2006), and Mg is accommodated commonly in dolomite. Phosphorus is consistently low in the samples analyzed in this study. According to Poole (2014), Ca and Mg are mainly in carbonate phases in the basin center, so Mg and Ca are good proxies for carbonate minerals. The concentrations of CaO and MgO in DP and JS and Shell have different characters: in DP, the averaged values of CaO and MgO increased from S1 to S2, then decreased from S2 to S3, as shown in Table 2.1; whereas in JS, CaO and MgO have the smallest values in S2 and S3, with CaO increasing upsection from S4 to S6. In contrast, the average values of MgO in S4, S5, S6 change little, with only slight difference among the last 3 lake stages. For Shell, CaO and MgO behaved coherently, similar to JS, the values of CaO and MgO in S2 and S3 are smallest, and then CaO and MgO increased from S3 to S4, with S4 recording the highest values. As shown in Figs. 2.5-2.7, the calculated carbonate concentrations in DP, JS and Shell show substantial variations throughout the sections. In DP, the carbonate increased from S1 to S2, and then decreased in S3; in Shell and JS, carbonate represents higher average values in S4 and S6, with S2 and S3 marking the lowest carbonate contents for both the basin center cores (JS and Shell). In the DP section, carbonate shows a bimodal distribution, with a few very high carbonate samples, and many with much lower carbonate content. High carbonate samples show low detrital sediment values and vice-versa. The

Shell and JS sections show less distinctly bimodal distribution, in part because of the wide variation of $Na_2O$.

Salinity Indicators

Saline minerals, like dawsonite and nahcolite, comprise a large part of the inventory of Na (Poole, 2014; Boak et al., 2016), so $Na_2O$ is a good proxy for lake salinity. Even in the basin margin, where nahcolite and dawsonite are absent, the presence of analcime indicates elevated salinity. In addition to sodium content, B/Ga, and Rb/K can also be used as paleo-salinity indicators for mudstone systems (Campbell and Lerbekmo, 1963; Campbell and Williams, 1965; Thompson, 1967; Scheffler et al., 2003; Ye et al., 2016). B/Ga is widely used as a paleo-salimeter due to the different behaviors of B and Ga in sediment deposition (Potter et al., 1963; Shimp et al., 1969; Couch, 1971; Ye et al., 2016), where B is usually concentrated under saline conditions and Ga is usually associated with Al. K in illite can be replaced by Rb because of their similar ionic radii (Doyle et al., 1998). Rb/K ratio in clay minerals deposited under saline conditions is higher than in freshwater environments (Taylor and McLennan, 1985). Therefore, Rb/K ratios in shales are reported to be positively related to salinity (Scheffler et al., 2003; Ocakoğlu et al., 2016).

There are large differences in sodium concentration between the basin margin and basin center (Figs 2.5-2.8). The average value of $Na_2O$ in DP is much lower than in JS and Shell (Table 2.1). For DP, the average value of $Na_2O$ in S1 is 2.79%, and then it decreases to 1.14% in S2, and increases to 1.94% in S3. For, JS and Shell, S2 and S3 represented the highest values of $Na_2O$, which was 4.38 (S2) and 17.08% (S3) for JS, and 11.08%(S2) and 13.57% (S3) for Shell, respectively. However, the sodium values for S4, S5, S6 in JS and Shell are sharply lower than S3 to S4, with S5 and S6 also at a low level of sodium (Table 2.1, Figs.2.5-2.7). Combined with B/Ga and Rb/K ratio, the salinity from the basin margin, DP, to basin center, Shell and JS, may be

better characterized. The average values of Rb/K(x$10^3$) from S1 to S3 has a decreasing trend in DP, with an overall average value of 4.2 (Table 2.1, Fig. 2.5). For the basin center, JS and Shell behave differently in terms of their B/Ga and Rb/K ratios in different stages: in JS, B/Ga has the highest value in S3 (22.35), whereas Shell has the highest B/Ga ratio in S5 (10.64); Rb/K ratios do not vary widely in different stages of Shell and JS (Figs 2.6 and 2.7, Table 2.1), with S1 (5.47) for Shell and S5(5.23) for JS, representing highest values, respectively. Rob/K does not change coherently with sodium concentrations in different lake stages (Table 2.1). Overall, the values of salinity indicators in the basin margin are smaller than the basin center in the lake development, but the elevated values of salinity in the basin margin seems to occur earlier than in the basin center, as shown in Figs 2.5 – 2.7.

Organic Carbon Content

TOC abundance clearly varies among the different stratigraphic units (Figs.2.5-2.7, Table 2.1). As shown in Fig.2.8, the overall TOC concentrations in the DP section are much lower than the values in JS and Shell sections. For the DP section, the average value of TOC in S1 (0.92%) is similar to S2 (0.8%), with S3 preserving the highest TOC (2.94%). For the more distal part of the lake, in the Shell well, the average TOC content has a relatively high value in S1 (10.81%), S2 (10.94%) and S3 (12.46%), and then decreases from S3 to S4 (5.77%), with S5 recording the highest TOC contents (15.46%). In the closing lake stage (S6), the TOC value decreases sharply, with average TOC (6.64%). In the JS core, the overall TOC concentrations are high, very similar to the Shell section: average TOC contents in S2, S3 and S4 are of 11.07%, 11.87%, 10.33%, respectively. The JS well also has the highest average TOC content in S5 (14.64%), and then the value decreases in S6 (4.58%).

Productivity Indicator

Phosphorous (P), an essential nutrient for marine phytoplankton growth, has been used as a productivity indicator in ancient sediments (Ingall et al., 1993; Rimmer et al., 2004; Schoepfer et al., 2015). Some authors used other geochemical proxies, like barium and biogenic Si to evaluate the role of productivity in the accumulation of organic-rich rocks (Brumsack, 2006; Tribovillard et al., 2006; Schoepfer et al., 2015; Shen et al., 2015; Dong et al., 2018). However, these do not work well in the Green River Formation of the Piceance Basin, because almost most Si is detrital in origin and no biogenic Si is available (Feng, 2011; Poole, 2014; Boak and Poole, 2015). In our study, P is used to indicate productivity in the lake water (Feng et al., 2011). As shown in Figs. 2.5-2.7, P concentrations in both the basin margin and the basin center are very low. The average value of P in the basin center is higher than in the basin margin (Fig.2.8 and Table 2.1). In the DP section, the variations of $P_2O_5$ in different lake stages are very small. In the JS and Shell sections, $P_2O_5$ changes throughout the sections are more obvious: in Shell, S4 and S5 have the highest values of $P_2O_5$ (S4=0.50%, S5=0.66%); similarly, JS also has the highest values of $P_2O_5$ in S4 and S5 (S4= 0.34%, S5=0.32%). However, the $P_2O_5$ concentration in different stages did not change as sharply in JS compared to Shell (Figs.2.6-2.7, Table 2.1). It is also important to note that the averages for S4 and S5 may be skewed by single values.

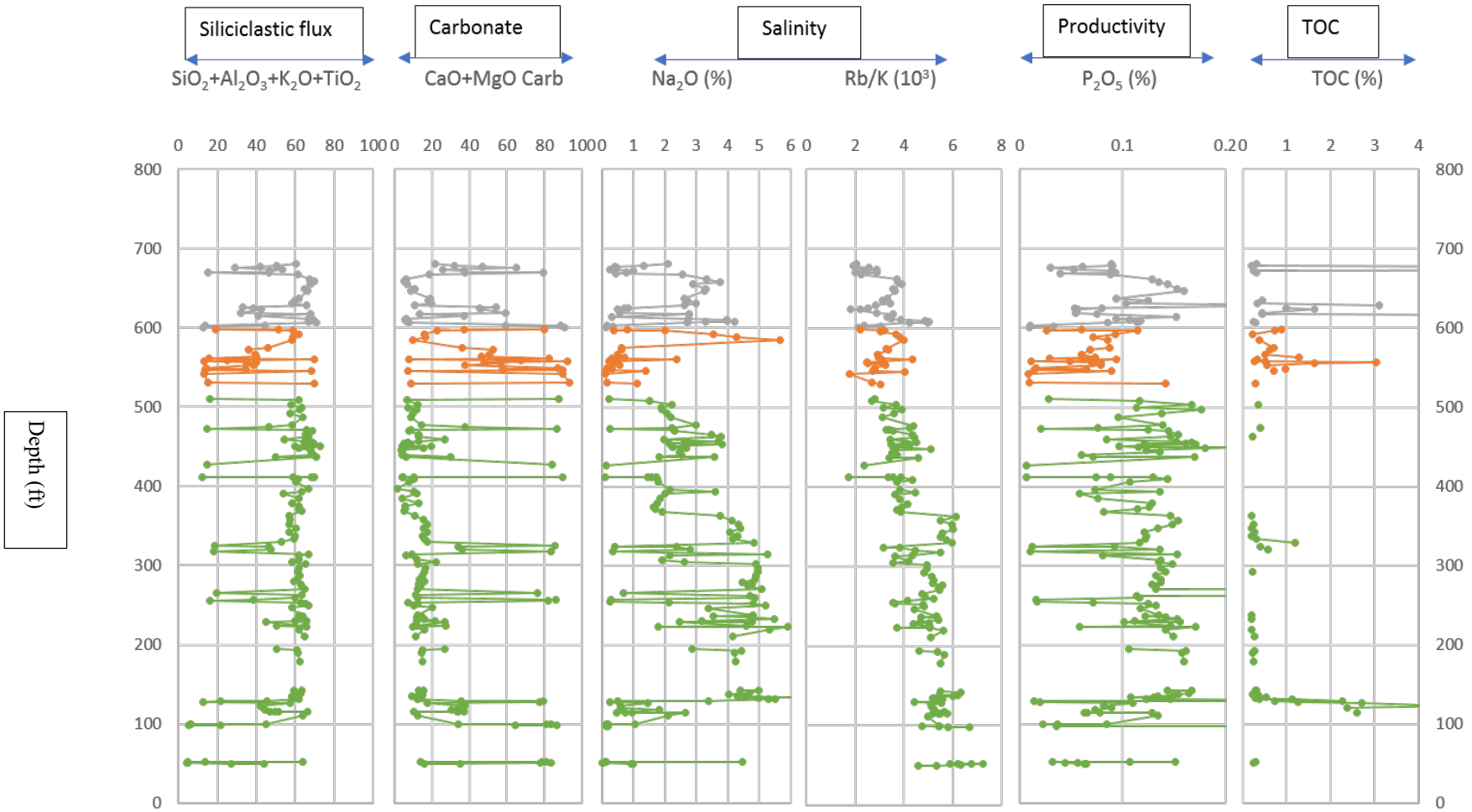



Figure 2.5. The distribution of typical geochemistry proxies derived from ICP-OES in Douglas Pass area (S1=Green line, S2=Orange line, S3=Grey line).

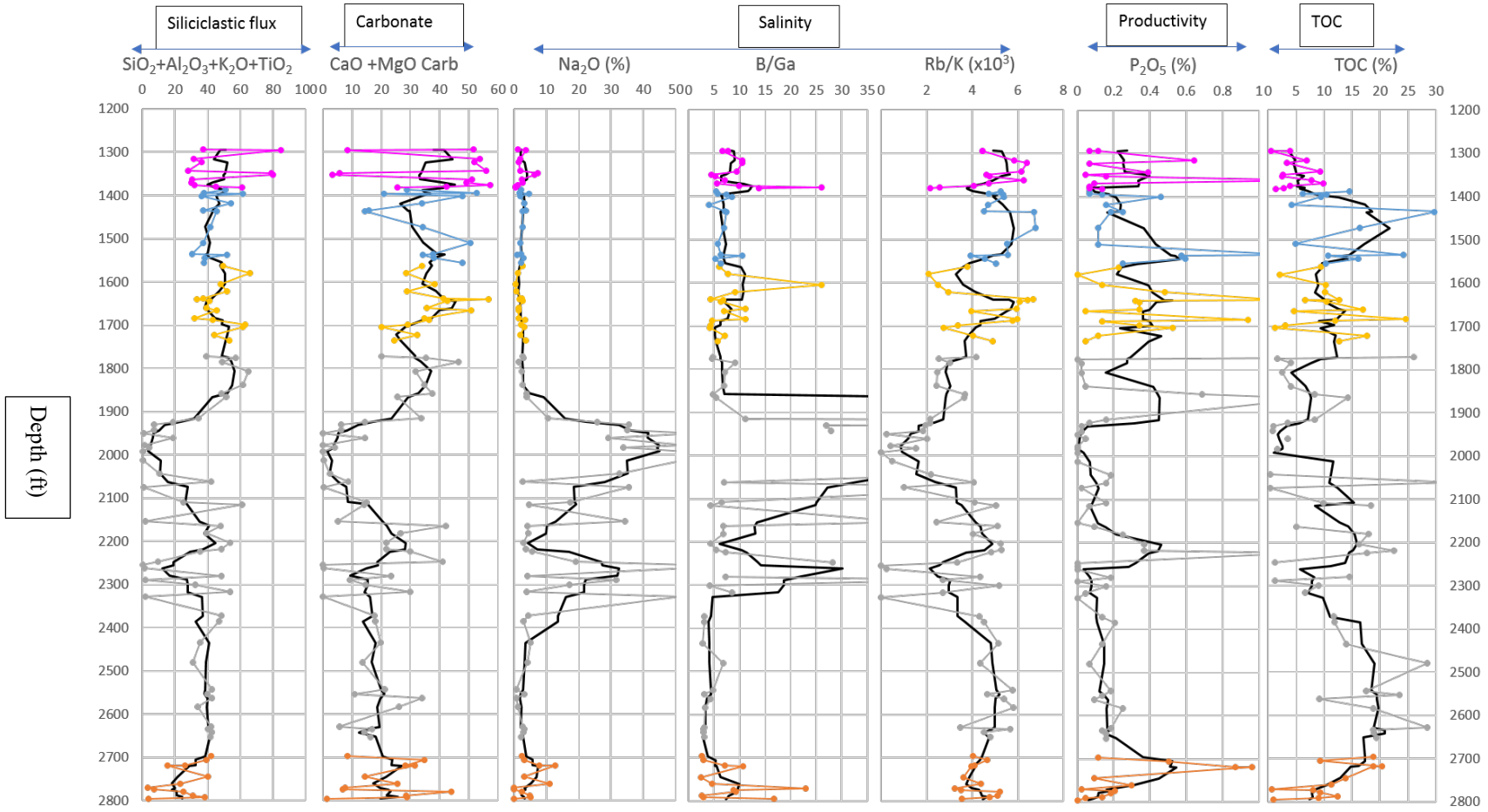



Figure 2.6. The Distribution of typical geochemistry proxies derived from ICP-OES in John Savage 24-1. Black lines are moving average of 5 samples (S2=Orange line, S3=Grey line, S4=Gold line, S5=Blue line, S6=Purple line).

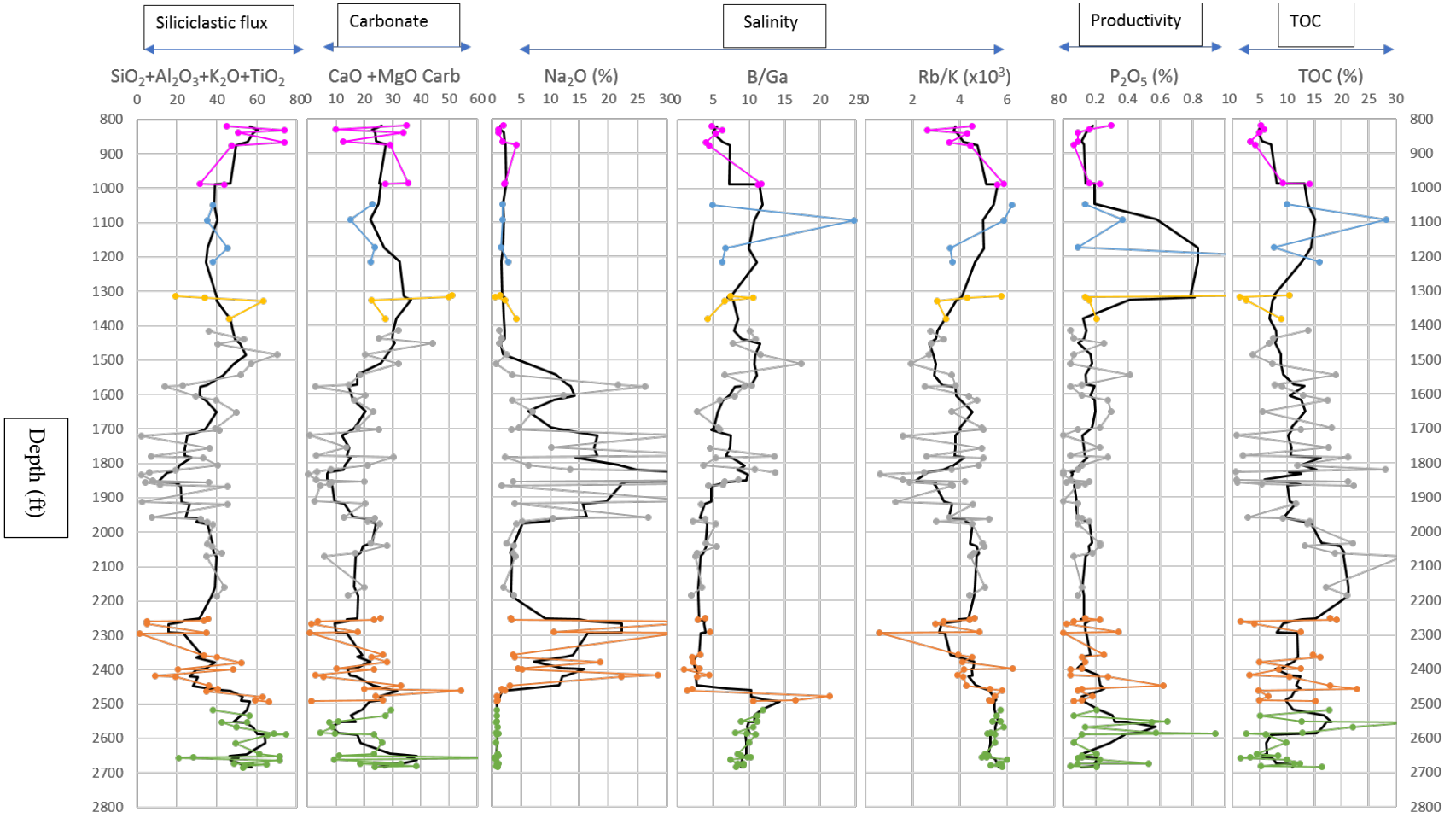



Figure 2.7. The Distribution of typical geochemistry proxies derived from ICP-OES in Shell 23X-2. Black lines are moving average of 5 samples (S1=Green line, S2=Orange line, S3=Grey line, S4=Gold line, S5=Blue line, S6=Purple line).

Table 2.1: Average Chemical Composition of Lake Stages in Three Stratigraphic Sections of the Green River Formation ($FeO_T$ = Total iron as FeO; TOC = TotalOrganic Carbon; Detrital= $SiO_2$+$Al_2O_3$+$K_2O$+$TiO_2$; Carb= $CaCO_3$ +$MgCO_3$; Rb/K*= Rb/K x $10^3$, DOP* = Degree of Pyritization (see text for explantion); EF = Enrichment Factor; n.a. = not analyzed.

| Section | Douglas Pass (Basin Margin) | | | Shell (Basin Center) | | | | | | John Savage (Basin Center) | | | | |
|---|---|---|---|---|---|---|---|---|---|---|---|---|---|---|
| Lake Stage | S1 | S2 | S3 | S1 | S2 | S3 | S4 | S5 | S6 | S2 | S3 | S4 | S5 | S6 |
| Depth (ft) | 49.2-510.4 | 529.4-598.4 | 600.4-680.4 | 2518-2685 | 2251.7-2493 | 1415-2185.4 | 1314-1381 | 1048-1215 | 819.7-989 | 2696.5-2795 | 1772-2652 | 1563-1735 | 1388-1555 | 1294-1382 |
| Interval (ft) | 461.1 | 69 | 80 | 167 | 241.3 | 770.4 | 67 | 167 | 169.3 | 98.5 | 880 | 172 | 167 | 88 |
| $SiO_2$ (wt%) | 40.34 | 28.72 | 37.77 | 39.82 | 25.52 | 22.77 | 30.02 | 28.18 | 38.05 | 19.05 | 23.24 | 35.33 | 33.73 | 37.09 |
| $Al_2O_3$ (wt%) | 10.17 | 7.64 | 10.73 | 10.14 | 5.61 | 5.42 | 6.26 | 7.06 | 8.55 | 4.36 | 5.59 | 8.71 | 7.50 | 8.35 |
| $K_2O$ (wt%) | 2.26 | 2.34 | 3.24 | 3.69 | 2.15 | 2.91 | 4.11 | 3.56 | 5.32 | 1.10 | 1.60 | 2.89 | 1.66 | 2.27 |
| $TiO_2$ (wt%) | 0.39 | 0.30 | 0.43 | 0.34 | 0.20 | 0.20 | 0.28 | 0.29 | 0.31 | 0.15 | 0.19 | 0.31 | 0.28 | 0.29 |
| CaO (wt%) | 9.46 | 18.53 | 10.71 | 7.31 | 6.07 | 5.48 | 13.87 | 7.82 | 10.01 | 7.87 | 5.84 | 12.58 | 13.62 | 15.05 |
| MgO (wt%) | 3.78 | 7.92 | 5.39 | 5.36 | 3.66 | 3.25 | 6.17 | 3.35 | 3.95 | 3.64 | 3.28 | 6.23 | 5.15 | 5.30 |
| $Na_2O$ (wt%) | 2.79 | 1.14 | 1.94 | 0.81 | 11.08 | 13.57 | 2.07 | 1.99 | 2.09 | 4.38 | 17.08 | 2.10 | 2.58 | 2.64 |
| FeO (wt%) | 3.25 | 2.28 | 3.60 | 4.09 | 2.05 | 1.67 | 2.09 | 2.21 | 2.54 | 1.41 | 1.86 | 3.21 | 2.33 | 2.51 |
| P (wt%) | 0.06 | 0.03 | 0.04 | 0.12 | 0.07 | 0.05 | 0.22 | 0.29 | 0.07 | 0.13 | 0.08 | 0.15 | 0.14 | 0.12 |
| TOC (wt%) | 0.92 | 0.80 | 2.94 | 10.81 | 10.94 | 12.46 | 5.77 | 15.46 | 6.64 | 11.07 | 11.87 | 10.33 | 14.64 | 4.58 |
| S (wt%) | 0.70 | 0.12 | 0.10 | 1.34 | 0.91 | 1.05 | 0.47 | 0.65 | 0.37 | 0.51 | 0.83 | 0.73 | 0.56 | 0.25 |
| As (ppm) | 14.07 | 11.20 | 14.28 | 35.88 | 25.06 | 27.63 | 18.00 | 62.50 | 41.14 | 15.00 | 28.22 | 34.50 | 29.69 | 26.89 |
| Mo (ppm) | 4.08 | 0.90 | 1.84 | 41.06 | 24.06 | 23.72 | 15.75 | 25.00 | 9.71 | 14.27 | 26.64 | 25.80 | 22.00 | 9.18 |
| U (ppm) | 4.27 | 4.53 | 4.17 | 8.59 | 3.26 | 3.09 | 4.02 | 7.83 | 3.82 | 1.63 | 3.98 | 5.11 | 5.98 | 3.43 |
| V (ppm) | 83.4 | 68.3 | 89.1 | 157 | 76.2 | 75.4 | 84.5 | 74.5 | 61.7 | 48.8 | 87.5 | 106 | 86.3 | 66.3 |
| Zn (ppm) | 68.28 | 50.02 | 82.46 | 103.67 | 54.76 | 53.37 | 52.50 | 72.00 | 54.29 | 38.00 | 75.86 | 121.73 | 131.31 | 48.92 |
| Cu (ppm) | 27.00 | 16.51 | 31.54 | 74.39 | 32.12 | 35.69 | 30.25 | 51.50 | 33.14 | 22.42 | 43.32 | 54.67 | 47.54 | 34.92 |
| B (ppm) | n.a | n.a | n.a | 122.44 | 25.38 | 51.76 | 61.25 | 71.00 | 78.43 | 28.50 | 55.69 | 76.71 | 67.00 | 80.80 |
| Ga (ppm) | n.a | n.a | n.a | 609.83 | 225.72 | 195.31 | 554.50 | 389.50 | 418.14 | 6.46 | 7.72 | 11.54 | 10.15 | 12.05 |
| Rb (ppm) | 87.01 | 63.90 | 86.65 | 83.86 | 42.68 | 44.59 | 66.45 | 64.98 | 86.56 | 39.28 | 54.11 | 89.66 | 70.72 | 76.73 |
| Detrital | 53.16 | 39.00 | 52.17 | 53.99 | 33.48 | 31.30 | 40.67 | 39.09 | 52.24 | 24.66 | 30.61 | 47.24 | 43.16 | 48.00 |
| Carbonate | 24.83 | 49.72 | 30.43 | 24.31 | 18.52 | 16.60 | 37.73 | 21.00 | 26.17 | 21.69 | 17.30 | 35.55 | 35.13 | 38.00 |
| B/Ga | n.a | n.a | n.a | 9.59 | 5.45 | 6.82 | 7.23 | 10.64 | 6.84 | 7.79 | 22.35 | 8.10 | 6.65 | 9.75 |
| Rb/K* | 4.69 | 3.09 | 3.10 | 5.47 | 4.38 | 3.62 | 4.14 | 4.84 | 4.42 | 4.18 | 3.23 | 4.48 | 5.23 | 4.71 |
| DOP* | 0.22 | 0.17 | 0.06 | 0.44 | 0.56 | 0.55 | 0.29 | 0.37 | 0.21 | 0.42 | 0.56 | 0.49 | 0.45 | 0.21 |
| EF Mo | 1.80 | 1.45 | 2.72 | 53.57 | 69.04 | 43.57 | 43.57 | 47.17 | 17.09 | 53.97 | 36.29 | 42.09 | 38.94 | 19.00 |
| EF U | 1.84 | 3.49 | 2.71 | 5.31 | 3.37 | 2.89 | 4.31 | 6.26 | 2.69 | 2.43 | 3.06 | 3.54 | 4.56 | 2.92 |
| EF As | 1.57 | 1.99 | 2.10 | 4.21 | 7.88 | 7.20 | 2.44 | 12.23 | 7.46 | 3.57 | 2.62 | 3.02 | 5.26 | 4.06 |
| EF V | 1.93 | 3.19 | 1.86 | 2.10 | 1.60 | 1.75 | 1.85 | 1.38 | 1.04 | 2.04 | 1.89 | 1.63 | 1.52 | 1.28 |
| EF Zn | 1.12 | 1.14 | 1.34 | 1.80 | 1.50 | 1.62 | 1.47 | 1.81 | 1.22 | 1.74 | 4.60 | 2.64 | 3.68 | 1.14 |
| EF Cu | 0.85 | 0.57 | 0.92 | 2.75 | 1.91 | 1.91 | 2.06 | 2.72 | 1.64 | 2.52 | 2.06 | 2.45 | 2.45 | 1.87 |

## Redox Indicators

### *Redox-Sensitive Trace Elements*

Certain trace elements, including uranium (U), molybdenum (Mo), arsenic (As), period IV transition metals (Fe, Co, Ni, Cu, Zn) and sulfur (S) commonly display strong enrichment under reducing conditions (Calvert and Pedersen, 1993; Tribovillard et al., 2006; Algeo and Tribovillard, 2009; Rowe et al., 2017; Dong et al., 2018). Mo, U, As, Cu, Zn have been selected to characterize the redox condition of the basin during sedimentation. Metal enrichment factors define the degree of enrichment of redox sensitive metals with respect to selected composite shale standards (Tribovillard et al., 2006; Boak et al., 2016).

The averaged values of enrichment factors for Mo, U, As, Cu, and Zn are summarized in Table 2.1 for DP, JS and Shell. No specific cut-off values have been defined for enrichment factors to differentiate degrees of reducing conditions (for example, oxic, dysoxic, anoxic). Thus, enrichment factors can generally be used primarily as relative measures of reducing tendency.

As shown in Table 2.1 and Fig.2.9, the average values of the enrichment factors for these selected trace elements are higher in the basin center (Shell and JS) than the basin margin (DP), confirming the pattern observed by Boak et al., 2016. From those trace metal enrichment factors throughout the Douglas Pass area, vertical variations from Mo, Cu, As, Zn, U can be observed (Table 2.1), but enrichments are relatively small, and Cu, As, Zn shows depletion with respect to the shale average.

In this study, the relationship of Mo and U enrichment to one another is plotted here (Fig. 2.10) for DP to define the redox signals for the basin margin (Algeo and Tribovillard, 2009; Tribovillard et al., 2012; Boak et al., 2016). The plot of Mo EF vs. U EF for the basin margin samples shows that most data fall into the area below the sea water line, indicating those samples were deposited under suboxic water condition, because those data are mainly in the suboxic zone (Tribovillard et al., 2012). For the basin center core, JS, the five trace elements behave differently from S2 to S6, with stage 3 covering the largest part of the section, reflecting the most intense variation in the enrichment factors. The average value of enrichment factors for each element in JS is summarized in Table 2.1. On the EF U-EF Mo cross-plot (Fig. 2.11), most data plot above sea water line, falling into the "particulate-shuttle" zone defined by Algeo and Tribovillard, 2009 and Tribovillard et al., 2012, indicating the operation of a particulate shuttle mechanism that scavenged Mo on Fe/Mn-oxyhydroxides that redissolved at depth, with Mo precipitating along with sulfides and/or organic matter at the sediment/water interface. As for Shell, EF Mo, EF As and EF Cu have similar trends through the whole section, with less variations in EF U and EF Zn (Table 2.1). Similar to JS, most of the data plot in the particulate shuttle zone as well, as shown in Fig.2.12.

*Degree of Pyritization (DOP)*

The degree of pyritization (DOP) is another parameter used in the shale system to characterize the redox condition. (Berner, 1984; Raiswell et al., 1988; Tuttle, 2009; Turner et al., 2016). Raiswell et al., 1998 stated that DOP reflects redox conditions prevailing during sediment accumulation, where DOP is the ratio of pyritic iron to total reactive iron (pyritic iron plus HCl-soluble iron). DOP values $\leq$0.42, indicate aerobic (normal marine) conditions; DOP values

between 0.42 and 0.75, indicate dysoxic conditions; and DOP values above 0.75, indicate euxinic conditions (Raiswell et al., 1988). More recent work (Raiswell et al., 2018) has offered more sophisticated measures of reducing conditions, but these require more sophisticated analytical data. Boak and Poole (2015) highlighted the presence of Fe only in pyrite or as carbonate (Fe-dolomite, ankerite, and siderite) in the basin center, and in limited quantity in clay minerals in the margin. It therefore appears reasonable to assume that total reactive iron would be closely equivalent to total Fe, whereas pyritic Fe could be calculated assuming S was present almost entirely as pyrite. Data from Tuttle (2009) indicate that, on average, about 20% of S is present in GRF samples as organic S, the above assumption would give a maximum DOP value, which is identified as DOP*. The relationship between Fe and S values is shown in Fig. 2.13, which implies different distribution patterns of Fe and S across the basin. The overall average DOP* value in DP is lower than JS and Shell (Fig.2.9, Table 2.1). The average values from S1 to S3 in DP decrease upward, from 0.22 to 0.17 to 0.06 for S1, S2 and S3, respectively, reflecting increasingly oxic conditions in the basin margin. whereas JS and Shell show slightly different trends in the development of different lake stages, with S3 (ave. DOP*=0.56) and S4 (ave. DOP*=0.49) marking the highest average values for JS and S2 (ave. DOP*=0.56) and S3 (ave. DOP*=0.55) recording the most saline zones for Shell, respectively), and then decreasing upward. In the closed lake stage S6, DOP has the smallest values in JS (ave DOP*=0.21) and Shell (ave. DOP*=0.21).

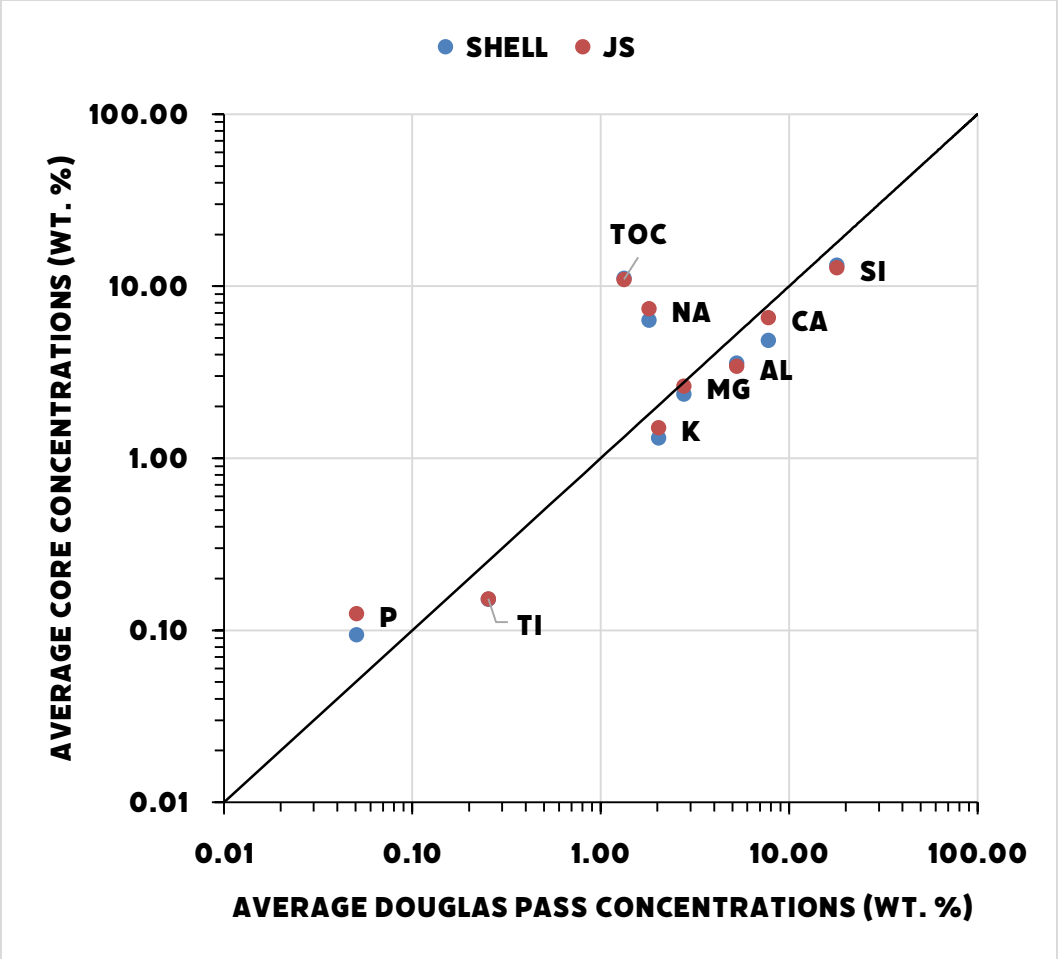



Fig. 2.8. The average concentration of selective major elements in DP, JS and Shell

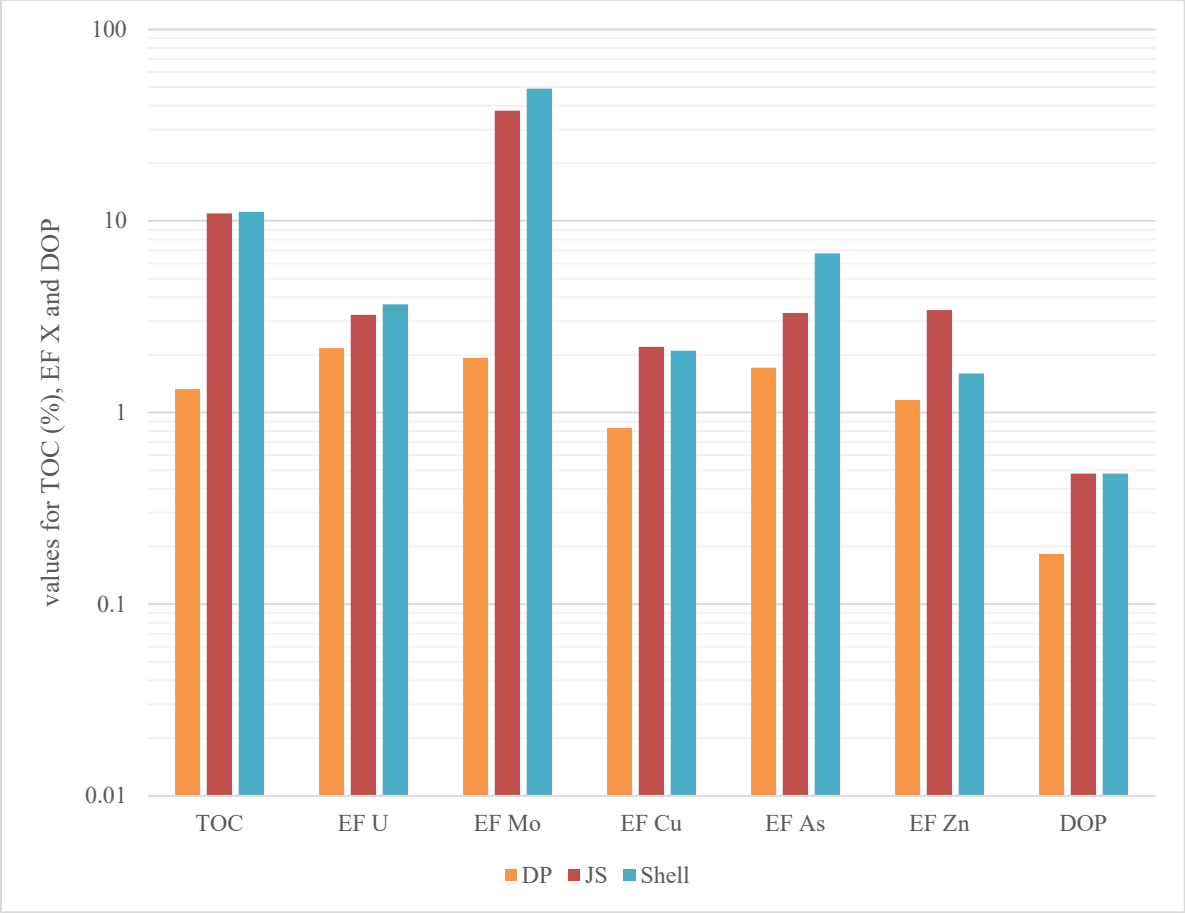



Fig.2.9. The average values of redox proxies and TOC from DP, JS and Shell, respectively, X = U, Mo, Cu, As, Zn.

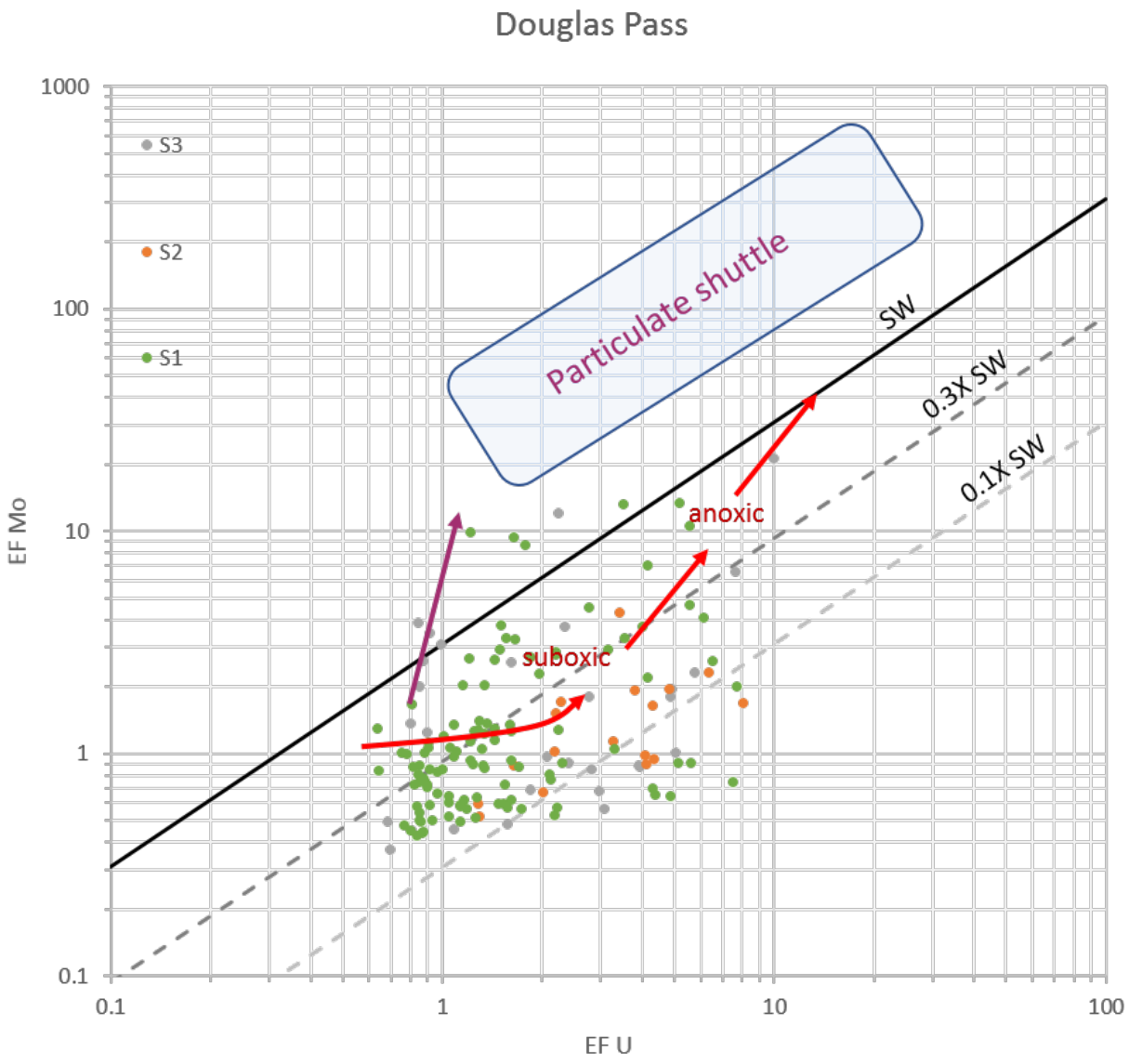



Fig. 2.10. U-EF vs. Mo-EF for Douglas Pass area (data from ICP-MS). Dotted lines show the Mo/U molar ratio (~7.5 in the Pacific region and ~ 7.9 in the Atlantic region), equal to the sea water value (1xSW) and fractions (0.1xSW, 0.3x SW) for the Black Sea.

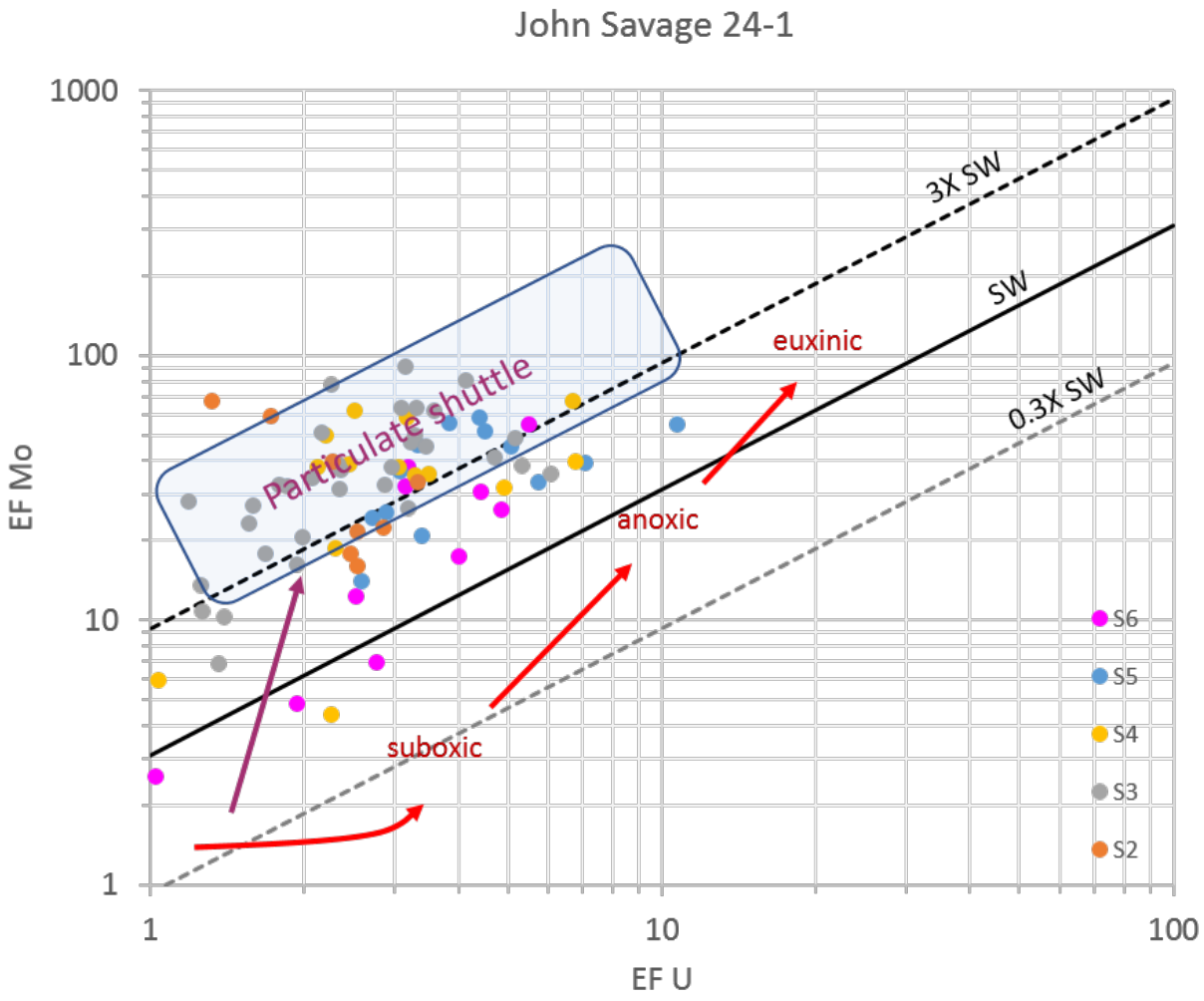



Fig. 2.11. U-EF vs. Mo-EF for core John Savage 24-1 (Data from ICP-MS); diagonal lines show Mo/U molar ratios at 0.3 time the seawater molar ratio (0.3X SW), seawater ratio (SW) and 3.0 times the seawater value (3X SW).

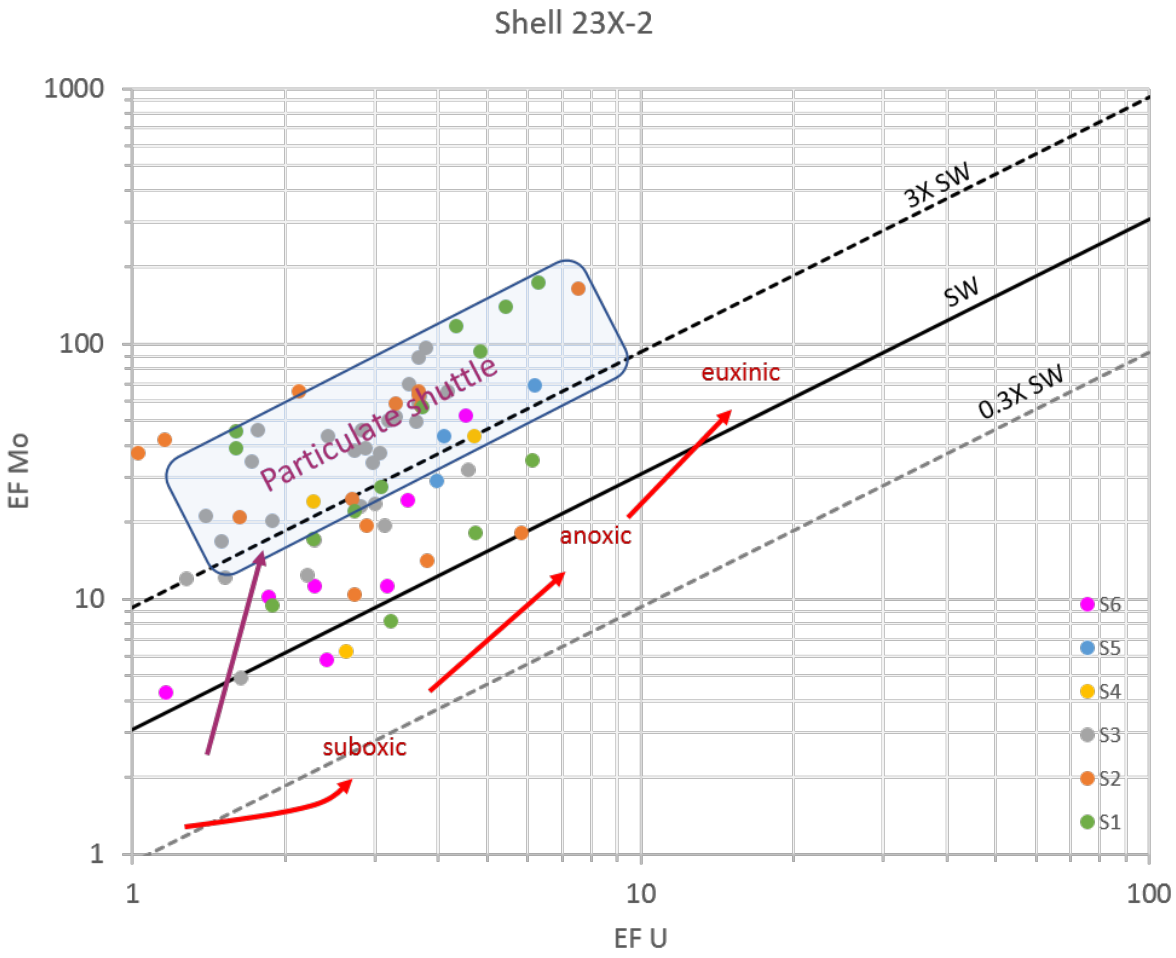



Fig. 2.12. U-EF vs. Mo-EF for core Shell 23X-2 (Data from ICP-MS); diagonal lines show Mo/U molar ratios at 0.3 time the seawater molar ratio (0.3X SW), seawater ratio (SW) and 3.0 times the seawater value (3X SW).

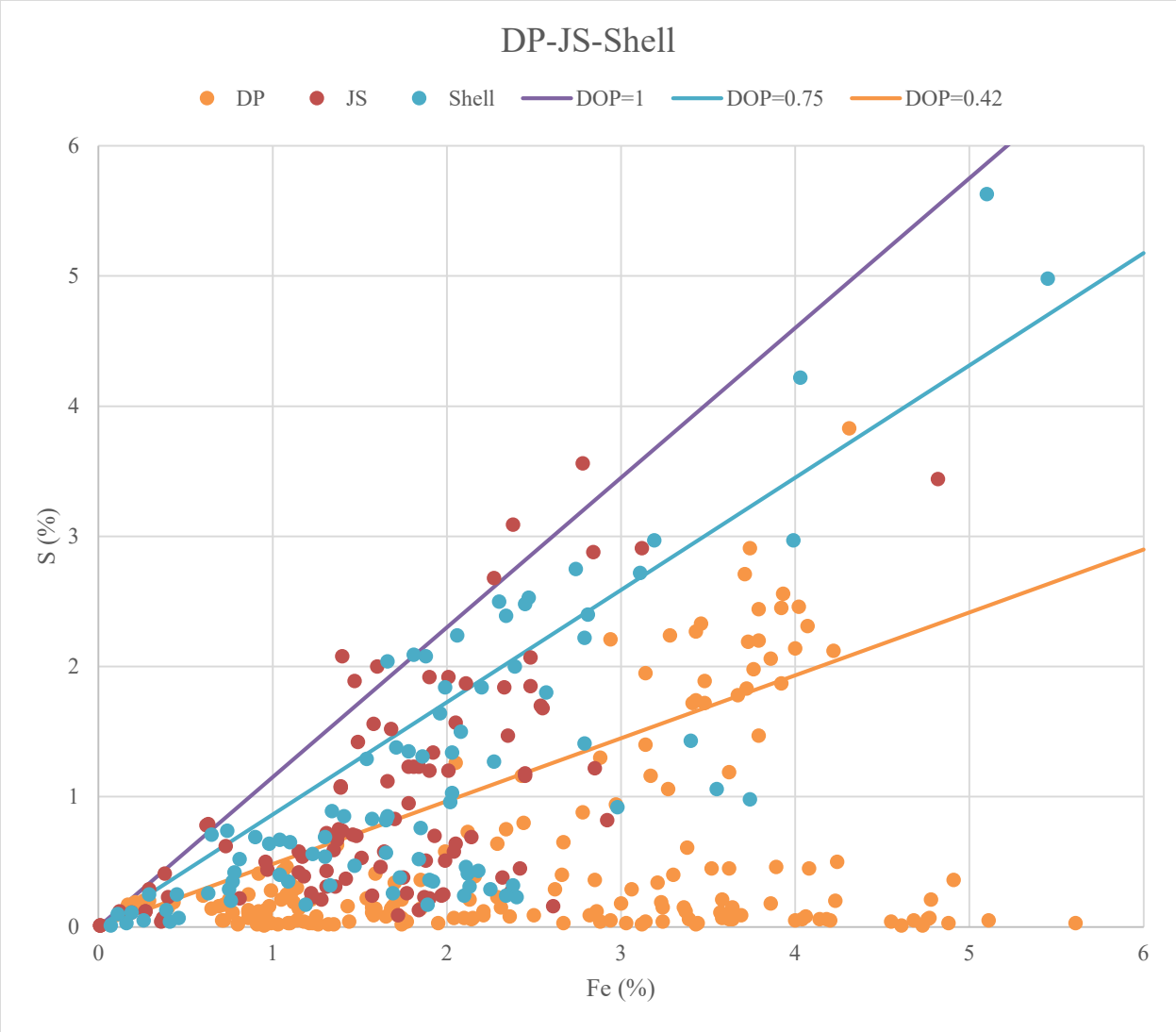



Figure 2.13. Plot of Fe vs S showing degree of pyritization (DOP) for basin margin samples and basin center samples. The lines at DOP=1 (euxinic), DOP=0.75 (anoxic/suboxic boundary), and DOP=0.42 (suboxic/oxic) are defined in Rainswell et al. (1988) and Rimmer et al. (2004).

## Discussion

### Climatic control on the clastic influx and carbonate deposition

Tectonic activities, local and regional climate variations, and changes in lake basin morphology can exert control on the deposition of lacustrine systems (Bohacs et al., 2000; Renaut and Gierlowski-Kordesch, 2010; Tänavsuu-Milkeviciene and Sarg, 2012; Tänavsuu-Milkeviciene et al., 2017). It is commonly agreed that climate-induced changes, on shorter timescales (thousands to hundreds of thousands of years), are dominant in controlling the deposition of the Green River Formation in all three lacustrine basins: the Piceance basin, the Uinta basin, and the Greater Green River basin (Picard and High, 1968; Fischer and Roberts, 1991; Cole, 1998; Smith et al., 2014). This conclusion is supported by lack of growth faults, passive fill of basins, and repetition of similar depositional sequences during the basin evolution (Tänavsuu-Milkeviciene et al.,2017). Sediment supply was mainly affected by climatic conditions on a relatively short time scale as stated by Tänavsuu-Milkeviciene et al. (2017). Therefore, variations in sediment inputs from the basin margin to basin center should give insight into the climatic changes.

As stated above, Si, Al, Ti, K proxies record the variations of the siliciclastic input in the evolution of the paleolake. Siliciclastic sediment input decreased from the basin margin to the center (Fig.2.14), as would be expected moving away from the basin margin sources toward the distal basin center. The Piceance lake evolution correlates well with the global climate reconstruction of Zachos et al. (2001, 2008) during the early to middle Eocene, according to Tänavsuu‐Milkeviciene et al (2012, 2017). During the early Eocene, sustained warming occurred and was followed by a substantial cooling trend throughout the middle Eocene (Bohaty and Zachos, 2003; Bijl et al., 2009). Stage 1 formed during the warming phase of the climate

optimum (Fig. 2.3). A change of abundant rainfall and high runoff to a somewhat more arid climate took place at the end of Stage 1. In DP, the detrital input was relatively constant and stable from S1, S2 to S3, which indicates relatively continuous sediment supply brought into the basin from abundant rainfall and high runoff in Stage 1 (Tänavsuu‐Milkeviciene et al., 2012; 2017). The high siliciclastic input into the marginal areas at the beginning of Stage 2 indicated increased seasonality and flash flood runoff. The peak of the climate optimum corresponds to Stage 3 and is marked by highly fluctuating cycles (Tänavsuu-Milkeviciene et al., 2012). Whereas in Shell and JS, the detrital flux deposited in the basin center decreased from S1 to S3, a result possibly influenced by aridity and increasing frequency of alternating wet and dry climatic conditions (Tänavsuu-Milkeviciene et al., 2012), consistent with the stratification of the lake in the depocenter. During the rising and high lake stages (Stages 4 and 5), relatively high siliciclastic inputs were observed in JS and Shell, indicating higher precipitation and increased inflow influenced by climate (Tänavsuu-Milkeviciene et al., 2012). These stages were followed by filling of the basin by the end of S6, which was largely controlled by tectonic activity that brought large amounts of siliciclastic materials to the basin (Carroll et al., 2006; Smith et al., 2008; Chetel et al., 2011). Overall, the characteristics of detrital sediment in deposition and distribution was strongly influenced by climate: in dry times, detrital input into the lake was relatively limited and focused at the margin; it increased during times of increased humidity and precipitation, which were closely related to the Early Eocene Climate Optimum (EECO) (Zachos et al., 2001; 2008; Tänavsuu-Milkeviciene et al., 2012; 2017; Smith et al., 2014).

Siliciclastic sediment input appears to decrease from the basin margin to the center (Figs.2.5-8). However, the change also reflects the dilution of both the clastic and carbonate sediments by organic matter and saline minerals in the basin center. In order to extract the detrital

flux between the basin margin and the center, the ratio of detrital input (Si, Al, K, Ti) to the sum of the detrital and carbonate input (Ca, Mg, Mn) has been made to test whether detrital input is decreased in the basin center, as shown in Fig.2.15. The variations in the ratios of clastic/clastic + carbonate fractions in the basin margin are larger and more frequent than in the basin center, because sediment sources and environments of deposition tend to shift more drastically and frequently in the shallow waters. The ratio of clastic/clastic + carbonate in different lake stages remain relatively high in the basin center, even in the most saline lake stages, S2 and S3 when the dilution of organic matter and elevated Na was removed. Thus, it confirms the previous interpretation that clastic sediment is predominant in the GRF, contrary to general descriptions suggesting that illitic Garden Gulch Member was clastic-dominated and the Parachute Creek Member was dolomitc (Dyni, 1976), and hence carbonate-dominated. In addition, during the rising lake (S4) and high lake (S5) stages, a slight decrease in the average value of this indicator is observed in Shell and JS, which might be expected as expansion of the lake starved the basin center of clastic sediment, even though clastic sediment inputs increased with cooler wetter conditions during that period. However, such inferences are fairly weak because of relatively sparser sampling of this interval. More detailed sampling is needed to fully evaluate the chemical trends that parallel those in the stratigraphic and sedimentologic record.

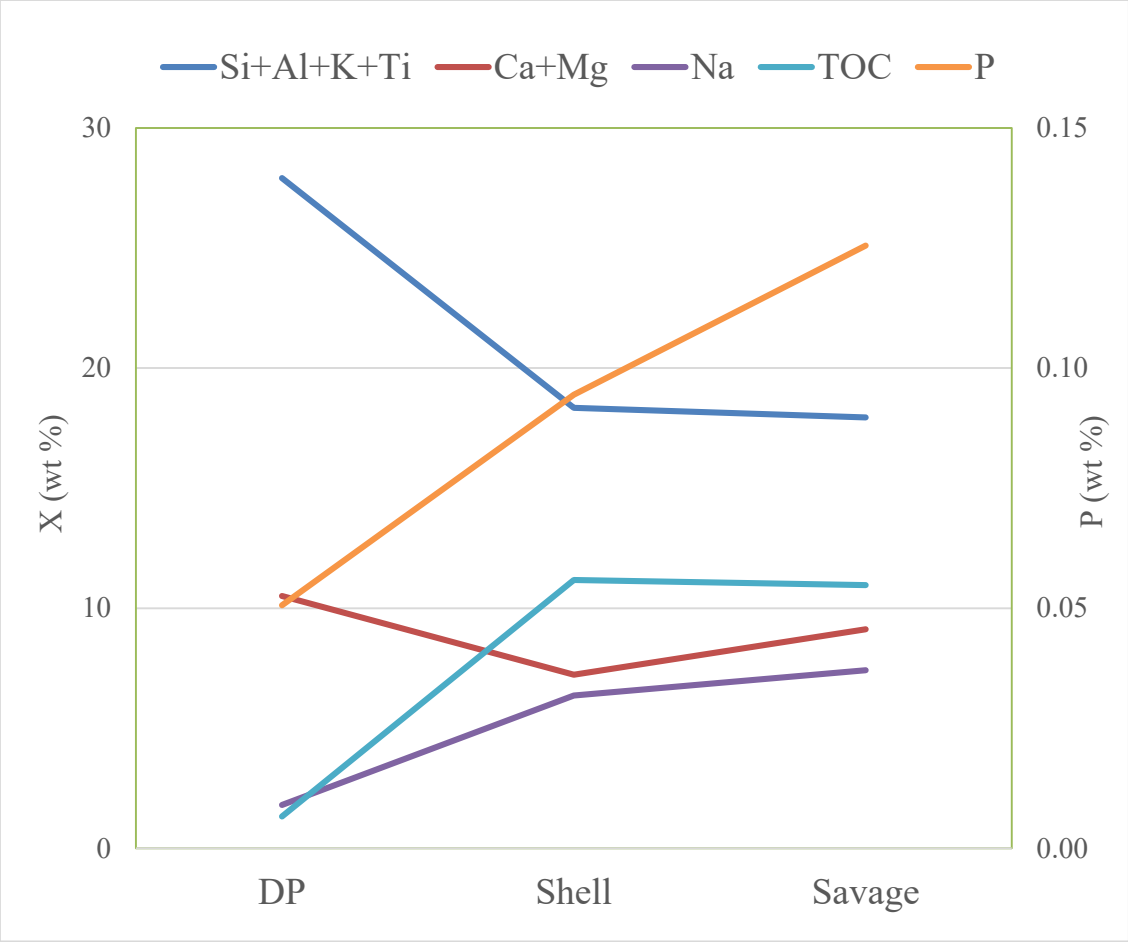



Fig. 2.14. The average values of detrital input, carbonate proxies, salinity and TOC from basin margin (DP) to center (Shell, JS). X= Si+Al+K+Ti, Ca+Mg, Na, and TOC.

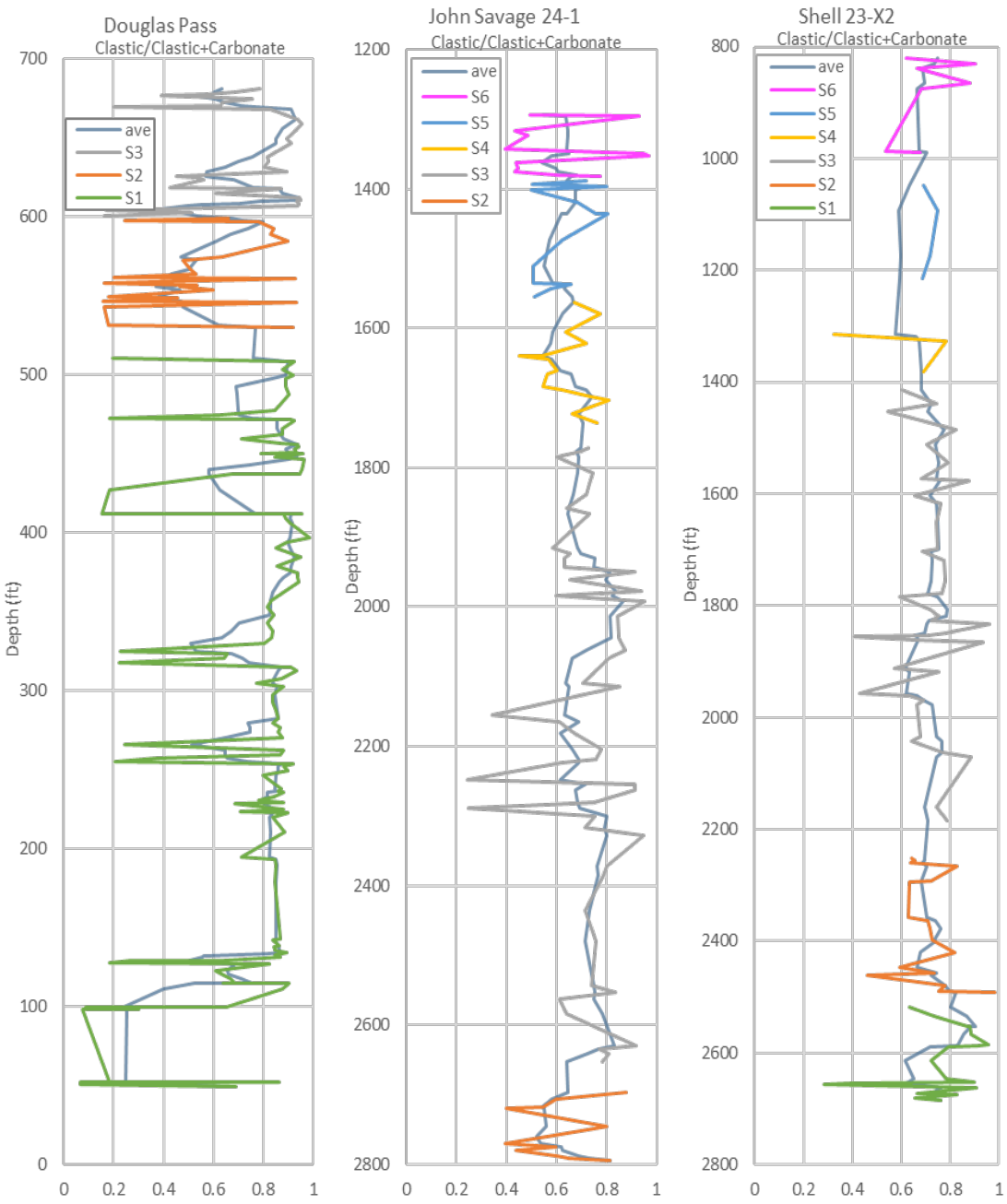



Fig.2.15. The ratio of detrital elements to detrital plus carbonate elements (Si+Al+Ti+K)/ (Si+Al+Ti+K+Ca+Mg+Mn) in Douglas Pass, John Savage 24-1, and Shell 23-X2 sections (S1 = Green line, S2 = Orange line, S3 = Grey line, S4 = Gold line, S5 = Blue line, S6 = Purple line, gray-blue line = 5-pointaverage).

Iron deficiency

Fe appears to be depleted as indicated by the cross-plot of Fe and Al (Fig.2.16). Fe/Al is low for nearly all the data regardless of the location where data were obtained, which suggests low mafic input. Similarly, period IV transition metal elements (Cu, Zn, V, Cr, Ni, Co) are also depleted compared to average shale, and only U, Mo, and As are enriched (Fig.2.17). There is a distinct difference in the behavior of two groups of common redox indicators: period IV transition metals (Cu, Zn, V, Cr, Ni, Co) show little consistent enrichment, whereas Mo shows fairly strong enrichment, and U shows some enrichment, as discussed above. As is less consistent but appears to show enrichment. These three elements are less strongly related to mafic constituents than the transition metals, and all these features imply a sparsity of mafic contributions to the source of GRF sediment. In the basin margin (DP), some carbonate-rich intervals show high Fe/Al ratios, as shown in Fig.2.16 and this feature was not observed in the basin center. However, most of these samples have very low Al values, suggesting that Fe present in these samples reflects pyrite or Fe-dolomite abundance, and is not directly related to clastic sedimentary contributions. Trace metals are closely related to delivery of detrital elements into the basin, especially period IV transition metals (Cu, Zn, V, Cr, Ni, Co), which are commonly related to iron concentration. Hence, reduced iron content from mafic sources will result in overall deficiency of those metals in sediments. This feature may explain the overall lack of enrichment of these trace metals in our study area and the limited utility of those trace metals (Cu, Zn, V, Cr, Ni, Co) in evaluating the relationships between trace metal redox proxies and total organic matter preservations in the lake development. This leaves only As, U, Mo as relatively reliable proxies. To address the issue, cluster analysis of these chemical elements, the subject of Chapter 3, will help determine the relationship between those trace metal proxies and TOC.

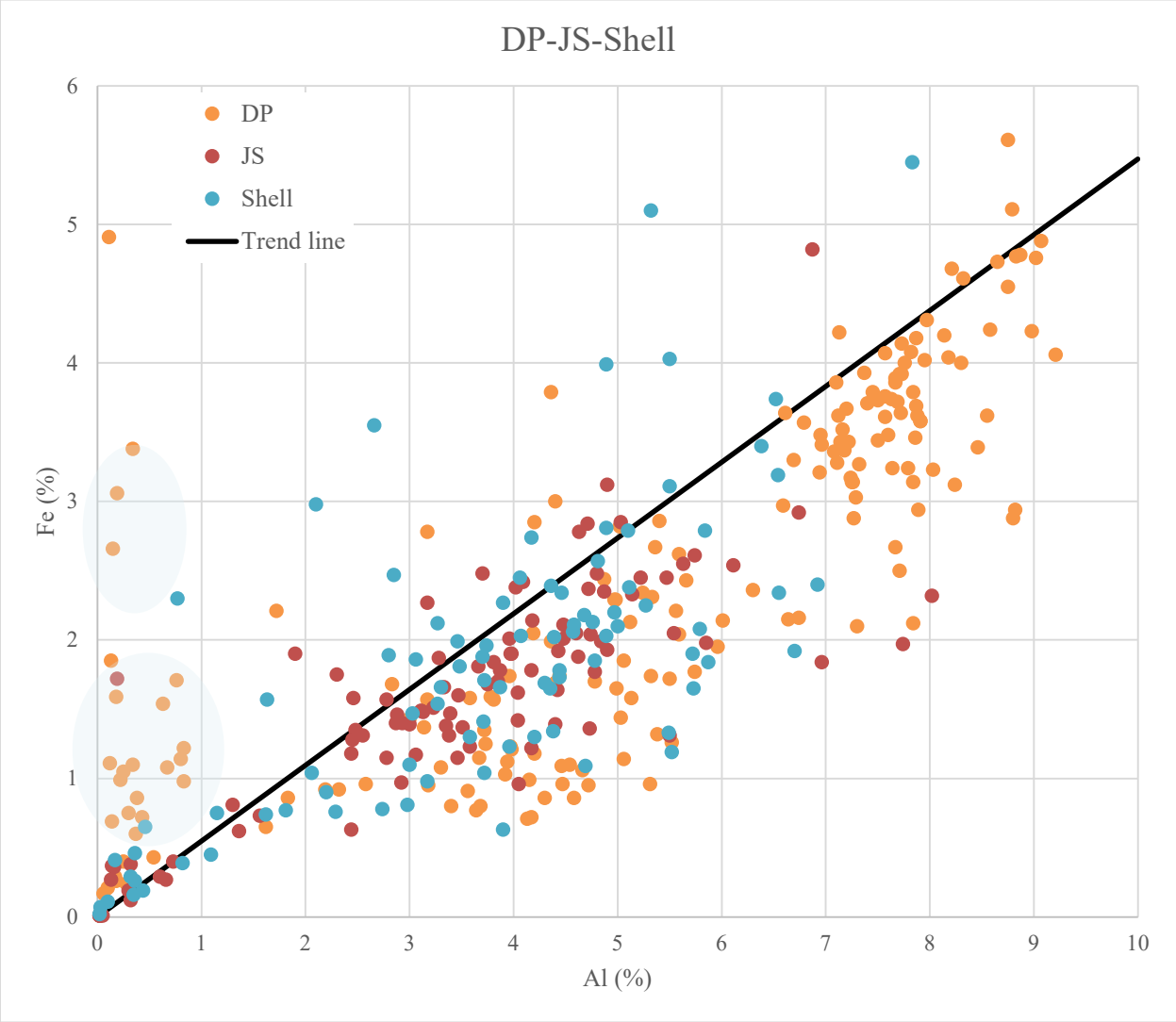



Fig. 2.16. Crossplot of Al vs Fe from basin margin (DP) to center (Shell, JS); the shaded area represents carbonate-rich samples. Trend line represents the ratio of Fe/Al for average shale from Wedepohl (1971).

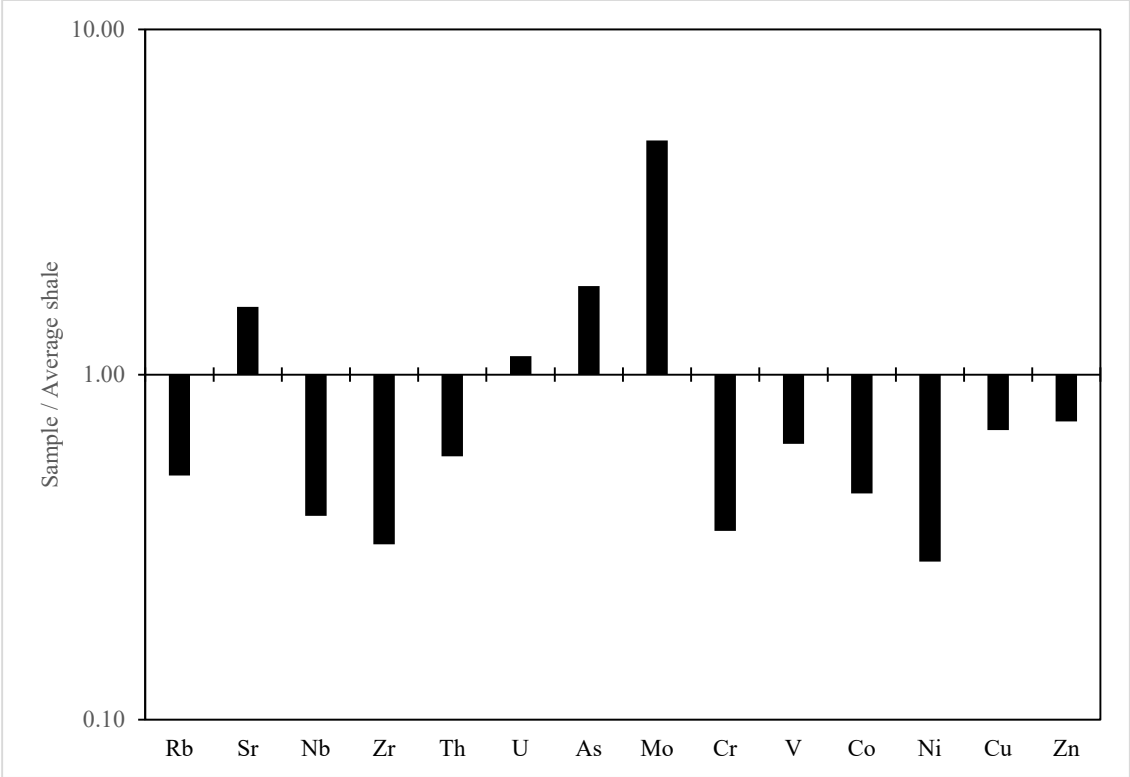



Fig.2.17. The Average Shale-normalized concentration of trace elements (Wedepohl, 1971).

Redox conditions

In this study, we integrated enrichment factors (EFs) of redox-sensitive trace metals, and degree of pyritization (DOP) to characterize the redox conditions of Lake Uinta in the Piceance basin. The basin margin and center demonstrated different redox conditions (Figs 2.9-2.12). For the basin margin, the distributions of trace metal proxies- Mo, U, As, Cu, Zn EF reflect relative changes of reducing conditions in different lake stages. However, there are no specific cut-off values derived from those EFs for evaluating reducing conditions of the lake, therefore, the cross-plot of EF U and EF Mo is used to differentiate the reducing conditions in the process of basin sedimentation, assuming that EF U-EF Mo relationships defined for marine shale systems (Algeo and Tribovillard, 2009; Tribovillard et al., 2012) can still be applied in the lacustrine system. All the data from DP, JS and Shell are plotted together on the diagram of EF U – EF Mo, which differentiates the basin margin from the basin center very clearly in reducing conditions (Fig. 2.18). As shown in Figs. 2.10 and 2.18, only a few data in S1 fall within the field indicating anoxic conditions, whereas most data fall into the oxic-suboxic region, consistent with Fe-S cross-plot in DP (Fig. 2.13) and DOP classifications of reducing conditions. The relatively higher values of DOP in S1 and S2, compared to S3 in DP, could reflect the effect of local climate change on the basin margin. In S1 and S2, nutrients were brought into the basin margin with clastic sediments by increasing runoff, promoting photosynthetic activity (Feng, 2011), which consumed oxygen in the water column. As a consequence, the conditions in S1 and S2 are somewhat more reducing than in S3, when evaporation rate was enhanced as temperature reached the peak for the EECO (Zachos et al., 2001; 2008; Tänavsuu‐Milkeviciene et al., 2012; 2017). However, the redox conditions in the basin margin vary widely, and the shallow level of the lake could more easily be affected by local environments. This would be in contrast to the basin center, where these local

effects are damped out, and redox conditions are driven by climate changes in the Eocene, the mechanism for controlling precipitation and evaporation of the lake.

For Shell and JS, the reducing conditions are similar in different stages of the lake. Stages 2 and 3 have the most reducing conditions (Table 2.1). Similar features are observed in JS and Shell: average DOP values in S2 and S3 are highest as well. However, the average DOP values in both the basin margin and basin center, are relatively low (Table 2.1), below the threshold value for anoxic or euxinic conditions (DOP >0.75) (Raiswell et al. 1988; Rimmer et al., 2004). Only S3 recorded euxinic conditions in a few samples from JS and Shell, consistent with the depletion features observed in major and trace metal elements compared to average shale. Our observation is similar to the suggestion by Boak et al. (2016) that relatively anoxic-euxinic conditions may have occurred at times beneath the sediment-water interface in the deep basin, whereas conditions above that interface may have been suboxic/dysoxic (Boak et al., 2016). Sulfur and iron concentrations in both basin margin and basin center are relatively low, which might limit the capacity of DOP as a redox indicator in our systems. Several authors note a number of complexities in interpreting redox stage from DOP (Lyons et al., 2003; Lash and Blood, 2014), such as effects of Fe/Al ratio and the Fe fraction contributed from clastic input.

Most of the data from JS and Shell cluster together and do not show sharp differences among the lake stages. Most of the data fall into a region identified by Algeo and Tribovillard (2009) as indicating the operation of a particulate shuttle, in which Fe and Mn oxyhydroxide particles formed in oxic waters scavenge Mo as they fall through the water column, and then dissolve at or near the sediment-water interface, where anoxic to euxinic conditions reduce the Fe and Mn to soluble forms. The Fe and Mn recirculate to the upper, more oxic waters, whereas the Mo is captured in the sediment by organic matter. This mechanism does not operate for U, and

therefore, the Mo/U ratio is increased by the process. Our data in the basin center has a similar EF U- EF Mo pattern to data from the Cariaco Basin listed by Algeo and Tribovillard (2009), implying dysoxic to weakly euxinic conditions in Lake Uinta, with more oxic shallow waters (Boak et al., 2016).

Overall, the variations of reducing conditions in basin margin and center (Figs. 2.9, 2.13 and 2.18) can be explained by the model of a deep, permanently stratified lake with chemical precipitation from the water column (Bradley and Eugster,1969; Desborough, 1978; Johnson, 1981, 1985; Tänavsuu-Milkeviciene et al., 2012). Redox conditions in different stages of the lake development are mainly controlled by Eocene climate changes (Zachos et al., 2001; 2008; Tänavsuu‐Milkeviciene et al., 2012; 2017; Smith et al., 2014). The relatively low values of enrichment factors of the transition metals are likely caused by depletion of mafic constituents in the sediments derived from the source rock.

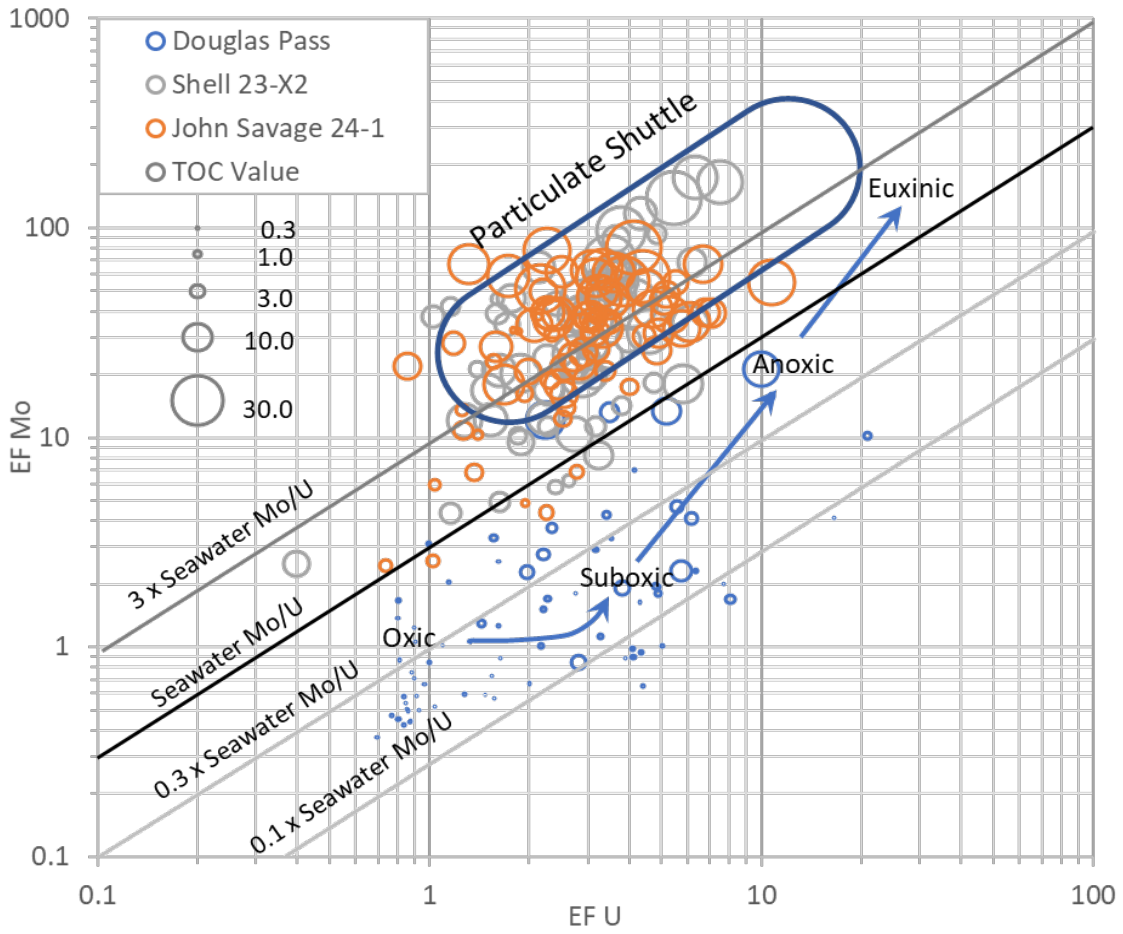



Fig.2.18. Uranium and molybdenum enrichment factor values for Douglas Pass area, John Savage 24-1 core, and Shell 23X-2 core. Oxic/Suboxic/ Anoxic/Euxinic regions from Tribovillard et al. (2012). Particulate shuttle region is explained further in the discussion section. Circle diameter is proportional to TOC.

Productivity and TOC Deposition

The distribution of Phosphorus (P) in sediments or sedimentary rocks is commonly linked to the supply of organic matter (Tribovillard et al., 2006). P is used as a productivity indicator in our study with caution, because P is soluble under anoxic conditions and can diffuse upward from the sediment to the water column (Tribovillard et al., 2006; Algeo and Ingall, 2007). As stated above, the average concentrations of P across the basin are relatively low during the lake

development in Eocene time, and the average values of P in the basin margin are lower than those in basin center, potentially reflecting productivity variations across the basin. The main source of P to the sediments includes phytoplankton necromass, plus fish scales and bones (Tribovillard et al., 2006). Fossil fish and ostracods were found in DP, at the basin margin (Tänavsuu-Milkeviciene et al.,2012; Johnson et al.,2010), representing high productivity in the margin area. However, the chemical log of P (Fig.2.5) shows concentrations of most samples throughout the margin section are below 0.2%, probably reflecting that high productivity develops in surface waters without the sediments recording any P enrichment, because P was soluble and cycling under reducing conditions. This redissolution could limit the preservation of P in the DP (Tribovillard et al., 2006).

In the basin center, the recorded relatively high P values in S4 and S5 are consistent with the observations of Feng (2011), corresponding to high clastic inputs in S4 and S5 and relatively low redox conditions as well, which indicates that high nutrients were brought into the basin center with clastic inputs by increasing runoff during these stages. Besides, elevated bioproductivities and the relatively low redox conditions reduce the reactive fraction of organic P in sediments so that high P concentrations can be preserved in the lake stages S4 and S5 (Tribovillard et al., 2006).

The deposition of total organic matter in the Piceance basin is mainly controlled by three factors: Production, Dilution and Destruction within the fourth (100k to 400kyr) and third-order sequences (~ 6myr) as explained in Feng (2011), with organic richness derived from the combination of the three factors (Bohacs, et al., 2000):

$$Organic\ Richness = \frac{Production - Destruction}{Dilution}$$

In this study, we further discuss how clastic sediments, redox condition and productivity affect TOC accumulation and preservation.

In the basin margin, the overall TOC concentrations in S1 and S2 in Fig.2.5 are very low, and correspond to low P values reflecting dilution by relatively high clastic sediment influx. The low retention of P and TOC is closely related to reducing conditions of water chemistry in the area. Organic matter was exposed to oxygenated conditions frequently in S1 and S2, experienced strong degradation, so that preservation (and therefore TOC content) was relatively low. As the lake level continued to rise in S3, more nutrients were brought in with increasing clastic input, and oxygen circulation may have decreased because of newly-formed weak stratification (Feng, 2011; Tänavsuu-Milkeviciene et al., 2012), leading to enhanced productivity, and higher TOC preservation in S3 compared to S1 and S2 in the DP area.

In the basin center, in Shell and JS, the average TOC concentrations are much higher than the basin margin and display different ranges in different stages of the paleolake. S5 records the highest TOC contents in both JS and Shell, associated with relatively high detrital sediment input, P values and relatively more reducing condition; S6 has the lowest TOC values in JS, whereas S4 and S6 record the lowest values in Shell. The low values in S4 in Shell probably reflect the very few samples taken in this zone such that a single very low sample from the L5 zone masks the real TOC distribution. The lowest TOC concentration should be in S6 rather than S4, based on the more detailed measurements of Fischer Assay in the USGS database. The relationship between phosphorous and TOC from DP, JS and Shell is shown in Fig.2.19, which shows there is little correlation between them, and indicates that preservation of TOC is not only controlled by productivity, but also reducing conditions, destruction and sediment/mineral dilution (Bohacs, et al., 2000; Feng, 2011). As shown in Fig.2.20, the EF Mo-TOC plot in JS and DP has a moderate

correlation, but has a very weak correlation in Shell, implying that the crossplot of Mo and TOC has to be used with caution, as other parameters, such as clay mineral content, salinity, and reducing condition may also have affected Mo and TOC distributions. Overall, the high TOC in the high lake stage (S5) of the basin center, indicates that productivity at that time was fairly high, reducing conditions were favorable for organic matter preservation, and dilution of clastic sediments was less than productivity, with much sediment trapped on a broad shelf at the margin. However, a complete interpretation requires a comprehensive stratigraphic, paleogeographic context and water chemistry (Eh, Ph, alkalinity and silica activity) investigation for the studied units. The deposition of TOC in the basin, mainly controlled by productivity, clastic input and redox conditions, reflects that climate change in Eocene time is dominant on a large scale.

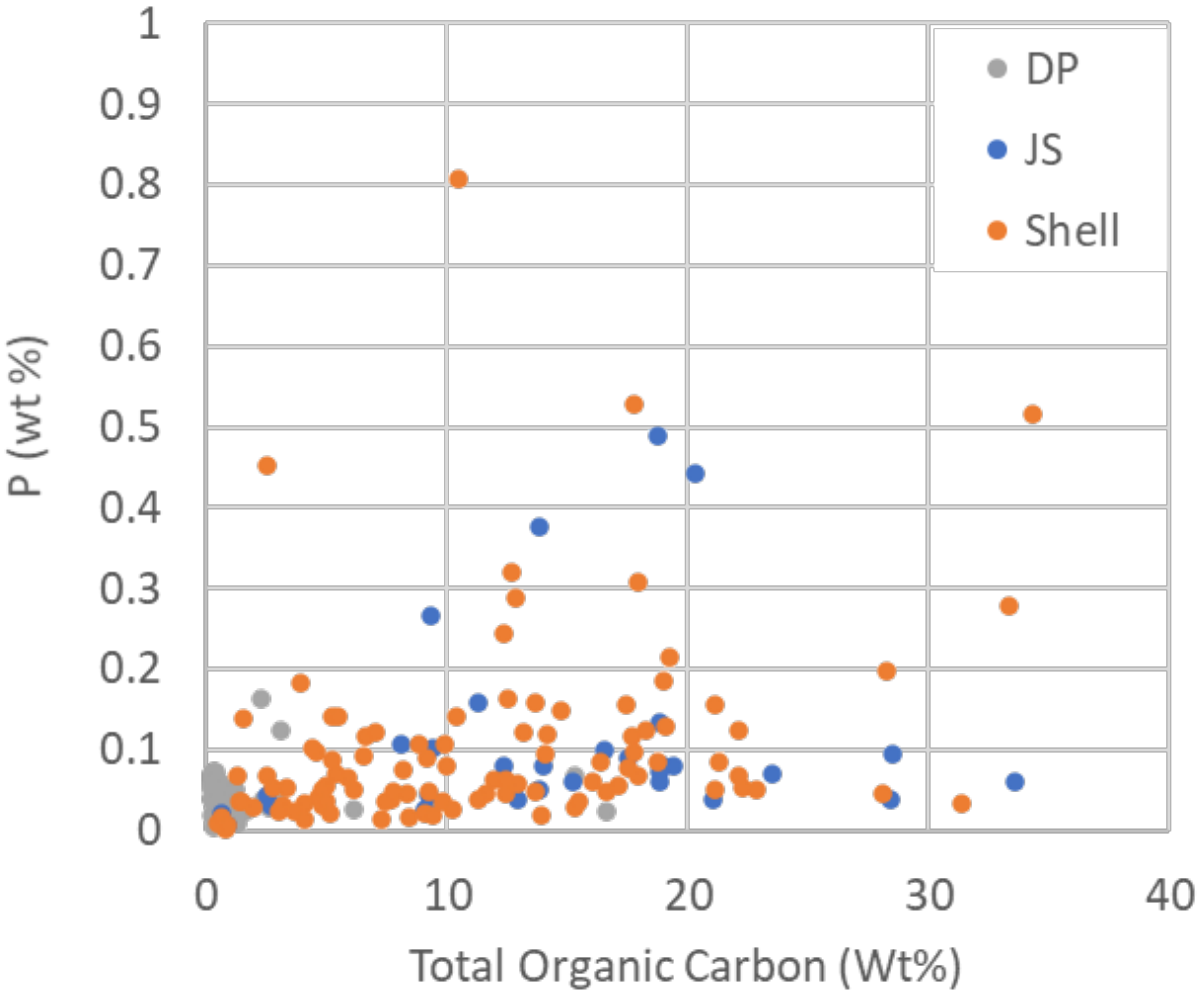



Figure 2.19. Plot of phosphorus and total organic carbon content of samples from all three sections.

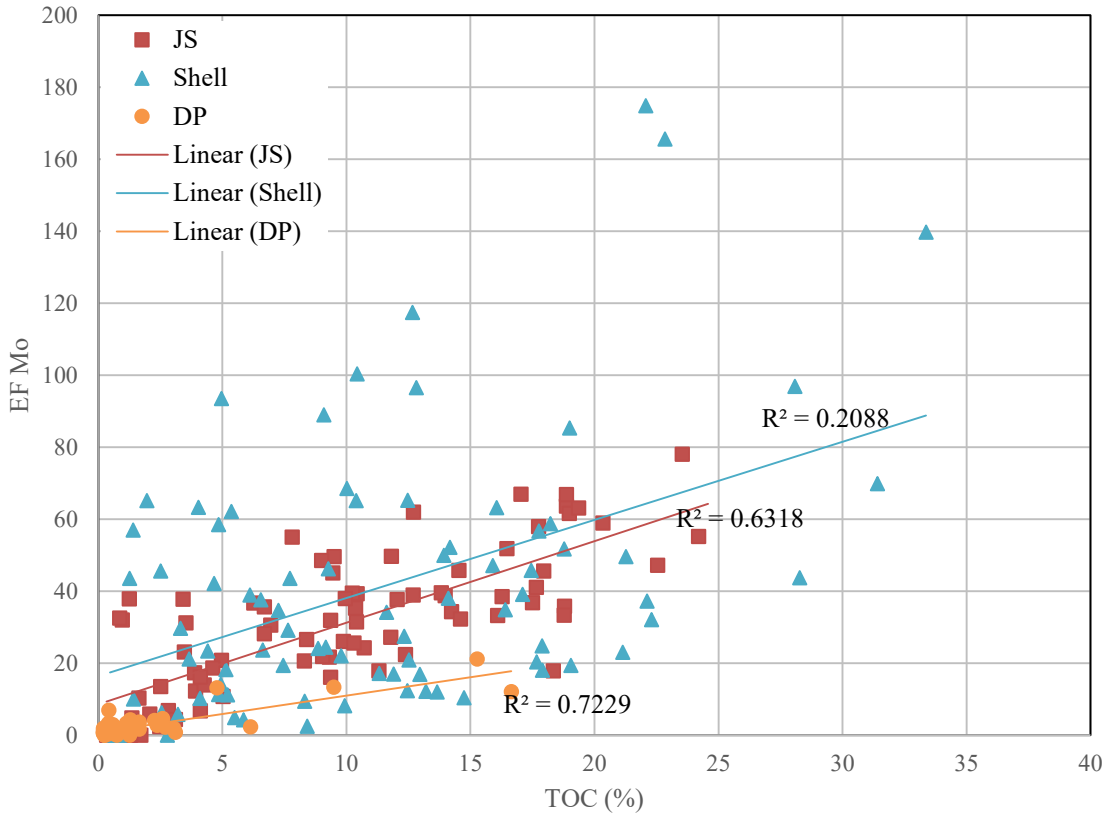



Fig. 2.20. Molybdenum enrichment factor (EF Mo) vs. TOC for samples from the basin center (JS and Shell) and basin margin (DP).

Variations in Salinity

Several paleo-salinity indicators were applied to characterize the salinity of the basin, but their features are not consistent in different stages of the basin development, regardless of the basin location. In DP, where there are higher clay mineral contents (Poole, 2014), Na concentrations are relatively low, compared to the basin center (Figs. 2.5 - 2.8). However, as shown in Table 2.1, Na concentrations in S1 are higher in DP than in the basin center (Shell), a novel finding that provides useful information about the evolution of salinity in the lake. One possible explanation is that, at the beginning of the lake expansion, S1, elevated salinity first occurred in the basin margin, because evaporative concentration is easier to achieve in the shallow basin margin than in the deep

lake, and that sodium first deposited, then redissolved in the basin margin was transported in to the basin center by saline density currents from the shallow shelf during the S1 and S2 stages. The validity of this assumption may potentially be tested by cluster analysis of salinity indicators in the basin, and will be discussed in more details in the next chapter. Later on, sodium was concentrated by extreme evaporation during the warmer, drier intervals in the basin center, resulting in formation of saline minerals in S2 and S3.

Boron incorporated in clays can be used as a paleosalinity indicator, because of its potential linear relationship with the salinity of the depositional environment (Landergren, 1958; Ye et al., 2016). B/Ga is also used as a paleosalimeter in both marine and lacustrine systems (Potter et al., 1963; Shimp et al., 1969; Chen et al., 1997; Yuri et al., 2008; Ye et al., 2016). Rb/K is as another paleosalinity proxy in mudstones, with higher Rb/K ratio in clay minerals representing higher salinity (Scheffler et al., 2003; Ocakoğlu et al., 2016; Ye et al., 2016).

In the basin margin, B data were not obtained, so we only discuss the relationship between Na and Rb/K* (representing Rb/K x $10^{-3}$), as shown in Fig.2.21. A moderate linear relationship was observed in S2 and S3, indicating that in a less saline environment, Rb/K ratio is a moderately useful indicator to gauge the saline condition of the lacustrine system. A similar relationship in S1 is complicated by the presence of a group of samples both very low in Na and high in Ca and Mg (indicating these are carbonate-rich rocks), but quite high in Rb/K*. Given that the Rb and K are interpreted as occurring in a very small amount of clay minerals, these may be indicating that Na has been reduced significantly by dilution from the carbonate fraction present. The overall correlation might be improved by recalculation on a carbonate-free basis. This serves as additional indicator, along with the analcime common to this section, that salinity was higher during this interval than earlier and, to some extent, later in the DP section. Additional basin margin sections

are needed to determine whether this saline/alkaline zone was a local feature or reflects widespread elevated salinity in the basin margin.

In the basin center, JS and Shell, Na, B/Ga and Rb/K ratios are combined to characterize the salinity trends of the paleolake. As shown in Figs. 2.21 and 2.22, JS and Shell share similar features: the most saline zones, S2 and S3 in JS and Shell, record a relative moderate positive linear relationship between Na and B/Ga ratios, but the link between Na and Rb/K* shows a weak negative trend, probably due to the breakdown of clay minerals in the saline stages. For Stages S4 to S6, the Na contents are extremely low, with average values in each stage around 2% in JS and Shell (Table 2.1). The low Na values reflect leaching of saline minerals in the upper portion of the section, as noted by (Dyni, 1996; Brownfield et al., 2010). On the other hand, in S2 and S3, a weak negative correlation exists between B/Ga and Rb/K*. One reasonable explanation for such relationships between B/Ga, Rb/K* and Na could be attributed to the mineralogic changes in different lake stages of the basin center. In S1, the fresh-brackish lake records low Na concentrations and large amount of illite, with inherited B, Ga, K, and Rb from its source regions. In the hypersaline lake stages S2 and S3, the breakdown of clay minerals releases B, Ga, K, and Rb but the Ga (which tends to occupy Al sites in minerals) and the K and Rb remain in the newly formed minerals (especially authigenic feldspar), whereas the B is transferred to the water column, and might be coprecipitated in a trace mineral at times of highest salinity (reflected in the high Na content). B/Ga and Rb/K can be used to estimate the relative paleosalinity in Piceance Basin samples to some extent, but the mineral distributions, especially the presence and concentration of clay minerals must also be considered when evaluating the salinity issue in the paleolake. Rb/K can serve as a paleosalinity indicator in sediments where clay minerals are preserved based on our study.

The salinity is mainly controlled by the balance of local precipitation and evaporation for the lake system, so the variation of salinity also reflects climate change in Eocene Epoch. The high salinity in S2 and S3 in the basin center, corresponds to low precipitation and high evaporation in more arid environments in the Eocene era, with S3 occurring at the warm, dry crest of the EECO (Zachos et al., 2001; 2008; Tänavsuu‐Milkeviciene et al., 2012; 2017; Smith et al., 2014). From S4 to S6, the climate became progressively cooler and more humid, as indicated by higher detrital sediment loads, brought by increased runoff.

The overall salinity change from the margin to the center can be summarized as follows: the appearance of elevated Na values in the basin margin (DP) at a time when Na values are lower in the basin center (Shell) suggests the possibility that evaporative concentration of Na in shallow marginal areas could have contributed to the later rise of Na in the center through formation of saline density currents. The presence of analcime is similar to results found in the Uinta Basin by Remy and Farrell (1989), who described features indicative of evaporation and potential redissolution of sodium in the margin. The subsequent evolution of salinity in the basin center is consistent with the statements of earlier researchers (Tänavsuu-Milkeviciene et al., 2012; 2017; Boak and Poole, 2015; Johnson, 1981; 1985). In S2 and S3, salinity of the lake reached its peak, with occurrences of thick saline mineral zones; In S4 and S5, salinity decreased but still remained high, as indicated by the extensive saline minerals in these intervals (commonly indicated primarily by solution cavities where nahcolite was leached long after deposition); the lake was freshening in S6 when it was filled with large amounts of clastic sediments.

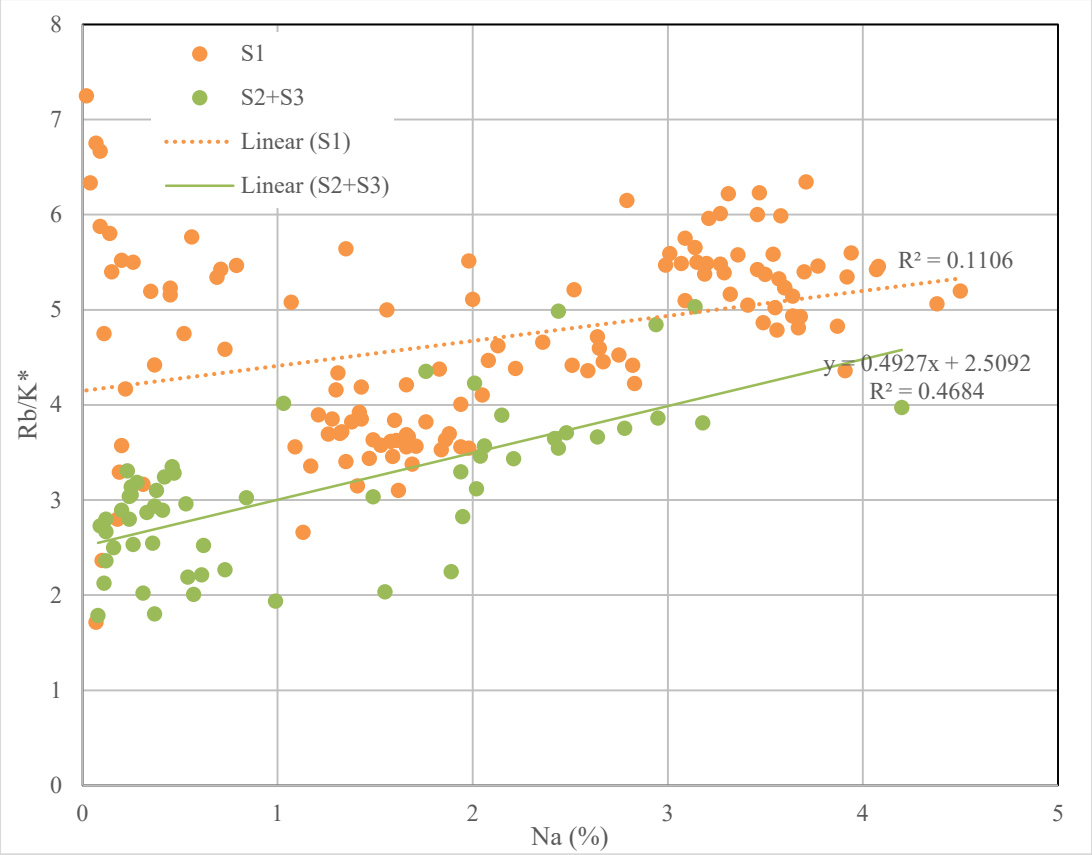



Fig. 2.21. Crossplot of Na vs. Rb/K* for samples from the basin margin (DP). Rb/K*= Rb/K x$10^3$.

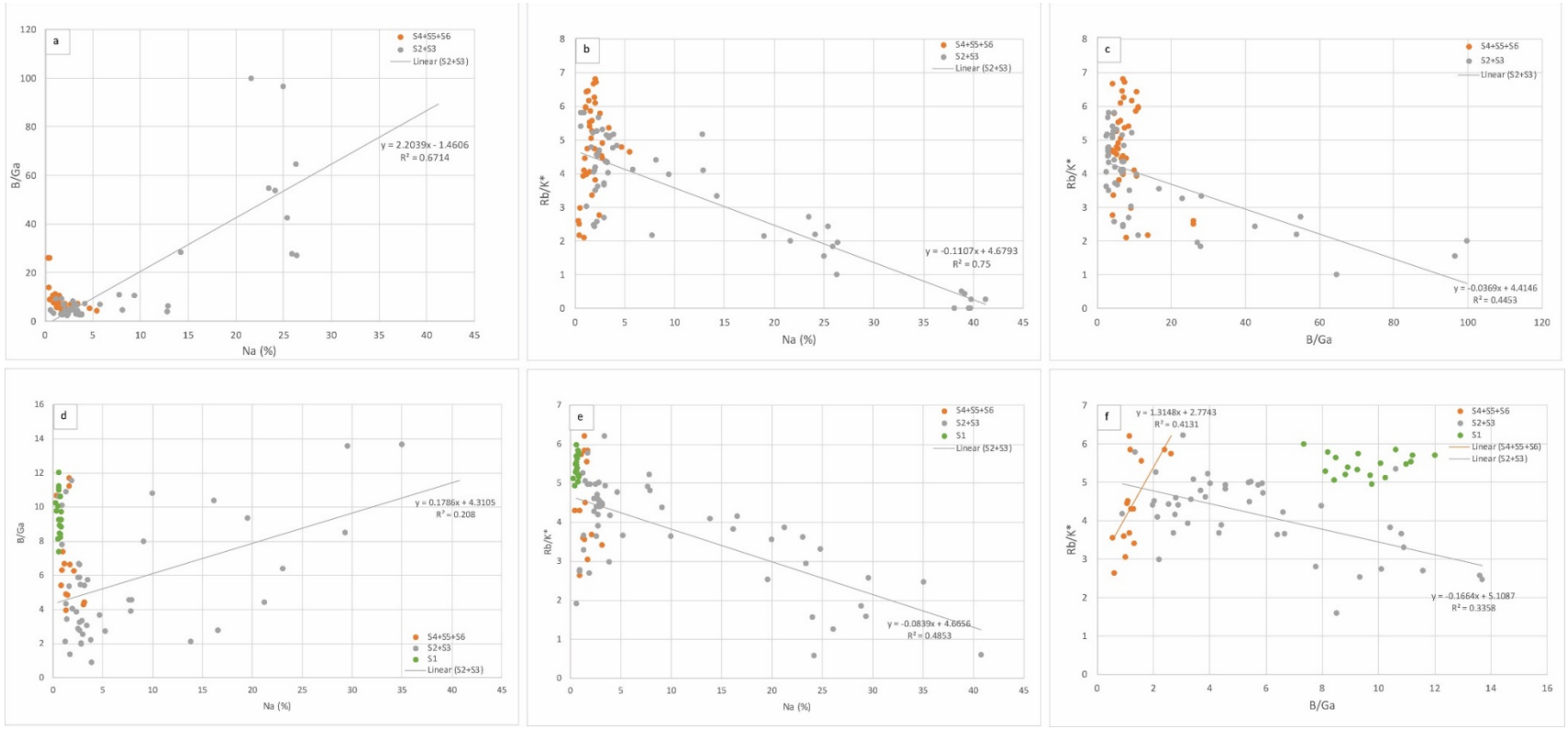



Fig. 2.22 a-f. Crossplot of Na vs B/Ga, Na vs Rb/K* and B/Ga vs Rb/K* for samples from JS and Shell in different lake stages, respectively. Rb/K*=Rb/K x $10^{-3}$. Figs. a- c are crossplots from JS and figs. d- f are crossplots from Shell.

## Conclusions

Our analysis of geochemical data from the basin margin, DP and basin center, JS and Shell unfolds the sedimentary process of the GRF in Piceance basin in the context of a stratified lake model. It helps provide new insight into the complex interactions among detrital flux, reducing conditions, paleoproductivity, organic matter accumulation and salinity across the basin.

(1) Our study demonstrates that major and trace metal elements can serve as useful proxies for clastic sediments, carbonate, reducing condition, paleoproductivity and salinity in a lacustrine system.

(2) Enrichment factors of Mo, U, As, $P_{IV}$ transition metals (Co, Ni, Cu, Zn etc), combined with DOP can be used to characterize the redox conditions of the paleolake; however, due to depletion of mafic sources, which resulted in deficiency of iron and transition metals compared to average shales, the applications of $P_{IV}$ transition metals (Co, Ni, Cu, Zn etc) as redox indicators were constrained, and only Mo, U and As clearly show enrichments under reducing conditions, because these elements are less strongly related to mafic constituents than the transition metals.

(3) We test the validity and limitation of B/Ga, Rb/K used as paleosalinity indicators in our basin, at least, when lack of sodium values, B/Ga and Rb/K can give us some insights about the salinity in the lacustrine system. The variations of clay minerals play a key role in controlling the deposition of B, Ga, Rb, and K and the reliability as paleosalinity indicators in the saline zones: when clay minerals are present, Rb/K shows a medium correlation with salinity.

(4) The appearance of elevated Na values in the basin margin (DP) at a time when Na values are lower in the basin center (Shell) suggests the possibility that evaporative concentration

of Na in shallow marginal areas could have contributed to the later rise of Na in the center through formation of saline density currents.

## Acknowledgements

We thank the Core Research Center, U.S. Geological Survey for the access to core analysis and sampling. We are grateful for the funding support from Center for Oil Shale Technology and Research, funded by Shell, ExxonMobil, and Total Petroleum, and the funding support from Oklahoma Geological Survey for field work and conference. Special thanks go to Dr. Justin Birdwell, from U.S. Geological Survey for helping us obtain the ICP data.

## References

Algeo, T.J., Ingall, E., 2007. Sedimentary Corg: P ratios, paleocean ventilation, and Phanerozoic atmospheric $pO_2$. Palaeogeography, Palaeoclimatology, Palaeoecology, 256(3-4): 130-155.

Algeo, T.J., Tribovillard, N., 2009. Environmental analysis of paleoceanographic systems based on molybdenum–uranium covariation. Chemical Geology, 268(3-4): 211-225.

Arthur, M.A., Sageman, B.B., 1994. Marine black shales: depositional mechanisms and environments of ancient deposits. Annual Review of Earth and Planetary Sciences, 22(1): 499-551.

Banner, J.L., 1995. Application of the trace element and isotope geochemistry of strontium to studies of carbonate diagenesis. Sedimentology, 42(5): 805-824.

Benitez-Nelson, C.R., 2000. The biogeochemical cycling of phosphorus in marine systems. Earth-Science Reviews, 51(1-4): 109-135.

Berner, R.A., 1984. Sedimentary pyrite formation: an update. Geochimica et cosmochimica Acta, 48(4): 605-615.

Boak, J., Poole, S., 2015. Mineralogy of the Green River Formation in the Piceance Creek Basin, Colorado, Stratigraphy and Paleolimnology of the Green River Formation, Western USA. Springer, pp. 183-209.

Boak, J., Poole, S., Feng, J., 2016. Geochemistry of the Green River Formation, Piceance Creek Basin, Colorado. in Dolan, MP, Higley, DK, and Lillis, PG, eds., Hydrocarbon Source Rocks in Unconventional Plays, Rocky Mountain Region, Rocky Mountain Association of Geologists: 295-318.

Boak, J., Poole, S., Sarg, J.F., Tänavsuu-Milkeviciene, K., 2013. Evolution of Lake Uinta as Defined by Mineralogy and Geochemistry of the Green River Formation in Colorado, Unconventional Resources Technology Conference. Society of Exploration Geophysicists, American Association of Petroleum Geologists, Society of Petroleum Engineers, pp. 1952-1961.

Bohacs, K.M., Carroll, A.R., Neal, J.E., Mankiewicz, P.J., 2000. Lake-basin type, source potential, and hydrocarbon character: an integrated sequence-stratigraphic-geochemical framework. Lake basins through space and time: AAPG Studies in Geology, 46: 3-34.

Bohacs, K.M., Grabowski Jr, G., Carroll, A.R., 2007. Lithofacies architecture and variations in expression of sequence stratigraphy within representative intervals of the Green River Formation, Greater Green River Basin, Wyoming and Colorado. *Mt. Geol.,* 44, 39-60.

Bradley, W.H., 1928. Zeolite beds in the Green River formation. Science, 67(1725): 73-74.

Bradley, W.H., 1931. Origin and microfossils of the oil shale of the Green River Formation of Colorado and Utah, U.S. Geological Survey Professional Paper 168, 58p.

Bradley, W.H., Eugster, H.P., 1969. Geochemistry and paleolimnology of the trona deposits and associated authigenic minerals of the Green River Formation of Wyoming. U.S. Geological Survey. Prof. Pap., 496-B, 71.

Brownfield, M.E., Mercier, T. J., Johnson, R C., Self, J.G., 2010. Nahcolite Resources in the Green River Formation, Piceance Basin, Colorado: U.S. Geological Survey Digital Data Series DDS-69-Y, chp. 2, 51p.

Brumsack, H.-J., 2006. The trace metal content of recent organic carbon-rich sediments: implications for Cretaceous black shale formation. Palaeogeography, Palaeoclimatology, Palaeoecology, 232(2-4): 344-361.

Calvert, S., Pedersen, T., 1993. Geochemistry of recent oxic and anoxic marine sediments: implications for the geological record. Marine geology, 113(1-2): 67-88.

Campbell, F., Lerbekmo, J., 1963. Mineralogic and chemical variations between Upper Cretaceous continental Belly River shales and marine Wapiabi shales in western Alberta, Canada. Sedimentology, 2(3): 215-226.

Campbell, F., Williams, G., 1965. Chemical composition of shales of Mannville group (lower Cretaceous) of central Alberta, Canada. AAPG Bulletin, 49(1): 81-87.

Caplan, M.L., Bustin, R.M., 1999. Palaeoceanographic controls on geochemical characteristics of organic-rich Exshaw mudrocks: role of enhanced primary production. Organic Geochemistry, 30(2-3): 161-188.

Carroll, A.R., Chetel, L.M., Smith, M.E., 2006. Feast to famine: Sediment supply control on Laramide basin fill. Geology, 34(3): 197-200.

Cashion, W.B., Donnell, J.R., 1972. Chart showing correlation of selected key units in the organic-rich sequence of the Green River Formation, Piceance Creek Basin, Colorado, and Uinta Basin, Utah. U.S. Geological Survey. Oil and Gas Investigations, Chart OC-65.

Chen, Z., Chen, Z., Zhang, W., 1997. Quaternary stratigraphy and trace-element indices of the Yangtze Delta, Eastern China, with special reference to marine transgressions. Quaternary Research, 47(2): 181-191.

Chetel, L.M. et al., 2011. Paleogeographic reconstruction of the Eocene Idaho River, North American Cordillera. Bulletin, 123(1-2): 71-88.

Clementz, M.T., Sewall, J.O., 2011. Latitudinal gradients in greenhouse seawater δ18O: evidence from Eocene sirenian tooth enamel. Science, 332(6028): 455-458.

Cole, R.D., 1998. Possible Milankovitch cycles in the Lower Parachute Creek Member of Green River Formation (Eocene), North-Central Piceance Creek Basin, Colorado: an analysis. J.K. Pitman, A.R. Carroll (Eds.), Modern & Ancient Lake Systems; New Problems and Perspectives, Utah Geological Association, Salt Lake City, United States (1998), pp. 233-259.

Cole, R.D., Picard, M.D., 1978. Comparative mineralogy of nearshore and offshore lacustrine lithofacies, Parachute Creek Member of the Green River Formation, Piceance Creek basin, Colorado, and eastern Uinta basin, Utah. Geological Society of America Bulletin, 89(10): 1441-1454.

Couch, E.L., 1971. Calculation of paleosalinities from boron and clay mineral data. AAPG Bulletin, 55(10): 1829-1837.

Dean, W.E., Arthur, M.A., 1989. Iron-sulfur-carbon relationships in organic-carbon-rich sequences I: Cretaceous Western Interior Seaway. American Journal of Science, 289(6): 708-743.

Dean, W.E., Pitman, J.K., Harrach, G.H., 1981. Geochemical and mineralogical analyses of U.S. Geological Survey oil-shale core CR-2, Piceance Creek basin, Colorado. U.S. Geological Survey open file report 81–596.

Desborough, G.A., 1978. A biogenic-chemical stratified lake model for the origin of oil shale of the Green River Formation: An alternative to the playa-lake model. Geological Society of America Bulletin, 89(7): 961-971.

Dickinson, W.R. et al., 1988. Paleogeographic and paleotectonic setting of Laramide sedimentary basins in the central Rocky Mountain region. Geological Society of America Bulletin, 100(7): 1023-1039.

Dong, T., Harris, N.B., Ayranci, K., 2018. Relative sea-level cycles and organic matter accumulation in shales of the Middle and Upper Devonian Horn River Group, northeastern British Columbia, Canada: Insights into sediment flux, redox conditions, and bioproductivity. GSA Bulletin, 130(5-6): 859-880.

Dong, T., Harris, N.B., Ayranci, K., Twemlow, C.E., Nassichuk, B.R., 2015. Porosity characteristics of the Devonian Horn River shale, Canada: Insights from lithofacies classification and shale composition. International Journal of Coal Geology, 141: 74-90.

Doyle, D.A. et al., 1998. The structure of the potassium channel: molecular basis of K+ conduction and selectivity. Science, 280(5360): 69-77.

Dyni, J.R., 1996. Sodium carbonate resources of the Green River Formation. US Geological Survey Open-File Report, 729: 39.

Dyni, J.R., 2006. Geology and Resources of Some World Oil-Shale Deposits. Scientific Investigations Report 2005-5294. US Geological Survey, Reston, VA.

Dyni, J.R., Hawkins, J.E., 1981. Lacustrine turbidites in the Green River Formation, northwestern Colorado. Geology, 9(5): 235-238.

Feng, J., 2011. Source rock characterization of the Green River oil shale, Piceance Creek Basin, Colorado, M.S thesis, Colorado School of Mines, Golden, 84p.

Fischer, A.G., Roberts, L.T., 1991. Cyclicity in the Green River formation (lacustrine Eocene) of Wyoming. Journal of Sedimentary Research, 61(7): 1146-1154.

Grabowski Jr, G.J., Pevear, D.R., 1985. Sedimentology and petrology of profundal lacustrine sediments, Mahogany zone of the Green River Formation, Piceance Creek Basin, northwest Colorado, *in* P. D. Crevello and P. M. Harris, eds., Deep water carbonates— A core workshop: SEPM Core Workshop 6, p. 386-430.

Harris, N.B., Mnich, C.A., Selby, D., Korn, D., 2013. Minor and trace element and Re–Os chemistry of the Upper Devonian Woodford Shale, Permian Basin, west Texas: insights into metal abundance and basin processes. Chemical Geology, 356: 76-93.

Hasiotis, S.T., Honey, J.G., 2000. Paleohydrologic and stratigraphic significance of crayfish burrows in continental deposits: examples from several Paleocene Laramide basins in the Rocky Mountains. Journal of Sedimentary Research, 70(1): 127-139.

Jagniecki, E.A., Lowenstein, T.K., 2015. Evaporites of the Green River Formation, Bridger and Piceance Creek Basins: deposition, diagenesis, paleobrine chemistry, and Eocene atmospheric CO 2, Stratigraphy and Paleolimnology of the Green River Formation, Western USA. Springer, pp. 277-312.

Johnson, R.C, Nichols, D.J, Hanley, J.H, 1988. Stratigraphic sections of Lower Tertiary strata and charts showing palynomorph and mollusk assemblages, Douglas Creek Arch area, Colorado and Utah: U.S. Geological Survey Miscellaneous Field Studies Map MF-1997. 2p.

Johnson, R.C., 1981. Stratigraphic evidence for a deep Eocene Lake Uinta, Piceance Creek Basin, Colorado. Geology, 9(2): 55-62.

Johnson, R.C., 1985. Early Cenozoic history of the Uinta and Piceance Creek basins, Utah and Colorado, with special reference to the development of Eocene Lake Uinta, *in* Flores, R.M., and Kaplan, S.S., eds, Cenozoic Paleogeography of the West-Central United States, Rocky Mountain Paleography Symposium 3: The Rocky Mountain Section, Society of Economic Paleontologists and Mineralogists p. 247-276.

Johnson, R.C., Mercier, T.J., Brownfield, M.E., Pantea, M.P., Self, J.G., 2010. An assessment of in-place oil shale resources in the Green River Formation, Piceance Basin, Colorado, U.S. Geological Survey Digital Data Series DDS-69-Y, pp. 187.

Katz, B., 1988. Clastic and carbonate lacustrine systems: an organic geochemical comparison (Green River Formation and East African lake sediments). Geological Society, London, Special Publications, 40(1): 81-90.

Landergren, S., 1958. On the distribution of boron on different size classes in marine clay sediments. Geologiska Föreningen i Stockholm Förhandlingar, 80(1): 104-107.

Lash, G.G., Blood, D.R., 2014. Organic matter accumulation, redox, and diagenetic history of the Marcellus Formation, southwestern Pennsylvania, Appalachian basin. Marine and Petroleum Geology, 57: 244-263.

Lyons, T.W., Werne, J.P., Hollander, D.J., Murray, R., 2003. Contrasting sulfur geochemistry and Fe/Al and Mo/Al ratios across the last oxic-to-anoxic transition in the Cariaco Basin, Venezuela. Chemical Geology, 195(1-4): 131-157.

Mason, G.M., 2007. Saline Minerals in the Green River Formation, Green River and Washakie Basins, Wyoming, 27th Oil Shale Symposium Colorado School of Mines.

Nandy, D., 2018. Dolomitization and Porosity Evolution of Middle Bakken Member, Elm Coulee Field and Facies Characterization, Chemostratigraphy and Organic-Richness of Upper Bakken Shale, Williston Basin, Ph.D Thesis, Colorado School of Mines, Golden, 186p.

Ocakoğlu, F. et al., 2016. A 2800-year multi-proxy sedimentary record of climate change from Lake Çubuk (Göynük, Bolu, NW Anatolia). The Holocene, 26(2): 205-221.

Pearce, T., Besly, B., Wray, D., Wright, D., 1999. Chemostratigraphy: a method to improve interwell correlation in barren sequences—a case study using onshore Duckmantian/Stephanian sequences (West Midlands, UK). Sedimentary Geology, 124(1-4): 197-220.

Pearce, T., Jarvis, I., 1992. Applications of geochemical data to modelling sediment dispersal patterns in distal turbidites; late Quaternary of the Madeira abyssal plain. Journal of Sedimentary Research, 62(6): 1112-1129.

Picard, M.D., High, L.R., 1968. Sedimentary cycles in the Green River Formation (Eocene), Uinta Basin, Utah. Journal of Sedimentary Research, 38(2): 378-383.

Pitman, J.K., 1996. Origin of primary and diagenetic carbonates in the lacustrine Green River Formation (Eocene), Colorado and Utah, U.S. Geological Survey Bulletin 2157, 20p.

Pitman, J.K., Fouch, T.D., Goldhaber, M.B., 1982. Depositional setting and diagenetic evolution of some Tertiary unconventional reservoir rocks, Uinta Basin, Utah. AAPG Bulletin, 66(10): 1581-1596.

Poole, S., 2014. Quantitative mineralogy and distributions of minerals of the green river formation, Piceance Creek Basin, Western Colorado, M.S. Thesis, Colorado School of Mines, Golden, 151p.

Potter, P.E., Shimp, N., Witters, J., 1963. Trace elements in marine and fresh-water argillaceous sediments. Geochimica et Cosmochimica Acta, 27(6): 669-694.

Raiswell, R., Buckley, F., Berner, R.A., Anderson, T., 1988. Degree of pyritization of iron as a paleoenvironmental indicator of bottom-water oxygenation. Journal of Sedimentary Research, 58(5): 812-819.

Raiswell, R., Hardisty, D.S., Lyons, T.W., Canfield, D.E.,Owens, J.D., Planavsky, N.J., Poulton, S.W., Reinhard, C.T., 2018. The iron paleoredox proxies: a guide to pitfalls, problems and proper practice Am. J. Sci., 318, pp. 491-526.

Ratcliffe, K., Wright, M., Spain, D., 2012. Unconventional methods for unconventional plays: using elemental data to understand shale resource plays, PESA News Resour., pp 55-60.

Remy, R.R., Ferrell, R.E., 1989. Distribution and origin of analcime in marginal lacustrine mudstones of the Green River Formation, south-central Uinta Basin, Utah. Clays and Clay minerals, 37(5): 419-432.

Renaut, R.W., Gierlowski-Kordesch, E.H., 2010, Lakes, in James, N.P., and Dalrymple, R.W., eds., Facies Models: Geological Association of Canada, IV Series,GEOtext 6, p. 541–575.

Rimmer, S.M., Thompson, J.A., Goodnight, S.A., Robl, T.L., 2004. Multiple controls on the preservation of organic matter in Devonian–Mississippian marine black shales: geochemical and petrographic evidence. Palaeogeography, Palaeoclimatology, Palaeoecology, 215(1-2): 125-154.

Ross, D.J., Bustin, R.M., 2009. Investigating the use of sedimentary geochemical proxies for paleoenvironment interpretation of thermally mature organic-rich strata: examples from the Devonian–Mississippian shales, Western Canadian Sedimentary Basin. Chemical Geology, 260(1-2): 1-19.

Rowe, H., Hughes, N., Robinson, K., 2012. The quantification and application of handheld energy-dispersive x-ray fluorescence (ED-XRF) in mudrock chemostratigraphy and geochemistry. Chemical Geology, 324: 122-131.

Rowe, H. et al., 2017. Chemostratigraphic insights into fluvio-lacustrine deposition, Yanchang Formation, Upper Triassic, Ordos Basin, China. Interpretation, 5(2): SF149-SF165.

Sageman, B.B., Lyons, T., 2003. Geochemistry of fine-grained sediments and sedimentary rocks. In Treatise on Geochemistry; Holland, H. D., Turekian, K. K., Eds.; Sediments, Diagenesis, and Sedimentary Rocks, Volume 7; Mackenzie, F. T., Series Ed. Elsevier-Pergamon, Oxford, U.K., 2003, pp 115-158.

Sarg, J.F., Suriamin, F., Tänavsuu-Milkeviciene, K., Humphrey, J.D., 2013. Lithofacies, stable isotopic composition, and stratigraphic evolution of microbial and associated carbonates, Green River Formation (Eocene), Piceance Basin, Colorado. AAPG bulletin, 97(11): 1937-1966.

Scheffler, K., Hoernes, S., Schwark, L., 2003. Global changes during Carboniferous–Permian glaciation of Gondwana: Linking polar and equatorial climate evolution by geochemical proxies. Geology, 31(7): 605-608.

Schoepfer, S.D. et al., 2015. Total organic carbon, organic phosphorus, and biogenic barium fluxes as proxies for paleomarine productivity. Earth-Science Reviews, 149: 23-52.

Shen, J. et al., 2015. Marine productivity changes during the end-Permian crisis and Early Triassic recovery. Earth-Science Reviews, 149: 136-162.

Shimp, N., Witters, J., Potter, P.E., Schleicher, J., 1969. Distinguishing marine and freshwater muds. The Journal of Geology, 77(5): 566-580.

Smith, M.E., Carroll, A.R., Scott, J.J., Singer, B.S., 2014. Early Eocene carbon isotope excursions and landscape destabilization at eccentricity minima: Green River Formation of Wyoming. Earth and Planetary Science Letters, 403: 393-406.

Smith, M.E., Carroll, A.R., Singer, B.S., 2008. Synoptic reconstruction of a major ancient lake system: Eocene Green River Formation, western United States. GSA bulletin, 120(1-2): 54-84.

Smith, M.E., Chamberlain, K., Singer, B., Carroll, A., 2010. Eocene clocks agree: Coeval 40Ar/39Ar, U-Pb, and astronomical ages from the Green River Formation. Geology, 38(6): 527-530.

Surdam, R.C., Parker, R.D., 1972. Authigenic aluminosilicate minerals in the tuffaceous rocks of the Green River Formation, Wyoming. Geological Society of America Bulletin, 83(3): 689-700.

Surdam, R.C., Stanley, K., 1980. Effects of changes in drainage-basin boundaries on sedimentation in Eocene Lakes Gosiute and Uinta of Wyoming, Utah, and Colorado. Geology, 8(3): 135-139.

Tänavsuu-Milkeviciene, K., Sarg, J.F., 2012. Evolution of an organic ‐ rich lake basin–stratigraphy, climate and tectonics: Piceance Creek basin, Eocene Green River Formation. Sedimentology, 59(6): 1735-1768.

Tänavsuu-Milkeviciene, K., Sarg, J.F., Bartov, Y., 2017. Depositional Cycles and Sequences in An Organic-Rich Lake Basin: Eocene Green River Formation, Lake Uinta, Colorado and Utah, USA. Journal of Sedimentary Research, 87(3): 210-229.

Taylor, S.R., McLennan, S.M., 1985. The continental crust: its composition and evolution, Blackwell Scientific, 312pp.

Thompson, G., 1968. Analyses of B, Ga, Rb and K in two deep-sea sediment cores; consideration of their use as paleoenvironmental indicators. Marine Geology, 6(6): 463-477.

Tribovillard, N., Algeo, T.J., Lyons, T., Riboulleau, A., 2006. Trace metals as paleoredox and paleoproductivity proxies: an update. Chemical geology, 232(1-2): 12-32.

Tribovillard, N.-P. et al., 1994. Geochemical study of organic-matter rich cycles from the Kimmeridge Clay Formation of Yorkshire (UK): productivity versus anoxia. Palaeogeography, Palaeoclimatology, Palaeoecology, 108(1-2): 165-181.

Turner, B., 2016. Utilization of chemostratigraphic proxies for generating and refining sequence stratigraphic frameworks in mudrocks and shales.

Turner, B., Tréanton, J., Slatt, R., 2016. The use of chemostratigraphy to refine ambiguous sequence stratigraphic correlations in marine mudrocks. An example from the Woodford Shale, Oklahoma, USA. Journal of the Geological Society: jgs2015-125.

Tuttle, M.L. 2009, A collection of chemical, mineralogical, and stable isotopic compositional data for Green River oil shale from depositional center cores in Colorado, Utah, and Wyoming: U.S. Geological Survey Open-File Report 2009–1274, 18 p.

Ver Straeten, C.A., Brett, C.E., Sageman, B.B., 2011. Mudrock sequence stratigraphy: a multi-proxy (sedimentological, paleobiological and geochemical) approach, Devonian Appalachian Basin. Palaeogeography, Palaeoclimatology, Palaeoecology, 304(1-2): 54-73.

Wedepohl, K., 1991. The composition of the upper earth's crust and the natural cycles of selected metals. Metals in natural raw materials. Natural Resources. In: Merian, E.(Ed.), Metals and Their Compounds in the Environment. VCH, Weinheim: 3-17.

Ye, C., Yang, Y., Fang, X., Zhang, W., 2016. Late Eocene clay boron-derived paleosalinity in the Qaidam Basin and its implications for regional tectonics and climate. Sedimentary geology, 346: 49-59.

Young, R.G., 1995b. Stratigraphy of Green River Formation in Piceance Creek Basin, Colorado, *in* Averett, W.R., ed., The Green River Formation in Piceance Creek and Eastern Uinta Basin, Field Trip Guidebook, 1-13.

Young, R.G., 1995a. Structural controls of the Piceance Creek Basin, Colorado, *in* Averett, W.R., ed., The Green River Formation in Piceance Creek and Eastern Uinta Basin, Field Guidebook, 23-29.

Yuri, Z.N., Eder, V., Zamirailova, A., 2008. Composition and formation environments of the Upper Jurassic–Lower Cretaceous black shale Bazhenov Formation (the central part of the West Siberian Basin). Marine and Petroleum Geology, 25(3): 289-306.

Zachos, J., Pagani, M., Sloan, L., Thomas, E., Billups, K., 2001. Trends, rhythms, and aberrations in global climate 65 Ma to present. science, 292(5517): 686-693.

Zachos, J.C., Dickens, G.R., Zeebe, R.E., 2008. An early Cenozoic perspective on greenhouse warming and carbon-cycle dynamics. Nature, 451(7176): 279.

# Chapter 3: Quantitative Analysis of the Green River Formation, Piceance Basin, Northwest Colorado

Tengfei Wu[1], Jeremy Boak[2], Justin E. Birdwell[3]

1. School of Geosciences, University of Oklahoma
2. Hurricane Peak Geosciences, Littleton, CO
3. U.S. Geological Survey, Denver

## Abstract

Hierarchical cluster analysis (HCA) was applied to a geochemical data set representing the Eocene Green River Formation in Piceance Basin to identify chemofacies in core and outcrop samples from the basin margin and the basin center. Inductively coupled plasma optical emission spectroscopy and mass spectrometry (ICP-OES/MS) and total organic carbon (TOC) content analyses were applied to 186 marginal outcrop and 190 basin center core samples. TOC values and twenty-five major and trace elements were used as variables to define statistical clusters of samples for each dataset and the overall dataset by HCA applying Euclidean Distance and Ward's Method algorithms. In the basin margin, five chemofacies were identified, highlighting geochemical variability within the stratigraphic section for Douglas Pass. The two stratigraphic classifications in the basin margin are discussed, which provides a different perspective to evaluate the sedimentary process of the margin area. In the basin center, five mostly similar chemofacies were determined by HCA for each of the two sets of core data reflecting the different geochemical properties from those identified in the basin margin. The chemofacies highlight modest relative enrichments or depletions compared to population mean values for most major and minor elements, but more substantial differences for trace elements. The shared chemofacies for the core

datasets have the following features: 1) high Ca, Mg, Sr and Mn; 2) high Si, Al, K, Ti, Zr, Nb; 3) high TOC, As and Mo; 4) high Na, with depletion of all other elements. These chemofacies correspond to carbonate-rich, highly siliciclastic, high redox potential and high salinity facies, respectively.

Combining the outcrop and core data, a basin-wide geochemical framework is obtained, with five chemofacies: 1) high Si, Al, Ti, K, P with low Ca, Mg, Sr, Mo, TOC; 2) high Ca, Mg, Sr, Mn with moderate enrichment in Si, K, P; 3) high Ca, Mg, Sr, Mn with low Si, Al, Ti, Fe, TOC; 4) high TOC, S, As, Mo, Cu with moderate Si, Al, Fe; 5) high Na and depletion of all other elements. Chemofacies 1 and 3 are dominant at the basin margin section and chemofacies 4 and 5 are dominant in the basin center, with chemofacies 2 being present across the basin, indicating distinct depositional conditions across the basin in terms of siliciclastic input, carbonate precipitation, redox conditions, salinity and organic matter productivity and preservation. The distinctions between the basin margin and the basin center provides further evidence supporting the stratified deep lake model and expanding our understanding Lake Uinta's history in the Piceance Basin. The close relationship of redox sensitive elements with TOC is identified, with especially As, U and Mo standing out in the lacustrine system. The early timing of saline conditions in the basin margin observed in the chemofacies log, further confirms our observation in the individual geochemical logs of the previous chapter.

## Introduction

The Eocene Green River Formation (GRF) in the Piceance Basin of Colorado is the richest oil shale deposit in the world (Dyni, 2006; Johnson et al., 2010) with over 350 billion barrels of

retort oil resource in place for oil shale capable of generating at least 25 gallons of oil per ton of rock by Fischer assay (Birdwell et al., 2013). The GRF in Colorado, Utah and Wyoming has received recurring attention from oil companies over the last 75 years due to its resource potential, particularly when the oil price has been high due mainly to production shortfalls from traditional petroleum resources or supply interruptions driven by geopolitical turmoil. As a consequence, geoscientists have conducted extensive study of the formation (Bradley, 1928; Smith and Milton, 1966; Surdam and Parker, 1972; Cole and Picard, 1978; Dean et al., 1981; Remy and Ferrell, 1989; Dyni, 1996; Pitman, 1996; Mason, 2007; Tuttle, 2009; Jagniecki and Lowenstein, 2015). Many previous studies have examined the geochemistry, mineralogy, source rock quality and sequence stratigraphy of the GRF (Dean et al., 1981; Katz, 1995; Feng, 2011; Tuttle, 2009; Johnson, 1985; Poole, 2014; Boak et al., 2016; Tänavsuu-Milkeviciene and Sarg, 2012; Johnson et al., 2018; Birdwell et al., 2019). Here, we have examined chemofacies in the GRF using Hierarchical Cluster Analysis (HCA) applied to major and trace element concentrations of oil shales sampled from outcrop and core to better understand variation in conditions over the history of paleo-Lake Uinta in the Piceance Basin. Particularly we seek to link chemofacies variability across the basin to lake history models developed based on stratigraphic, geochemical/mineralogical and Fischer assay studies conducted over the last 40 years, which are key to understanding how the depositional environment changed over the ~7 Ma history of lacustrine deposition in the Piceance Basin during the Eocene.

HCA is a widely applied data clustering method in Earth Sciences (Davis, 1986; Cloutier et al., 2008) and is often used in the classification of hydrogeochemical datasets (Steinhorst and Williams, 1985; Schot and van der Wal, 1992; Güler et al., 2002). Recently, the application of HCA to shale inorganic properties has been demonstrated to be a useful tool for identifying non-

obvious groupings and trends in large geochemical datasets (Turner et al., 2016; Offurum, 2016; Galvis-Portilla, 2017). HCA is a unique way of visualizing or analyzing each sample as an assemblage of a large set of properties and grouping samples based on their overall degree of similarity to other samples in the population (Phillips, 1991). The newly-formed clusters can be considered to be chemically distinct units or chemofacies (Offurum, 2016). Combined with other geochemical and mineralogical trends and observations and the well-developed stratigraphic framework for the GRF in the Piceance Basin (Cashion and Donnell, 1972; Johnson, 1985; Johnson et al., 2010; Tänavsuu-Milkeviciene and Sarg, 2012), the HCA chemofacies can be used to help interpret changing depositional and diagenetic conditions in the lake. In addition, the difference in chemofacies between the basin margin and the basin center likely reflect variations in detrital input, carbonate precipitation, saline mineral formation, organic matter deposition and redox conditions across the lake at different lake history stages. The chemofacies analysis can therefore provide insights into paleogeographic and stratigraphic trends noted in recent studies of organic matter and mineral distributions in the Piceance Basin (Johnson et al., 2018; Birdwell et al., 2019). In addition, the chemofacies features identified from the basin margin and the basin center may reinforce characteristics that are not obvious to extract from individual geochemical logs as described in Boak et al (2021). In the following sections, we discuss how the chemofacies analysis was conducted and how it aids in refining our understanding of the sedimentary history of Lake Uinta, the depositional environment of the Piceance Basin, and how mineral distributions relate to the chemofacies during lake development in the Eocene Epoch.

## Stratigraphy and Geologic Setting

The GRF in the Piceance Basin in the basin center is mainly composed of the Garden Gulch Member and the Parachute Creek Member, which intertongue with the fluvial Wasatch Formation below and the fluvial and volcaniclastic Uinta Formation above, as shown in Fig.1 (Cashion and Donnell, 1972; 1974). The Garden Gulch Member is a clay-mineral rich oil shale unit, overlain by the Parachute Creek Member, which consists of dolomitic-feldspathic and saline-mineral rich oil shale zones. This shift in mineralogy at around the R2 zone has been attributed to diagenetic alteration of clay minerals to form authigenic feldspars, dawsonite, and analcime (Poole, 2014; Boak and Poole, 2015). These oil shale units grade into marginal lacustrine rocks of the Douglas Creek Member on the western margin of the basin, and the Anvil Points Member on the eastern margin (Fig.3.1) (Suriamin, 2010; Johnson et al., 2010). The GRF in the Piceance Basin is about 3000 feet thick near the center of the basin, and around 700 ft thick in the basin margin, at the Douglas Pass outcrop (Johnson et al., 2010; Tänavsuu-Milkeviciene and Sarg, 2012). Green River oil shale-bearing strata have been divided into alternating layers of kerogen-rich zones (R-zones) with high oil yield based on Fischer assay analysis, and kerogen-poor or lean zones (L-zones) with lower Fischer assay yields (Cashion and Donnell, 1972). Rich and Lean zones are laterally continuous, forming approximately chronostratigraphic units, and many of them are correlative across both the Uinta and Piceance Basins (Smith, 1983; Johnson et al., 2010). These rich and lean zones start at the top of the Long Point Bed (Johnson, 1984) and terminate at the top of the Parachute Creek member with the R8 zone, a unit that contains interbedded fluvial-volcanic and oil shale beds (Dyni, 2008; Johnson et al., 2010; Tänavsuu-Milkeviciene and Sarg, 2012). The Garden Gulch Member consists of the R0 through the L1 zones and the Parachute Creek Member contains the R2 through R8 zones (Dyni, 2008; Johnson et al., 2010).

Several scales of stratigraphic cyclicity have been observed in this lacustrine system, from kilometers to meters thick, or in a hierarchy from formation and member scale to sequence-set, sequence, and parasequence scales (Bohacs et al., 2000). Two scales of stratigraphic cyclicity are recognized: fourth order sequences on the order of 100-400 ky in time length, and a third order sequence, over a period of 5 Myr, during the deposition of the GRF lacustrine sediments between *ca* 53 and *ca* 48 Ma (Smith et al., 2008; 2010). Tänavsuu-Milkeviciene and Sarg (2012) identify six evolutionary lake stages recognized by integration of facies association analysis, depositional trends, and gamma ray and Fischer assay data expanding on the similar five stage model of Johnson (1985). The six lake stages are: Stage 1, early brackish lake, R0 through R1; Stage 2, transitional lake, L1 through L3; Stage 3, highly fluctuating lake, R4 through L5; Stage 4, rising lake R6 and L6; Stage 5, high lake, R7 (Mahogany zone); Stage 6, closing lake, A-groove through R8. Stage 1 formed prior to the Early Eocene Climate Optimum (EECO). Stage 2 formed as a saline-restricted lake at the beginning of the Eocene climate optimum and then was followed by a highly fluctuating lake, Stage 3, during the peak of the EECO, indicating rapid climate changes. After the climate optimum, Stages 4, a rising lake and 5 a stable high stand developed, respectively, as the climate became more humid. Stage 6, marked the closing of the lake, which was caused by increased clastic sediment input from the north due to the influence of both climate change and volcanic/tectonic activity (Johnson et al., 2019). Oil shale deposition first ended in the northern part of the basin, and then ceased farther south as the lake in Piceance Basin was infilled by the Uinta Formation clastic sediments (Tänavsuu-Milkeviciene and Sarg, 2010; 2012; Johnson et al., 2019). The stage boundaries for the basin margin section only extend to the B-groove (or "L6", which precedes the Mahogany zone) and differ from those defined by Tänavsuu-Milkeviciene and Sarg (2010; 2012), based on recent reinterpretation (Birdwell et al., 2019).

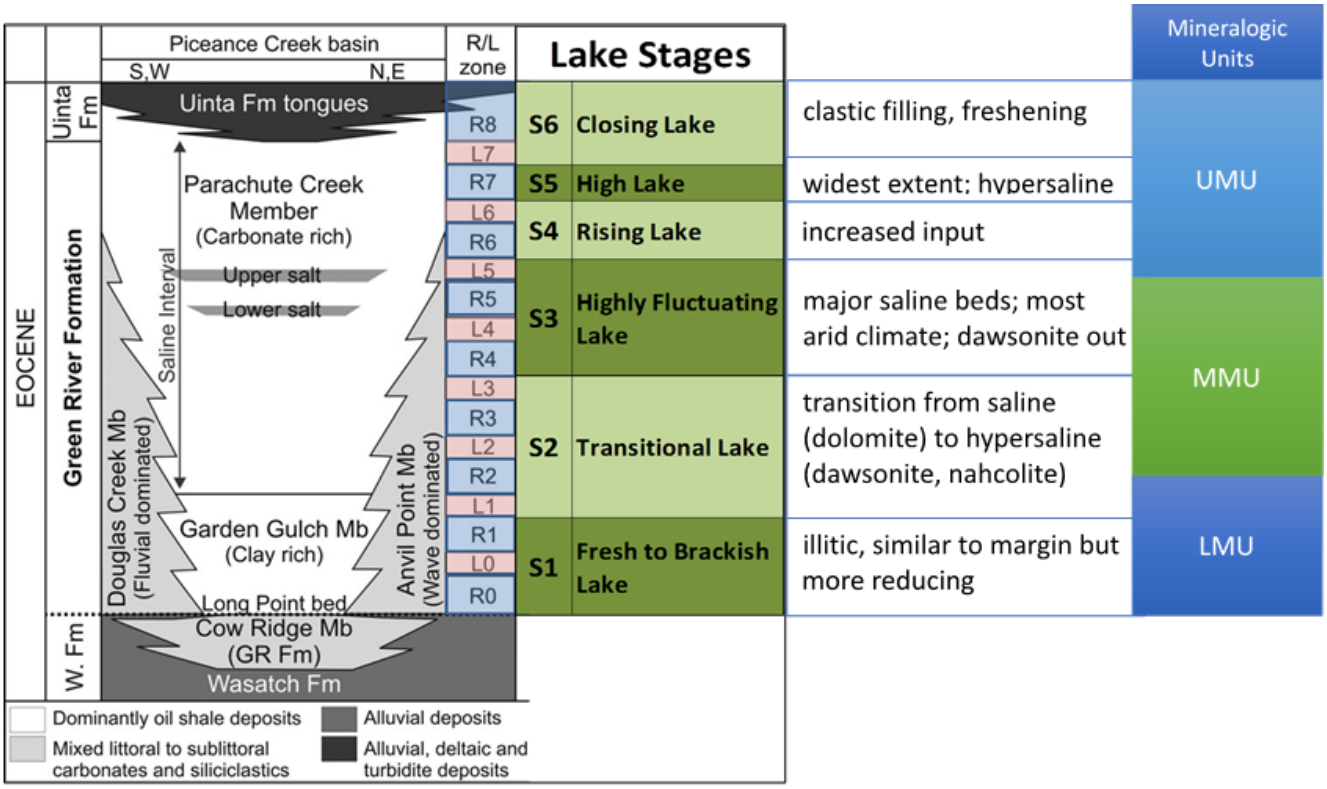



**Figure 3.1.** Stratigraphy of the Eocene Green River Formation, rich and lean oil shale zones (Cashion and Donnell, 1972, 1974), Lake Stages of Tänavsuu-Milkeviciene and Sarg (2012), and mineralogic units defined in Boak et al. (2013).

## Materials and Methods

### Sample Information

Samples representative of the basin margins were collected from an outcrop section at Douglas Pass in Garfield County, Colorado (abbreviated DP; n = 186; collected along Hwy 139 from 39°35'54.06"N, 108°49'3.00"W to 39°35'49.44"N, 108°48'22.14"W). Basin center samples were taken from three cores housed at the U.S. Geological Survey Core Research Center (CRC) in Denver, CO for this study: Shell 23X-2 (also referred to as Shell; n = 100; located at 39°54'19.7"N 108°21'44.1"W, CRC no. C042), John Savage 24-1 (abbreviated JS; n = 90; located at 39°57'18.6"N 108°20'01.4"W, USGS Core Research Center no. B801). Locations of the outcrop

and core holes are shown in Fig. 2. The Shell 23X-2 well is located in the depocenter of the basin and the interval is 1,919 ft thick, recording the complete depositional history of the formation. The core was sampled and analyzed carefully where lithofacies changes or distinctive sedimentary structures were observed (Tänavsuu-Milkeviciene and Sarg, 2012). The John Savage 24-1 well is located in the depocenter as well, is 1,504 ft thick and has well-preserved saline mineral zones, but pure halite intervals were not sampled for analysis.

Geochemical Analyses

The core and outcrop samples were analyzed by AGAT Laboratories (Calgary, Alberta, Canada) under a USGS contract using methods developed by the USGS Minerals Resources Program (USGS MRP, 2019a). This study focuses on data obtained for the DP, Shell and JS samples using Method 18 for sixty elements by Inductively Coupled Plasma-Optical Emission Spectroscopy-Mass Spectroscopy (ICP-OES-MS) with preparation using a sodium peroxide fusion (ICP-60). In this process, samples (0.5 g crushed to -200 mesh) are fused at 750°C with sodium peroxide and the fusion cake is dissolved in a dilute nitric acid. The resulting solution is analyzed by ICP. Data are deemed acceptable if recovery of each element is ± 15% at five times the Lower Limit of Determination (LOD) and the calculated Relative Standard Deviation (RSD) of duplicate samples is no greater than 15%. Detailed information on the ICP analytical protocols is presented by Harris et al. (2013) and Dong et al. (2015). After the analysis, all the results obtained from samples pass through two levels of data validation by AGAT and USGS reviewers. These procedures are available online (USGS MRP, 2019a). USGS geochemical reference materials (GRMs) SCO-1, SGR-1b, SBC-1 and ShBOQ-1 were analyzed as blinds for quality control purposes (USGS MRP, 2019b).

Total organic carbon (TOC) content was determined by the USGS Petroleum Geochemistry Research Laboratory (Denver, CO) using the LECO method (Jarvie, 1991). Samples were analyzed for TOC and total carbon content using a LECO$^{TM}$ C744 Carbon Analyzer following the manufacturer's instructions. TOC was determined after carbonate removal using 6M hydrochloric acid and rinsing with deionized water. Blanks, manufacturer's calibration standards, USGS shale GRMs and internal laboratory check standards were run for quality control purposes.

Data Analysis Methods

Cluster analysis is a multivariate statistical approach used to sort data plotted in multidimensional space based on the degree of similarity between each individual datum and its neighboring "clusters" (Güler et al., 2002). The application of Hierarchical Cluster Analysis (HCA) can provide new insight into geochemical data and extract significant information from large datasets. The traditional approach has involved treating each sample variable (each element and TOC measurement value) as a one-dimensional characteristic, whereas HCA treats each sample as an assemblage of the elements (Phillips, 1991). The purpose of HCA is to create relatively independent clusters by maximizing the distances between clusters and minimizing distances within particular clusters. The analysis begins with each sample or variable, assigns these samples or variables to a cluster, and agglomerates them in a hierarchy of larger and larger clusters until finally a single cluster contains all the samples or variables. This is typically displayed graphically as a dendrogram. When the identified clusters are linked with different elements, geological features can be identified and classified accordingly, based on elemental correlations and known geochemical relationships (e.g., mineralogical associations). Chemofacies, defined as clusters of samples with similar chemistry can then be defined to

summarize and represent geochemical variability within stratigraphic successions based on the HCA results (Turner, 2016). The defined chemofacies are expected to reveal non-obvious information and associations that would not be apparent when viewing elemental profiles separately (Nance and Rowe, 2015; Turner, 2016; Boak et al., 2021). When performing HCA, two key variables need to be considered: (1) how the cluster's centroid should be defined; and (2) how distances should be measured between data and centroids. In this study, *Euclidean distance* and *Ward's linkage method* (Ward, 1963; Turner and Closs, 2009) were selected based on their prior success in similar geological statistical applications (Güler et al., 2002, Turner et al., 2016). These methods are shown schematically in Figs. 3.3 and 3.4.

HCA was applied to the individual data collections for the DP, JS, and Shell sample sets using the Minitab® 18 software package (Minitab LLC, State College, PA). Geological interpretation of the output clusters is based on an elemental enrichment/depletion ratio computed for each cluster. We used the approach developed by Phillips (1991) to calculate enrichment ratios (ER), in which the average concentration of each element in each cluster is divided by the average concentration of each element in the total sample set. Each cluster can then be characterized by specific elemental enrichments (ER > 1) or depletions (ER < 1) as illustrated in a colored-graded matrix (Galvis-Portilla, 2017). The advantage of using this matrix of enrichment/depletion ratios is that it facilitates and simplifies identification of elemental enrichments or depletions in each cluster, and these features are then used to describe the chemofacies.

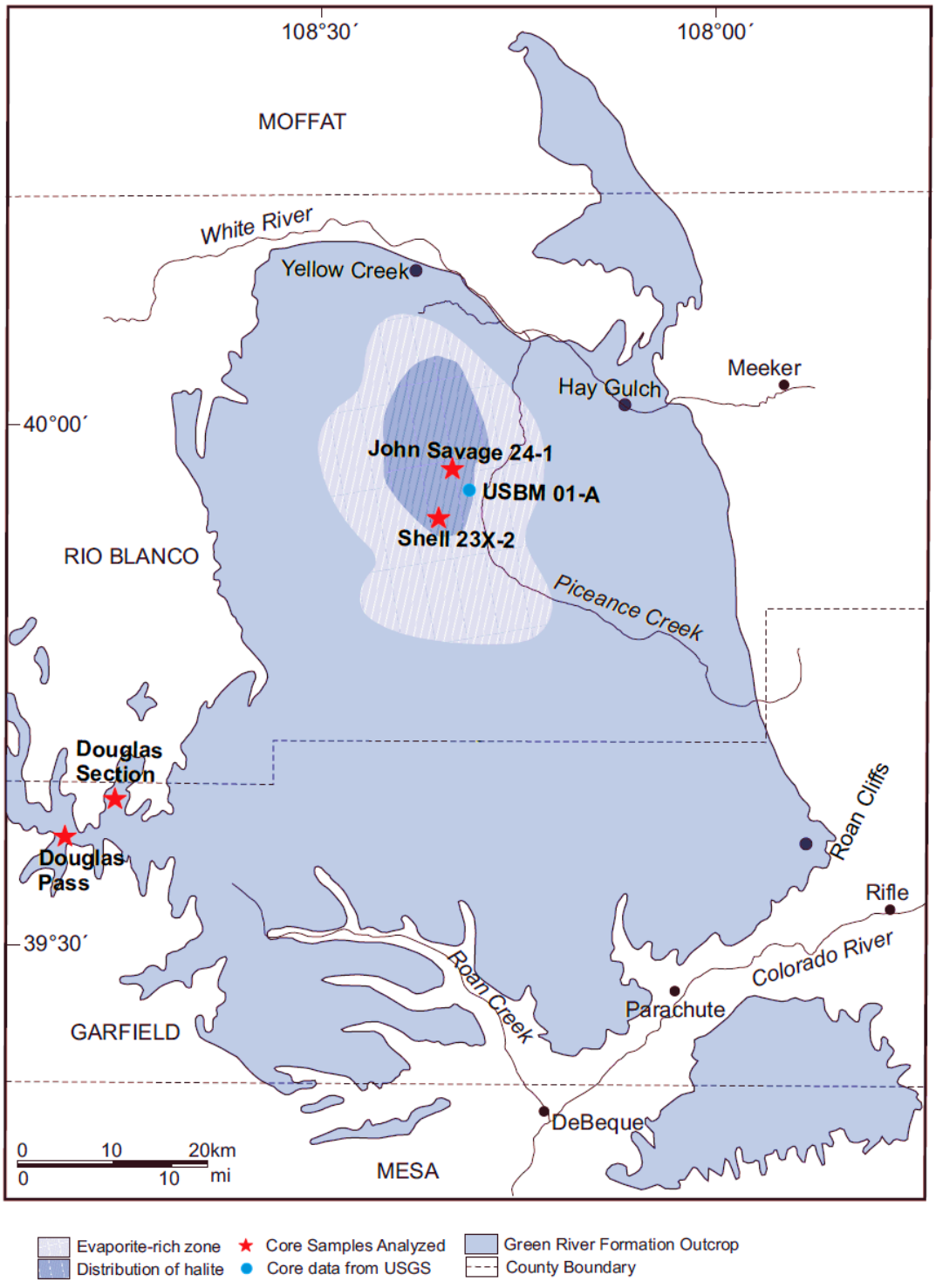



**Figure 3.2.** Map of Piceance Creek Basin with outcrop and well locations. Shaded area in the northern part of the basin indicates area with bedded evaporite deposits in basin depocenter (modified after Dyni, 1996 and Tänavsuu-Milkeviciene and Sarg, 2012).

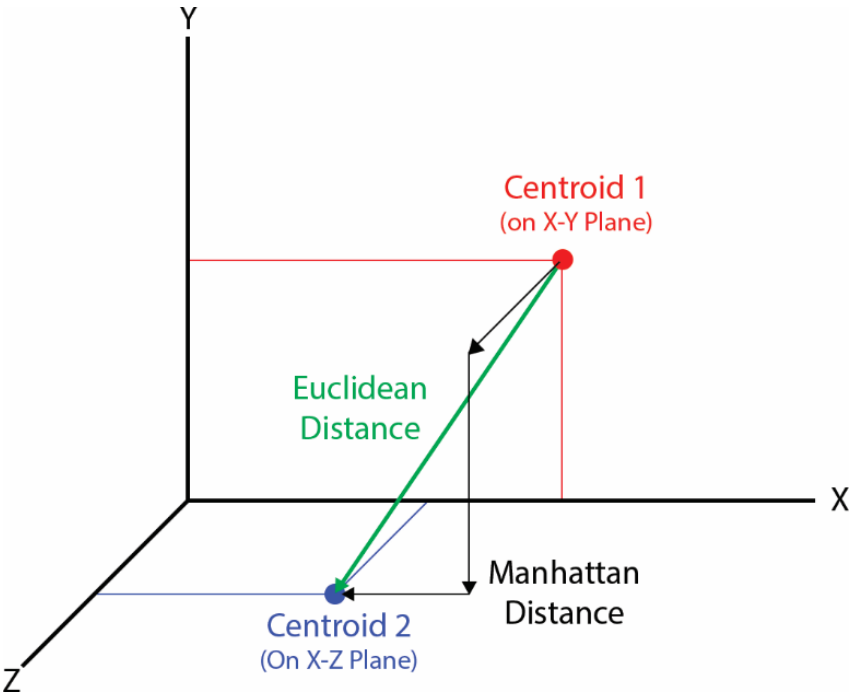



**Figure 3.3.** Difference Between Euclidean Distances and Manhattan Distances. This example is simplified to three variables (X, Y, and Z). Euclidean distances (green) are simply measured along the shortest direct route between centroids. Manhattan distances (black) are measured along a single variable at a time (After Turner and Closs, 2009, Modified from Turner, 2016).

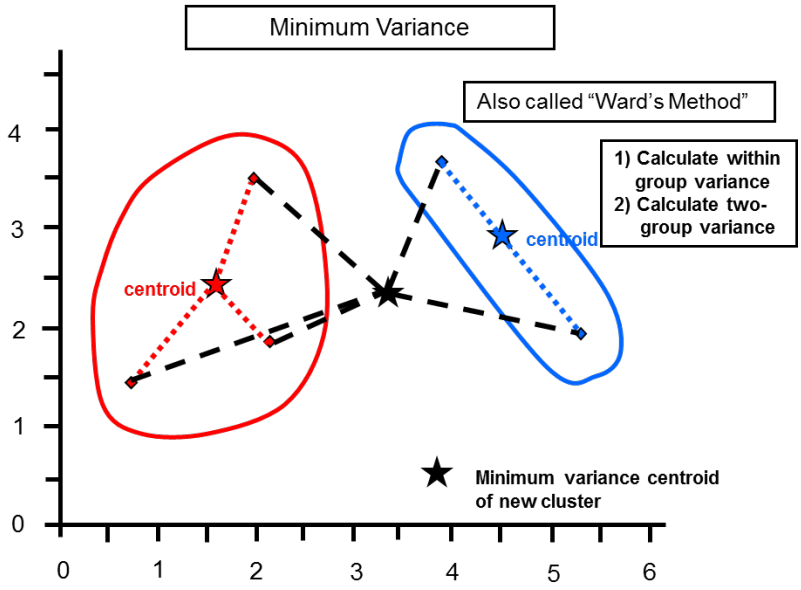



**Figure 3.4.** Schematic Illustrating Distances Using Ward's Method (Ward, 1963). This simplified example uses only two variables. From Turner and Cloos, 2009.

## Results

Chemofacies derived from the integration of DP, JS and Shell

To facilitate a meaningful comparison of the similarities and differences between the samples in these datasets, data from the DP, Shell, and JS were combined and analyzed by HCA, generating a set of five chemofacies (Table 3.1; Fig. 3.5). This analysis can be used to elucidate facies relationships across the basin as depositional conditions and sedimentary processes in the lake changed over the course of the Eocene.

A suite of 25 major and trace elements and the TOC concentrations were compiled and analyzed by HCA, derived from 376 samples, based on their consistent abundance in the sample sets and their known relevance to assessing geochemical and mineralogical features in lacustrine and marine sedimentary rocks. To determine the chemofacies (CF) type, average concentrations each of the elements in the clusters are compared to the average concentration of the sum of that element in the full dataset using the following equation (Phillips, 1991):

*Enrichment ratio (ER) = Avg. conc. of element X in cluster/ Avg. conc. of element X from all samples in the study area*

The enrichment or depletion of certain elements in the clusters are then used to identify chemofacies.

A variety of techniques are available to determine the number of clusters in a data set (Ketchen and Shook, 1996). For this study, the Elbow Method was applied to determine the ideal number of clusters, combined with K-Means algorithm, which is one of the most popular and simplest clustering methods (Ng, 2012; Kodinariya and Makwana, 2013). These results are summarized in Table 3.1 and Figure 3.5. The geochemical features of the chemofacies from the combined (COM) dataset are compared to the sample suite average in the following:

COM-1 is enriched in Si, Al, Ti, K, and P, shows enrichment of Fe, S, and Period IV transition metals (V, Cr, Co, Ni, Cu, Zn – hereafter referred to as $P_{IV}$ transition metals) but is depleted with respect to Mo, As and U. The cluster is depleted in Ca, Mg, Sr, Na, and TOC. It represents siliciclastic sediment, including sandstone deposited in a reducing environment with little organic matter preserved.

COM-2 is moderately enriched in Ca, Mg, Sr, and Mn with near average Si, Al, Ti, K, and P content, and it is depleted in Fe, S, $P_{IV}$ transition metals, As, Mo, and U, and Na. It represents slightly carbonate enriched mudstone formed in relatively oxidizing conditions, with moderate amounts of organic matter preserved.

COM-3, the smallest cluster, is strongly enriched in Ca, Mg, Sr and Mn and it is depleted in Fe, S, $P_{IV}$ transition metals, Na, and TOC, while As, Mo and U are close to average values of the whole formation. It represents carbonate sediment deposited under the most oxic conditions of any chemofacies, with little organic matter deposited or preserved.

COM-4 is the chemofacies most enriched in TOC as well as S, As, Mo, U and $P_{IV}$ transition metals, with moderate enrichment in Fe, but has approximately average Si, Al, Ti, and K, and is depleted in Ca, Mg, Sr, Mn, and Na. It represents mudstone with the highest organic content deposited under reducing conditions.

COM-5 is strongly enriched in Na, and very strongly depleted in all other elements. It represents saline evaporitic sedimentary rock deposited under hypersaline conditions exclusively in the basin center.

Table 3.1. Matrix of average elemental enrichment ratios (ER - enrichment or depletion ratio compared to the average concentration of that element in the whole dataset) by cluster in the combined dataset. The color gradient of this matrix ranges vertically across each cluster based on variations of ER among elements. Note: N= number, ave= average.

| Variable | ave of all | #1 ave | #1 ER | #2 ave | #2 ER | #3 ave | #3 ER | #4 ave | #4 ER | #5 ave | #5 ER |
|---|---|---|---|---|---|---|---|---|---|---|---|
| Si, wt% | 15.47 | 21.29 | 1.38 | 16.25 | 1.05 | 6.32 | 0.41 | 16.78 | 1.08 | 2.14 | 0.14 |
| Al, wt% | 4.37 | 7.65 | 1.75 | 3.92 | 0.90 | 0.39 | 0.09 | 4.76 | 1.09 | 0.43 | 0.10 |
| Ti, wt% | 0.19 | 0.34 | 1.84 | 0.16 | 0.89 | 0.01 | 0.07 | 0.19 | 1.01 | 0.02 | 0.08 |
| K, wt% | 1.72 | 2.59 | 1.50 | 1.80 | 1.04 | 0.17 | 0.10 | 1.80 | 1.05 | 0.30 | 0.18 |
| Fe, wt% | 2.11 | 3.53 | 1.67 | 1.63 | 0.77 | 1.23 | 0.58 | 2.52 | 1.20 | 0.38 | 0.18 |
| Rb, ppm | 71.43 | 116.67 | 1.63 | 67.90 | 0.95 | 5.66 | 0.08 | 80.18 | 1.12 | 7.39 | 0.10 |
| Th, ppm | 6.95 | 12.49 | 1.80 | 5.92 | 0.85 | 4.20 | 0.60 | 6.45 | 0.93 | 0.58 | 0.08 |
| Nb, ppm | 7.02 | 13.28 | 1.89 | 6.18 | 0.88 | 0.57 | 0.08 | 6.91 | 0.98 | 0.27 | 0.04 |
| Zr, ppm | 51.57 | 77.96 | 1.51 | 48.47 | 0.94 | 6.25 | 0.12 | 65.32 | 1.27 | 6.14 | 0.12 |
| Ca, wt% | 6.75 | 3.15 | 0.47 | 8.00 | 1.19 | 22.27 | 3.30 | 5.12 | 0.76 | 1.13 | 0.17 |
| Mg, wt% | 2.61 | 1.30 | 0.50 | 2.93 | 1.12 | 8.04 | 3.08 | 2.34 | 0.90 | 0.65 | 0.25 |
| Sr, ppm | 470.83 | 207.50 | 0.44 | 564.46 | 1.20 | 1488.31 | 3.16 | 386.73 | 0.82 | 76.57 | 0.16 |
| Mn, ppm | 366.60 | 487.48 | 1.33 | 362.27 | 0.99 | 691.62 | 1.89 | 259.51 | 0.71 | 34.80 | 0.09 |
| Na, wt% | 4.33 | 2.86 | 0.66 | 2.27 | 0.53 | 0.18 | 0.04 | 1.82 | 0.42 | 25.52 | 5.90 |
| P, wt% | 0.30 | 0.56 | 1.87 | 0.25 | 0.82 | 0.44 | 1.48 | 0.17 | 0.56 | 0.02 | 0.06 |
| S, wt% | 0.62 | 0.75 | 1.20 | 0.36 | 0.58 | 0.25 | 0.41 | 1.34 | 2.14 | 0.23 | 0.37 |
| As, ppm | 18.04 | 10.40 | 0.58 | 13.94 | 0.77 | 17.56 | 0.97 | 41.81 | 2.32 | 5.06 | 0.28 |
| Mo, ppm | 12.40 | 1.34 | 0.11 | 7.97 | 0.64 | 12.89 | 1.04 | 38.26 | 3.09 | 4.29 | 0.35 |
| Co, ppm | 8.60 | 12.53 | 1.46 | 6.46 | 0.75 | 2.43 | 0.28 | 14.14 | 1.65 | 1.06 | 0.12 |
| Cr, ppm | 31.74 | 52.25 | 1.65 | 28.29 | 0.89 | 5.27 | 0.17 | 38.77 | 1.22 | 1.37 | 0.04 |
| Cu, ppm | 31.10 | 38.16 | 1.23 | 23.74 | 0.76 | 0.30 | 0.01 | 61.91 | 1.99 | 4.89 | 0.16 |
| Ni, ppm | 19.52 | 27.35 | 1.40 | 15.50 | 0.79 | 3.76 | 0.19 | 31.68 | 1.62 | 4.03 | 0.21 |
| U, ppm | 4.18 | 3.82 | 0.91 | 3.57 | 0.85 | 5.09 | 1.22 | 7.25 | 1.73 | 0.48 | 0.12 |
| V, ppm | 81.97 | 109.31 | 1.33 | 71.16 | 0.87 | 30.20 | 0.37 | 123.87 | 1.51 | 12.77 | 0.16 |
| Zn, ppm | 69.44 | 103.88 | 1.50 | 49.67 | 0.72 | 10.30 | 0.15 | 117.68 | 1.69 | 13.09 | 0.19 |
| TOC, wt% | 5.53 | 0.39 | 0.07 | 5.62 | 1.02 | 0.10 | 0.02 | 15.39 | 2.79 | 1.83 | 0.33 |
| N of sample | 376 | 89 | | 149 | | 29 | | 74 | | 35 | |

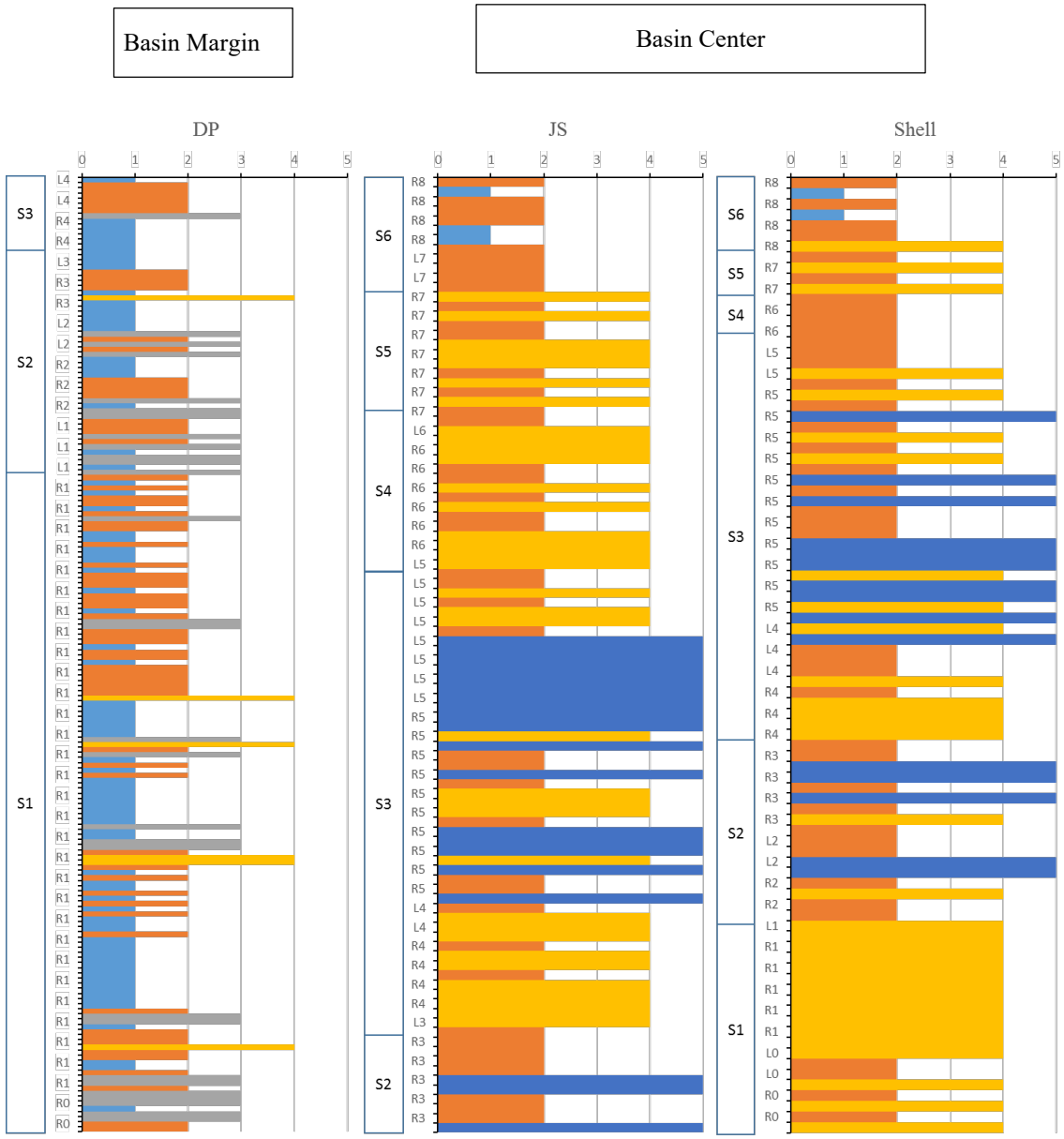



Fig. 3.5. Chemofacies logs generated from the combined dataset of DP, Shell and JS.

Table 3.2. Key chemical features of combined dataset from chemofacies of DP, Shell, and JS

| | **Cluster** | **1** | **2** | **3** | **4** | **5** |
|---|---|---|---|---|---|---|
| Name | | Low TOC Mudstone | Medium TOC Mudstone | Low TOC Carbonate | High TOC Mudstone | Saline Minerals |
| Siliciclastic | Si, Al, K, Fe, Ti, Rb, Zr, Nb | ++ | 0 | —— | 0 | — |
| Carbonate | Ca, Mg, Mn, Sr | — | + | ++ | — | —— |
| Saline | Na | — | — | —— | — | ++ |
| Pyrite | Fe, S | + | — | — | + | —— |
| $P_{IV}$ Transition Metal | V, Cr, Co, Ni, Cu, Zn | + | — | — | ++ | —— |
| Other Redox | Mo, As, U | — | — | —— | ++ | — |
| Organic Matter | TOC | — | 0 | —— | ++ | — |
| Phosphate | P | ++ | + | — | — | —— |

+ = enriched; ++ = most enriched; — = depleted; —— = most depleted; 0 = ~equal to average

To help in visualizing the characteristics of each facies, Figure 3.6 plots average values for the sum of three siliciclastic elements (Si, Al, K) against three carbonate elements (Ca, Mg, Mn), with the bubble size proportional to TOC. Each of the elements in these groups and TOC tend to show significant enrichment or depletion in different chemofacies as defined by the cluster analysis. Fields of various informal rock types (drawn to cover the area of all similar chemofacies averages – see later figures) are shown.

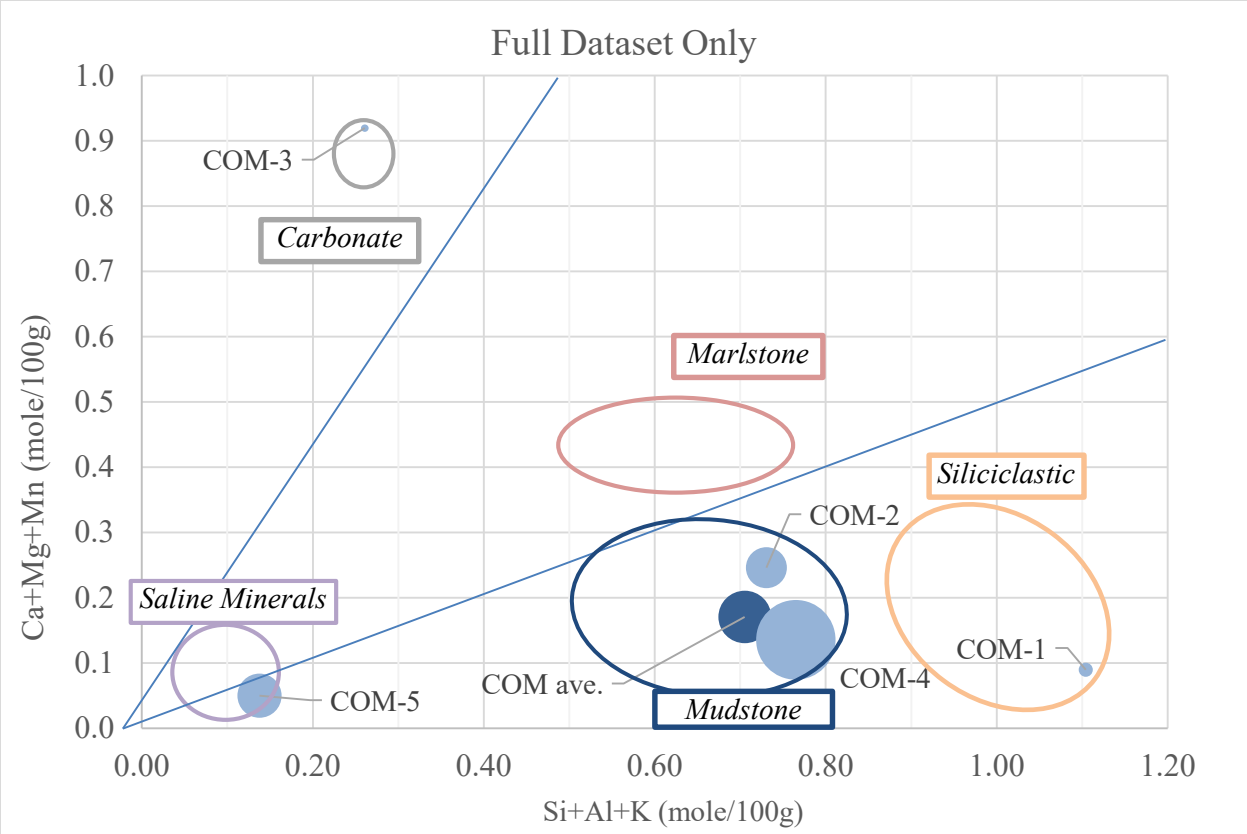



Fig.3.6. Crossplot of the sum of siliciclastic index elements and the sum of carbonate index elements of average values for chemofacies defined from the integrated DP, JS and Shell datasets. Ovals illustrate geochemically defined facies terms used throughout the chapter. Datapoint size is proportional to TOC.

In order to refine our understanding of chemical facies in the GRF, HCA was also performed on each individual dataset from the DP, JS, and Shell sections.

Chemofacies in the Basin Margin

Five chemofacies were identified within the stratigraphic section for DP, summarized in Table 3.3 and plotted as a chemofacies log in Fig. 3.7. The five chemofacies are described as follows:

DP-1 is characterized by enrichment of Si, Al, Fe, K, Ti, $P_{IV}$ transition metals and Na with relatively lower Ca, Mg, Sr, S, As, U, Mo and TOC content. The chemofacies represents low TOC siliciclastic sediment deposited in a reducing environment.

DP-2 is characterized by enrichment in Ca, Mg, Sr, and Mn, with relatively low concentrations of $P_{IV}$ transition metals and other redox sensitive elements (Mo, U, As). This chemofacies also has the highest TOC content (although distinctly less enriched than basin center facies), and relatively depleted Na and S content. It consists of slightly organic-enriched mixed siliciclastic and carbonate sediment with slight enrichment of the carbonate component (informally, marlstone).

DP-3 is characterized by substantial enrichment in Ca, Mg, Sr, and Mn, as well as the highest relative U, As and Mo content, with corresponding depletion of siliciclastic (Si, Al, Ti, and K), sulfide (Fe, As) and saline (Na) components. This facies represents low TOC carbonate sediment, deposited in an environment with slightly reducing conditions.

DP-4 is characterized by enrichment of Si and K with very low relative contents of redox sensitive elements ($P_{IV}$ transition metals, Fe, S, Mo, U, As) and no TOC content. The chemofacies consists of arkosic siliciclastic sediment, primarily sandstone.

DP-5 is enriched in Si, Al, and Ti, and has the highest enrichment in S, Fe, and Na of the DP chemofacies, with high relative $P_{IV}$ transition metal content, and low relative concentrations of Ca, Mg, Sr, Mo, and TOC. The chemofacies represents low TOC pyritic siliciclastic (possibly silty) sediment deposited under the most reducing conditions in the section.

The specific features of these chemofacies are summarized in Table 3.4 as a color-coded matrix.

| Variable | ave of all | Cluster 1 | Cluster 2 | Cluster 3 | Cluster 4 | Cluster 5 |
|---|---|---|---|---|---|---|
| Si, wt % | 17.91 | 1.17 | 0.86 | 0.37 | 1.38 | 1.18 |
| Al, wt % | 5.26 | 1.44 | 0.76 | 0.10 | 0.85 | 1.42 |
| Ti, wt % | 0.23 | 1.47 | 0.73 | 0.08 | 0.77 | 1.49 |
| K, wt % | 2.03 | 1.32 | 1.01 | 0.11 | 1.16 | 1.07 |
| Fe, wt % | 2.48 | 1.39 | 0.72 | 0.51 | 0.45 | 1.49 |
| Rb, ppm | 83.97 | 1.38 | 0.83 | 0.09 | 1.00 | 1.35 |
| Zr, ppm | 53.05 | 1.38 | 0.93 | 0.16 | 0.70 | 1.38 |
| Nb, ppm | 8.84 | 1.46 | 0.79 | 0.09 | 0.71 | 1.48 |
| Th, ppm | 9.41 | 1.30 | 0.81 | 0.46 | 0.72 | 1.41 |
| Ca, wt % | 7.75 | 0.41 | 1.41 | 2.81 | 0.23 | 0.44 |
| Mg, wt % | 2.76 | 0.48 | 1.26 | 2.86 | 0.18 | 0.48 |
| Sr, ppm | 523.66 | 0.41 | 1.39 | 2.78 | 0.31 | 0.43 |
| Mn, ppm | 519.27 | 0.93 | 1.16 | 1.32 | 0.44 | 1.04 |
| U, ppm | 4.29 | 0.90 | 1.21 | 1.19 | 0.42 | 1.20 |
| Na, wt % | 1.80 | 1.42 | 0.45 | 0.13 | 0.84 | 1.92 |
| P, wt % | 0.05 | 1.15 | 0.77 | 0.88 | 0.91 | 1.20 |
| S, wt % | 0.52 | 0.48 | 0.56 | 0.51 | 0.07 | 4.24 |
| As, ppm | 13.74 | 0.70 | 0.99 | 1.85 | 0.73 | 1.01 |
| Mo, ppm | 3.27 | 0.37 | 0.76 | 3.85 | 0.24 | 0.37 |
| Co, ppm | 8.64 | 1.39 | 0.72 | 0.30 | 0.63 | 1.58 |
| Cr, ppm | 35.78 | 1.43 | 0.89 | 0.18 | 0.42 | 1.53 |
| Cu, ppm | 23.55 | 1.60 | 0.66 | 0.03 | 0.44 | 1.61 |
| Ni, ppm | 18.11 | 1.44 | 0.78 | 0.24 | 0.45 | 1.58 |
| V, ppm | 82.45 | 1.33 | 0.97 | 0.39 | 0.41 | 1.45 |
| Zn, ppm | 68.44 | 1.52 | 0.74 | 0.17 | 0.43 | 1.56 |
| TOC, wt % | 0.53 | 0.55 | 3.44 | 0.22 | 0.00 | 0.11 |
| N of sample | 186 | 65 | 41 | 30 | 23 | 27 |

Table 3.3. Matrix of average elemental enrichment ratios (ER - enrichment or depletion ratio compared to the average concentration of that element in the whole dataset) by cluster in Douglas Pass. The color gradient of this matrix ranges vertically across each cluster based on variations of ER among elements. Note: N= number, ave= average.

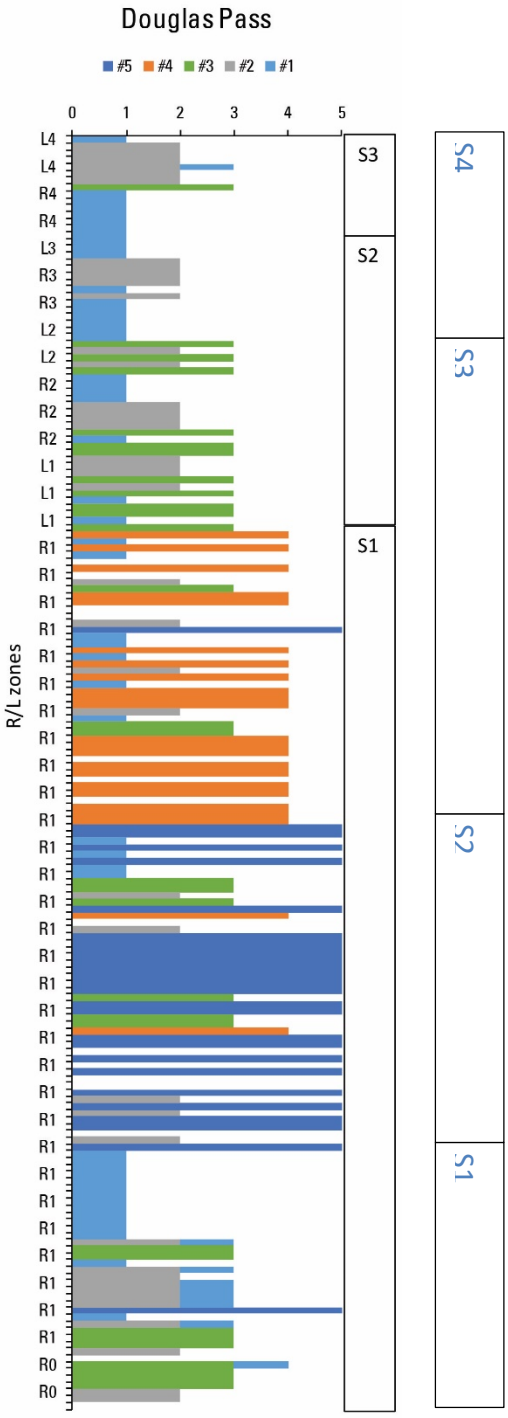



Fig.3.7. Computed Chemofacies of Douglas Pass area, with 5 facies identified (note: on the right side, the lake stage boundaries with stage symbol in color are from Tänavsuu-Milkeviciene and Sarg) (2012).

Table 3.4. Key chemical features of chemofacies of Douglas Pass.

| | Cluster | 1 | 2 | 3 | 4 | 5 |
|---|---|---|---|---|---|---|
| Name | | Low TOC Siliciclastic | High TOC Marlstone | High Mo, As Carbonate | Arkosic Sandstone | Sodic Pyritic Siliciclastic |
| Siliciclastic | Si, Al, K, Ti, Rb | ++ | – | — | + | + |
| Carbonate | Ca, Mg, Mn, Sr | — | + | ++ | 0 | — |
| Saline | Na | + | — | — | 0 | ++ |
| Pyrite | Fe, S | + | — | — | —— | ++ |
| $P_{IV}$ Transition Metal | V, Cr, Co, Ni, Cu, Zn | + | — | — | – | ++ |
| Other Redox | Mo, As, U | — | — | ++ | —— | — |
| Organic Matter | TOC | — | ++ | — | —— | — |
| Phosphate | P | + | — | — | — | ++ |

+ = enriched; ++ = most enriched; — = depleted; —— = most depleted

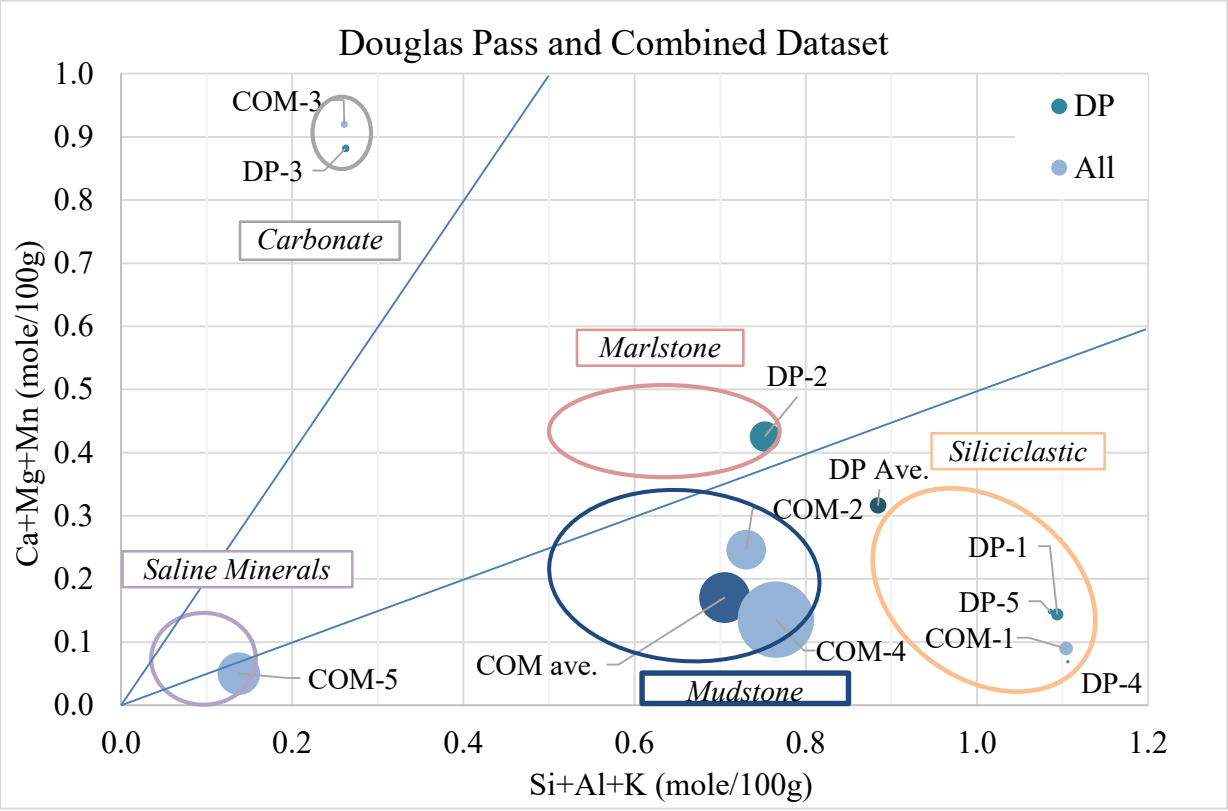



Figure 3.8: Crossplot of the sum of siliciclastic index elements and the sum of carbonate index elements of average values for chemofacies defined from the combined DP, JS and Shell datasets, and from the DP dataset alone. Ovals illustrate range for geochemically defined facies terms used throughout the chapter. Datapoint size is proportional to TOC.

Chemofacies in the Basin Center

Application of HCA to the basin center core samples yielded a different set of chemofacies from those identified in the marginal DP section. For the Shell dataset, 28 elements and TOC were included in the HCA and the following five chemofacies were identified (Table 3.5; Fig. 3.9):

Shell-1 is characterized by enrichment of carbonate-related elements (Ca, Mg, P, Sr, and Mn) with average values of elements related to siliciclastic minerals (Si, Al, Ti, Fe, and K), relative depletion of redox-sensitive elements, and lower TOC enrichment (average 10 wt%) than other chemofacies except Shell-5 saline facies in this well (overall average = ~11 wt%). It consists of high TOC marlstone (informal lithologic classification, shown in Table 3.6).

Shell-2 is characterized by enrichment of Si, Al, Ti, K, Zr, B, and redox-sensitive elements (Fe, S, $P_{IV}$ transition metals, Mo, U, As), with near average TOC content and low Na. It represents high-TOC siliciclastic-rich sediment with enrichment of elements indicating dysoxic to anoxic conditions, and high TOC content.

Shell-3 is characterized by average values of Si, Al, Ti, K, the highest relative TOC values and is enriched in Fe, S, $P_{IV}$ transition metals, As, and Mo, with relatively low Na, Ca, Mg and Sr content. This chemofacies represents high TOC mudstone.

Shell-4 is characterized by high TOC, depletion in Si, Al, Ti, K, Rb, Zr, average values of Ca, Mg, Sr, Mn and with low relative Fe, S, Mo, Cu, and U content. This chemofacies represents high TOC, slightly carbonate enriched mudstone.

Shell-5 is characterized by strong enrichment in Na, and depletion in every other element. It represents the saline mineral depositional environment during the hypersaline stage of Lake Uinta (Stages 2 and 3).

Figure 3.10 provides a plot of siliciclastic and carbonate element groups and TOC, following the model of Figure 3.6, with points for the combined dataset as well as for Shell.

| Variable | ave of all | Cluster 1 | Cluster 2 | Cluster 3 | Cluster 4 | Cluster 5 |
|---|---|---|---|---|---|---|
| Si, wt % | 13.31 | 1.03 | 1.54 | 1.11 | 0.84 | 0.16 |
| Al, wt % | 3.58 | 1.08 | 1.58 | 1.04 | 0.82 | 0.12 |
| Ti, wt % | 0.15 | 1.15 | 1.52 | 1.02 | 0.84 | 0.11 |
| K, wt % | 1.32 | 1.09 | 1.66 | 0.96 | 0.71 | 0.19 |
| Fe, wt % | 1.82 | 1.08 | 1.62 | 1.16 | 0.58 | 0.25 |
| B, ppm | 68.09 | 0.94 | 2.06 | 0.89 | 0.50 | 0.10 |
| Ga, ppm | 9.37 | 1.11 | 1.55 | 1.04 | 0.82 | 0.13 |
| Rb, ppm | 57.18 | 1.08 | 1.61 | 1.06 | 0.77 | 0.12 |
| Th, ppm | 4.46 | 1.19 | 1.57 | 1.00 | 0.74 | 0.12 |
| Nb, ppm | 5.20 | 1.19 | 1.62 | 0.96 | 0.76 | 0.03 |
| Zr, ppm | 55.88 | 0.97 | 1.93 | 0.83 | 0.67 | 0.11 |
| Ca, wt % | 4.86 | 1.85 | 0.80 | 0.81 | 1.05 | 0.18 |
| Mg, wt % | 2.37 | 1.70 | 0.99 | 0.80 | 0.97 | 0.19 |
| Sr, ppm | 336.81 | 1.89 | 0.88 | 0.76 | 0.96 | 0.15 |
| Mn, ppm | 215.61 | 1.35 | 1.25 | 0.96 | 0.98 | 0.13 |
| Na, wt % | 6.36 | 0.34 | 0.15 | 0.33 | 0.93 | 4.15 |
| P, wt % | 0.09 | 1.54 | 1.14 | 0.82 | 0.98 | 0.18 |
| S, wt % | 0.87 | 0.53 | 1.83 | 1.67 | 0.51 | 0.30 |
| As, ppm | 27.30 | 0.66 | 1.34 | 1.90 | 0.75 | 0.38 |
| Mo, ppm | 24.02 | 0.63 | 1.95 | 1.41 | 0.46 | 0.27 |
| Co, ppm | 9.20 | 0.83 | 1.68 | 1.47 | 0.62 | 0.15 |
| Cr, ppm | 27.82 | 1.17 | 1.58 | 1.04 | 0.81 | 0.00 |
| Cu, ppm | 39.84 | 0.89 | 1.76 | 1.36 | 0.57 | 0.10 |
| Ni, ppm | 20.80 | 0.95 | 1.65 | 1.25 | 0.69 | 0.15 |
| U, ppm | 4.46 | 1.16 | 1.69 | 1.10 | 0.55 | 0.12 |
| V, ppm | 87.77 | 1.02 | 1.64 | 1.18 | 0.69 | 0.14 |
| Zn, ppm | 61.59 | 0.95 | 1.64 | 1.29 | 0.70 | 0.12 |
| TOC, wt % | 10.80 | 0.71 | 0.95 | 1.83 | 1.37 | 0.20 |
| N of sample | 90 | 21 | 23 | 14 | 18 | 14 |

Table 3.5. Matrix of average elemental enrichment ratios (ER - enrichment or depletion ratio compared to the average concentration of that element in the whole dataset) by cluster in Shell 23X-2 well. The color gradient of this matrix ranges vertically across each cluster based on variations of ER among elements. Note: N= number, ave= average.

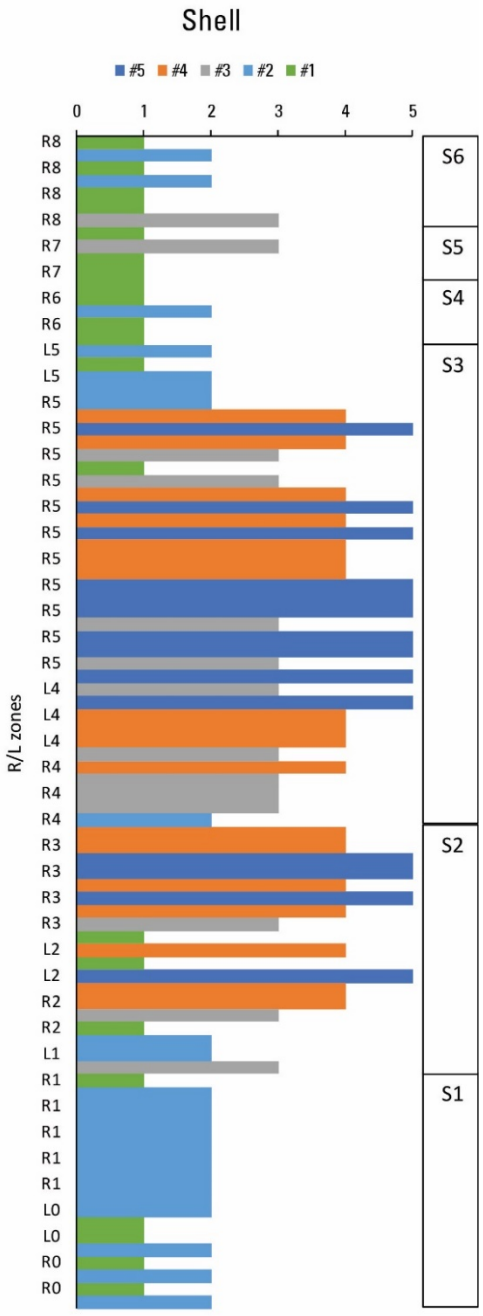



Fig.3.9. Computed Chemofacies of Shell 23X-2, with 5 facies identified.

Table 3.6. Key chemical features of chemofacies of Shell 23X-2 well

| | Cluster | 1 | 2 | 3 | 4 | 5 |
|---|---|---|---|---|---|---|
| Name | | High TOC Marlstone | High TOC Siliciclastic | High TOC Mudstone | High TOC Mudstone | Saline |
| Siliciclastic | Si, Al, K, Ti, Rb, Ga | 0 | ++ | 0 | — | —— |
| Carbonate | Ca, Mg, Mn, Sr | ++ | — | — | + | —— |
| Saline | Na | — | —— | — | 0 | ++ |
| Pyrite | Fe, S | — | ++ | + | — | —— |
| $P_{IV}$ Transition Metal | V, Cr, Co, Ni, Cu, Zn | — | ++ | + | — | —— |
| Other Redox | Mo, As, U | — | ++ | + | — | —— |
| Organic Matter | TOC | — | — | ++ | + | —— |
| Phosphate | P | ++ | + | — | 0 | —— |

+ = enriched; ++ = most enriched; — = depleted; —— = most depleted; 0 = ~equal to average

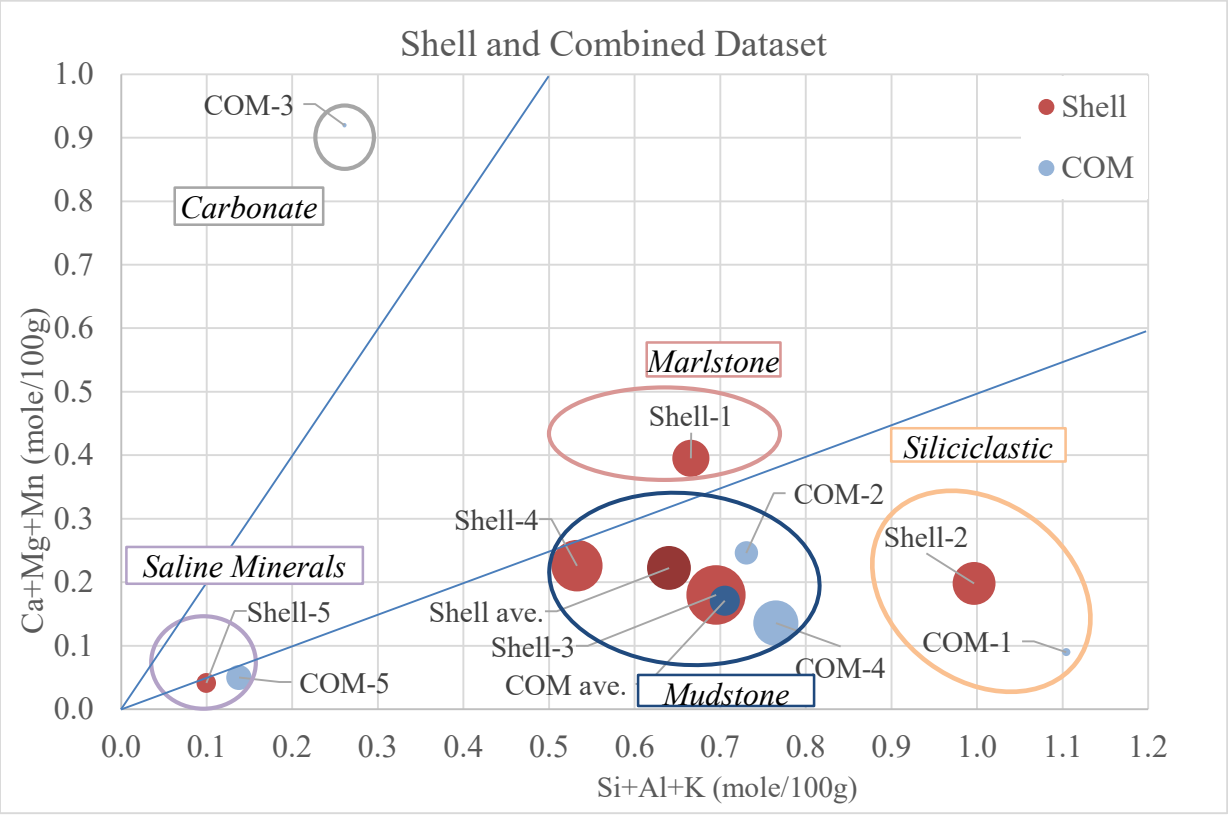



Figure 3.10: Crossplot of the sum of siliciclastic index elements and the sum of carbonate index elements of average values for chemofacies defined from the combined DP, JS and Shell datasets, and from the Shell dataset alone. Ovals illustrate geochemically defined facies terms used throughout the chapter. Datapoint size is proportional to TOC.

Five chemofacies were defined in the JS well dataset (Table 3.7; Fig. 3.11). These chemofacies showed similar features to those identified in the Shell dataset. The chemofacies from the John Savage well are the following:

JS-1 is characterized by enrichment of Ca, Mg, Mn, Sr, and P, approximately average values of Si, Al, Ti, Fe, Zr, K, and Na, depletion of redox elements ($P_{IV}$ transition metals, As, Mo, U, S) and TOC equal to the average value for the entire well. This chemofacies represents relatively high TOC marlstone with less reducing conditions than JS-2, JS-3 and JS-4 in the well. It resembles chemofacies Shell-1. Note that the phrase high TOC here reflects a comparison to source rocks in general, where an average value of 10.8 wt % is quite high, even though GRF rocks commonly reach much higher values.

JS-2 is characterized by enrichment in Si, Al, K, Ti, Fe, and Zr, as well as in $P_{IV}$ transition metals, and depletion in Na, TOC, As, and Mo, with Ca, Mg, and Sr close to average value of the whole well. This chemofacies represents moderate TOC siliciclastic sediment formed under relatively reducing conditions. It resembles chemofacies Shell-2.

JS-3 is characterized by modest enrichment in Si, Al, Ti, Fe, and Zr, high enrichment in TOC, S, As; moderate enrichment in $P_{IV}$ transition metals, U, and Mo, and depletion in Ca, Mg, and Sr. It represents high TOC mudstone deposited under reducing conditions. It resembles chemofacies Shell-3 but is richer in the siliciclastic constituents.

JS-4 is characterized by moderate enrichment in Si, Al, Ti, K, enrichment in $P_{IV}$ transition metals and strong enrichment in As, Mo, U, P and TOC with relative depletion of Na and the carbonate-related elements Ca and Mg. It represents high TOC mudstone deposited under strongly reducing conditions. It is distinct from Shell-4 in showing higher enrichment in the siliciclastic constituents.

JS-5 is characterized by strong enrichment in Na, and depletion in all other elements. It represents saline mineral deposits formed under the highest salinity conditions. It represents the saline mineral-rich sediment primarily deposited in Stages 2 and 3. It resembles chemofacies Shell-5.

| Variable | ave of all | Cluster 1 | Cluster 2 | Cluster 3 | Cluster 4 | Cluster 5 |
|---|---|---|---|---|---|---|
| Si, wt % | 12.87 | 0.98 | 1.61 | 1.13 | 1.14 | 0.10 |
| Al, wt % | 3.43 | 0.92 | 1.68 | 1.13 | 1.32 | 0.07 |
| Ti, wt % | 0.14 | 0.96 | 1.60 | 1.14 | 1.32 | 0.06 |
| K, wt % | 1.51 | 0.86 | 1.89 | 1.01 | 1.15 | 0.12 |
| Fe, wt % | 1.67 | 0.92 | 1.53 | 1.15 | 1.67 | 0.09 |
| B, ppm | 73.64 | 1.20 | 1.58 | 0.70 | 0.90 | 0.25 |
| Ga, ppm | 8.98 | 0.94 | 1.65 | 1.13 | 1.28 | 0.07 |
| Rb, ppm | 60.91 | 1.00 | 1.55 | 1.17 | 1.15 | 0.06 |
| Nb, ppm | 5.29 | 0.94 | 1.75 | 1.07 | 1.25 | 0.02 |
| Th, ppm | 4.62 | 1.00 | 1.58 | 0.97 | 1.62 | 0.10 |
| Zr, ppm | 44.94 | 0.96 | 1.61 | 1.12 | 1.31 | 0.08 |
| Ca, wt % | 6.58 | 1.50 | 1.01 | 0.88 | 0.90 | 0.11 |
| Mg, wt % | 2.55 | 1.41 | 1.18 | 0.90 | 0.73 | 0.14 |
| Sr, ppm | 493.18 | 1.53 | 0.98 | 0.77 | 1.17 | 0.11 |
| Mn, ppm | 218.54 | 1.14 | 1.48 | 0.97 | 1.14 | 0.09 |
| Na, wt % | 7.19 | 0.56 | 0.31 | 0.44 | 0.26 | 3.70 |
| P, wt % | 0.11 | 1.35 | 0.89 | 0.80 | 2.47 | 0.11 |
| S, wt % | 0.60 | 0.70 | 0.79 | 2.19 | 1.88 | 0.19 |
| As, ppm | 17.71 | 0.70 | 0.89 | 1.75 | 3.39 | 0.03 |
| Mo, ppm | 18.90 | 0.76 | 0.88 | 1.59 | 3.46 | 0.09 |
| Co, ppm | 7.96 | 0.82 | 1.37 | 1.38 | 2.19 | 0.06 |
| Cr, ppm | 27.76 | 0.97 | 1.57 | 1.19 | 1.39 | 0.00 |
| Cu, ppm | 37.29 | 0.90 | 1.29 | 1.36 | 2.02 | 0.07 |
| Ni, ppm | 20.97 | 0.86 | 1.26 | 1.37 | 2.04 | 0.17 |
| U, ppm | 3.75 | 0.83 | 1.26 | 1.20 | 3.04 | 0.07 |
| V, ppm | 75.87 | 0.93 | 1.38 | 1.34 | 1.59 | 0.09 |
| Zn, ppm | 78.38 | 0.72 | 1.15 | 0.99 | 4.67 | 0.12 |
| TOC, wt % | 10.08 | 1.00 | 0.67 | 1.78 | 2.15 | 0.09 |
| N of sample | 0 | 36 | 21 | 20 | 6 | 17 |

Table 3.7. Matrix of average elemental enrichment ratios (ER - enrichment or depletion ratio compared to the average concentration of that element in the whole dataset) by cluster in John Savage. The color gradient of this matrix ranges vertically across each cluster based on variations of ER among elements. Note: N= number, ave= average.

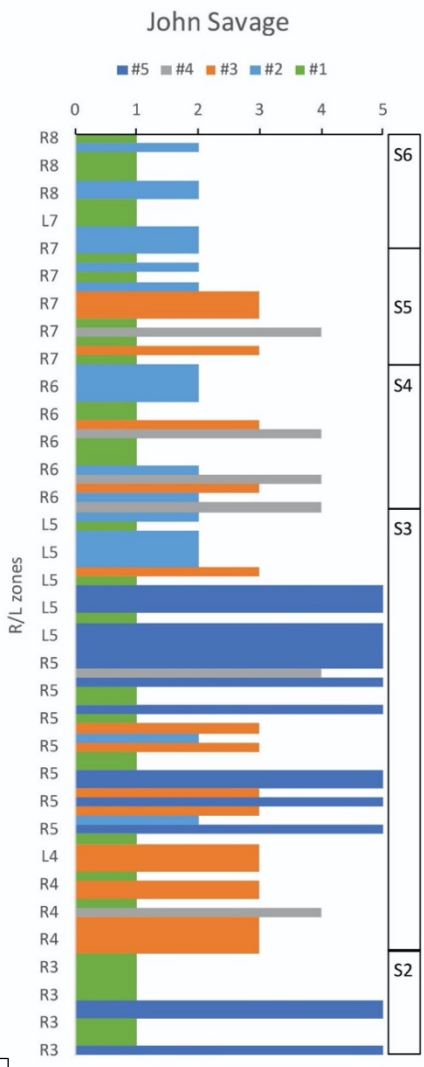



Fig.3.11. Computed Chemofacies of John Savage 24-1, with 5 facies identified.

Table 3.8. Key chemical features of chemofacies of John Savage well

| | **Cluster #** | **1** | **2** | **3** | **4** | **5** |
|---|---|---|---|---|---|---|
| Constituent | Elements | High TOC Marlstone | Medium TOC Siliciclastic | High TOC Mudstone | High TOC Mudstone | Saline Mineral |
| Siliciclastic | Si, Al, K, Ti, Rb, Ga | 0 | ++ | + | + | —— |
| Carbonate | Ca, Mg, Mn, Sr | ++ | 0 | — | — | —— |
| Saline | Na | — | — | — | —— | ++ |
| Pyite | Fe, S | — | ++ | + | — | —— |
| $P_{IV}$ Transition Metal | V, Cr, Co, Ni, Cu, Zn | — | + | + | ++ | —— |
| Other Redox | Mo, As, U | — | — | + | ++ | —— |
| Organic Matter | TOC | 0 | — | + | ++ | —— |
| Phosphate | P | + | — | — | ++ | —— |

+

= enriched; ++ = most enriched; — = depleted; —— = most depleted; 0 = ~equal to average

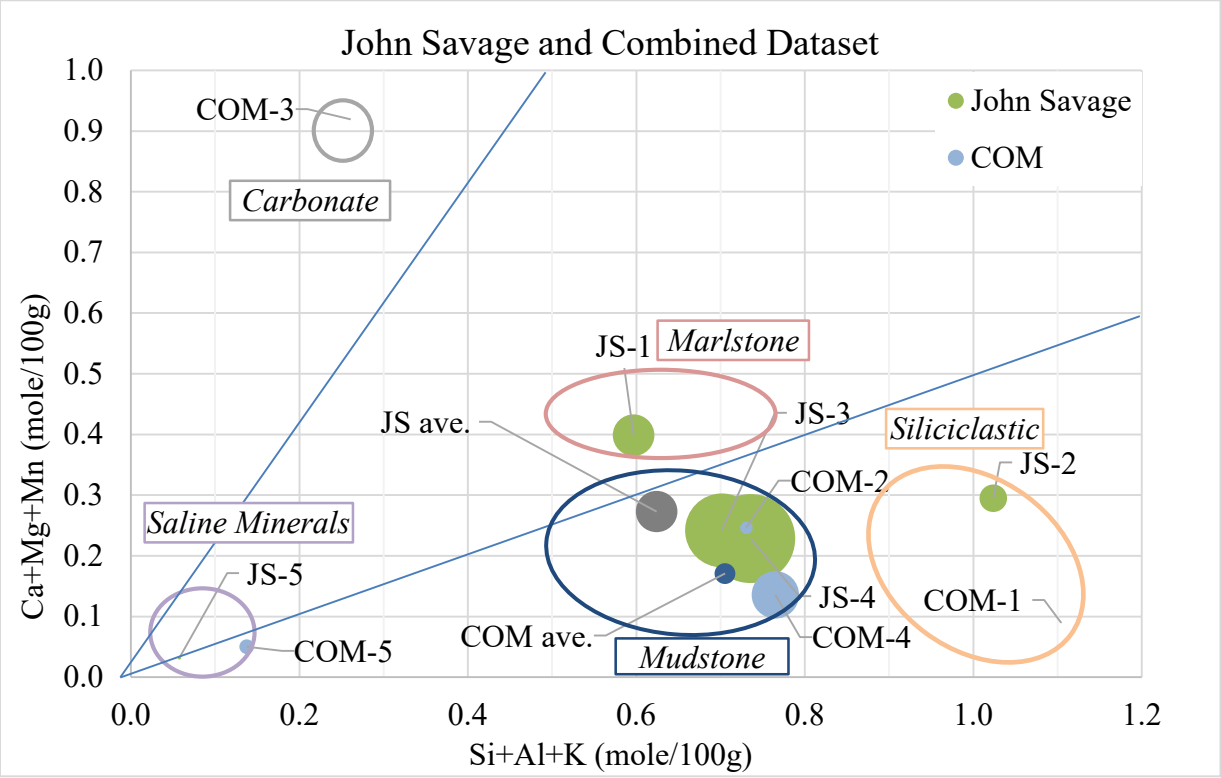



Fig. 3.12: Crossplot of the sum of siliciclastic index elements and the sum of carbonate index elements of average values for chemofacies defined from the combined DP, JS and Shell datasets, and from the JS dataset alone. Ovals illustrate geochemically defined facies terms used throughout the chapter. Datapoint size is proportional to TOC.

## Discussion

### Chemofacies of the combined dataset

The chemofacies defined for the combined dataset show clear differences between the basin margin and the basin center (Fig.3.5). The DP sample set from the basin margin includes most of the samples of COM-1 and all the COM-3 samples, whereas the Shell, and JS samples from the basin center include all but six of the samples of COM-4 and all of the COM-5 samples. COM-1 and 3 represent highly siliciclastic and carbonate-rich facies, respectively; while COM-4 and COM-5 reflect high TOC mudstone and high saline mudstone (Tables 3.1 and 3.2). Only COM-2, the low TOC mudstone chemofacies, is common in both the basin margin and basin center (Fig. 3.5), which represents dolomitic mudstone facies, specifically. The distributions of 5 chemofacies average values in terms of siliciclastic index elements (Si, Al, K) and carbonate index elements (Ca, Mg, Mn) is shown in Fig.3.6, which demonstrates the chemical features of each chemofacies very clearly. It is also important to note that the COM-1 low TOC siliciclastic facies occurs in the basin center, but only in the uppermost sections, when the basin was being filled by siliciclastic sediments derived from the north (Birdwell et al., 2019) in the closing stage of the paleolake. Overall, the basin margin mainly represents the low TOC siliciclastic and carbonate facies with less reducing conditions, and the basin center mainly represents high TOC and high saline mineral facies, with more reducing conditions.

### Chemofacies of the Basin Margin

In the basin margin, the 5 chemofacies emphasize the strong differentiation between the siliciclastic inputs, which includes DP-1, DP-4, DP-5, and carbonate inputs in DP-3. DP-1, DP-4 and DP-5 represent high siliciclastic, low carbonate component siltstone, sandstone, and mudstone, respectively. DP-2, the intermediate composition marlstone (an informal term), has the highest

TOC and is sparse to absent from the middle part of the section (Fig.3.8). The DP section shows a sequence of variations in lithofacies, TOC, redox conditions and salinity, which are reflected in the changes of chemofacies throughout the section (Fig.3.8; Tables 3.3 and 3.4). As shown in Fig.3.7, Johnson et al (1985) and Tänavsuu-Milkeviciene and Sarg (2012) defined different boundaries for lake stages in the basin margin.

According to the stage boundaries of Johnson et al (1985), most samples were collected from lake stage 1, which contains all 5 chemofacies, with DP-4 and DP-5 observed only in this stage. DP-5 represents pyritic and sodic mudstone, where DP-4 represents siltstone/sandstone with depleted redox sensitive elements and low TOC. Each is dominant in a portion of the stage, DP-5 in the middle, and DP-4 in the top. The lower part of the stage consists of DP-1, 2 and 3, and these facies are sparely distributed through the upper parts of the stage. In Stage 2, DP-3, the carbonate facies, is very common, and interbedded with DP-1 and DP-2 through the lower half, but sparse to absent in the upper part and Stage 3 as well. In Stages 2 and 3, DP-1, 2, 3 are common and DP-4 and 5 are missing, implying a deepening upward depositional process. In the upper part of Stage 2 and Stage 3, the section is mainly composed of DP-1 and 2, with only few occurrences of DP-3.

The stage definitions from Tänavsuu-Milkeviciene and Sarg (2012) in the basin margin provides another version of the paleolake evolution. According to Tänavsuu-Milkeviciene and Sarg (2012), Stage 1 includes a mix of samples from facies DP-1, DP-2 and DP-3. Stage 2 is almost entirely composed of DP-5, with a few DP-1, DP-3 and DP-4 in between. The lower part of Stage 3 includes almost all the DP-4, the sandy facies and the upper Stage 3 includes only DP-1, DP-2 and DP-3, with DP-4 and DP-5 missing. Stage 4 is mainly dominated by DP-1, low TOC siliciclastic facies and DP-2, the high TOC marlstone facies, with only one sample of the carbonate

chemofacies, DP-3. The stratigraphic classification from Tänavsuu-Milkeviciene and Sarg (2012) covers more stages of lake development in the basin margin area and presents a different evolutionary history of the paleolake in the basin margin area. During the fresh-brackish lake stage 1, it is mainly characterized by detrital sediments and carbonate facies, implying the beginning of the basin development; During the transitional lake stage 2, DP-5, the pyritic siliciclastic facies with highest salinity and significant enrichement of redox-sensitive elements stands out, corresponding to the interpretation of Wu et al. (2021) in the previous geochemistry chapter, that elevated evaporation occurred in this stage, concentrating sodium in the margin as the temperature rose (Zachos et al., 2001; 2008; Smith et al., 2014). In the highly fluctuating lake stage 3, the sandstone facies is dominant in the early stage and then switches to carbonate facies, and siliciclastic facies, indicating changes of mineral types and water depth during the driest and hottest period of the EECO. In the rising lake stage 4, only siliciclastic facies and marlstone facies are observed, which reflect more detrital sediment inputs, and presumably further deepening of the lake.

As shown in Fig.3.7, DP-5, the high salinity siliciclastic facies occurs at the beginning of Stage 2, and this chemofacies is almost completely confined to Stage 2, which suggests that this stage has stratigraphic significances, even if the Stage 1 definition of Johnson et al (1985) is accepted. The shift to chemofacies DP-4 occurs at the boundary of Stages 2 and 3, and the end of common carbonate facies occurs at the boundary of Stages 3 and 4. Thus, the stage boundaries of Tänavsuu-Milkeviciene and Sarg (2012) define sequence stratigraphic as well as chemostratigraphic changes that require more detailed investigation to resolve differences in interpretation. No matter which definition is accepted, the early timing of high sodic enrichment in the basin margin further confirms our interpretation of the occurrence of hypersalinity in the

basin margin in the previous chapter (Boak et al., 2021). Whether the sodic interval is a local phenomenon or whether it occurs widely on the margin of Lake Uinta will require additional basin margin profiles to determine.

It is worth noting that the coherence in enrichment of most $P_{IV}$ transitional metals is observed in the 5 DP chemofacies of the basin margin, but that other redox sensitive elements (U, Mo, As) are not consistently coherent with them. Additionally, whole-rock concentrations are depleted with respect to average shale values (Boak et al., 2021). However, it is very challenging to evaluate the variations of reducing conditions in the basin margin area, because the shallow lake is more easily affected by the local facies variations (Feng, 2011), as it lies above the chemocline of the stratified lake. Below the chemocline in the basin center, variations in chemofacies are more likely to reflect lake-wide changes driven by climate change. It is interesting to point out that DP-3, the carbonate chemofacies, is enriched in Mo and U compared to the average value, and that DP-2, with the highest TOC, shows all $P_{IV}$ transition metals depleted. It is evident that redox conditions were complex and will require more detailed sample analysis in this area so that the puzzle can be solved in future studies.

Chemofacies of the Basin Center

In the basin center, the distributions of chemofacies in the Shell and JS wells are, in general, very different from those of the basin margin section. The Shell section is more complete and covers samples from all six lake stages. Stage S1 is dominated by Shell-1 and Shell-2, high TOC marlstone and siliciclastic sediments, respectively. Stages S2 and S3 are dominated by Shell- 3, 4 and 5, high TOC and high $P_{IV}$ transition metal mudstone (Shell-3), high TOC mudstone with low redox sensitive elements (Shell-4), and high salinity (Shell-5), respectively. Stages S4, S5 and S6 are mainly characterized by Shell-1, 2 and 3, with no Shell- 4 and 5 samples observed in those

stages (Fig. 3.9). This pattern is consistent with the trends identified from the chemical logs of the Shell core (Boak et al., 2021), with Na content sharply reduced by leaching (Dyni, 1974; Beard et al., 1974; Birdwell et al, 2019). There may also be a signal of increase in siliciclastic input due to higher humidity and increased inflow in the later stages (Smith et al., 2008; Tänavsuu-Milkeviciene et al., 2012).

For the JS core samples, Stages S2 and S3 are dominated by JS-1, 3 and 5, characterized as high TOC marlstone, high TOC mudstone, and saline mineral, quite similar to the features identified from the same stages in Shell 23X-2. Stages S4 and S5 are composed of JS-1, 2, 3 and 4, represented by high TOC marlstone, medium TOC siliciclastic, high TOC mudstone with redox sensitive element enrichment, and high TOC mudstone with strong redox sensitive element enrichment. The shift reflects both dissolution of saline minerals in the leached zone, and possible increasing siliciclastic input and decreasing salinity after S3. Chemofacies, JS-2, the medium TOC mudstone is rare below zone L5 near the top of S3, reflecting the earliest stages of the influx of siliciclastic sediment driven both by cooler wetter conditions, and ultimately the infilling of the lake. Stage S6 is mainly composed of JS-1 and 2, marking the end of the lake by increasing siliciclastic input to fill in the basin (Carroll et al., 2006; Poole, 2014; Tänavsuu-Milkeviciene and Sarg, 2012; Wu et al., 2021).

Overall, it is important to note that the chemofacies of the two basin center sections are quite similar. Shell-1 and JS-1 are both marlstone of similar compositions and lower TOC with some enrichment in redox sensitive elements (Figs. 3.9 and 3.11); Shell-2 and JS-2 are high siliciclastic lower carbonate mudstone with moderate TOC; Shell-3 and JS-3 are common mudstone with high TOC and significant enrichment in redox sensitive elements; Shell-5 and JS-5 are high saline mudstone (Table 3.6 and 3.8).

On the other hand, some differences are observed between Shell-4 and JS-4. Shell-4 shows a somewhat higher average ratio of Ca + Mg to Si + Al + K than JS-4 (Figs. 3.10 and 3.12). Shell-4 is depleted in redox-sensitive elements, whereas JS-4 has the highest enrichments in these elements. According to Boak et al (2013), and Poole (2014), three mineralogic units are identified based on the changes in index minerals in the basin center, *i.e,* Lower Mineralogic Unit (LMU), Middle Mineralogic Unit (MMU), and Upper Mineralogic Unit (UMU). Shell-1 and Shell-2 comprise most of the samples in the LMU, but are largely absent in the MMU. Shell-4 and Shell-5 are largely absent in both the LMU and UMU. Therefore, there is a shift in chemofacies from Shell-1 and Shell-2 to Shell-3 and Shell-4, and then back to Shell-1 and Shell-2 upward in the Shell section (Fig.3.9), which indicates that Shell-4 replaces Shell-1, and is lower in both the silicate and carbonate fractions because it is more enriched in TOC; Shell-3 replaces Shell-2, and is richer in TOC, but lower in silicate fraction because of the dilution effect of TOC in Shell-3. As shown in Fig.3.11, JS-1 occurs throughout much of the section and JS-2 does not appear until R5, and is most common in the UMU. The LMU was not penetrated by the JS well. It is possible that the differences among statistical clusters between the two wells are a consequence of the incomplete sampling of the lower section in the JS well. This question will require more study on the formation in the future to get a more comprehensive comparison.

From Tables 3.5-3.8, it is noted that high TOC is closely associated with high concentration of redox sensitive elements, which indicates organic matter preservation is maintained under more reducing conditions, as shown in Shell-3, Shell-4, and JS-3 and JS-4, the organic rich, high $P_{IV}$ transition metals chemofacies. This relationship corresponds to our discoveries in the individual geochemical logs of the previous chapter. Mo, U and As are mainly associated with high TOC in

the basin center, implying the validity of these trace metal proxies to evaluate the organic matter deposition in the lacustrine system of the Piceance Basin.

These chemofacies accentuate the distinction between the more bimodal dolomitic and siliciclastic, less anoxic, and lower TOC environments of the basin margin, on the one hand, and the more compositionally mixed mudstone and marlstone, and more reducing, TOC-richer, and saline evaporative environments of the basin center. These differences are related to the balance of siliciclastic input, carbonate precipitation, organic productivity, reducing conditions and salinity (Boak et al, 2021), which are likely to have varied in the shallower margins relative to the deeper depocenter due to lake stratification.

The chemofacies also make one thing apparent that is not easily seen in the raw geochemical data. There is clear coherence among most of the $P_{IV}$ transition metals analyzed. V, Co, Ni, Cu, and Zn are generally either enriched or depleted in a given chemofacies, although the degree of enrichment or depletion may vary from element to element. As noted in the previous chapter, $P_{IV}$ transition metals do not show very strong enrichments when normalized to Al and to average shale (Tribovillard, 2006), in part due to an inferred depletion in mafic constituents in the source rocks for the GRF. This made drawing conclusions regarding the redox conditions during deposition difficult. The persistent coherence of enrichment or depletion of these metals in statistically defined chemofacies suggests at least that relative redox conditions may be inferred. Especially where other redox sensitive elements (Mo, As, U) are also coherent in a given facies, interpretations are more robust than might be possible on the basis of individual elements.

The timing of rising salinity in DP seems to occur around the time when shale zones R1 - L1 formed (Fig.3.7), regardless which stratigraphic classification we were referring to, earlier than the basin center in Shell, where shale zones L2 – R 3 marked the beginning of high salinity

(Figs.3.9 and 3.11). It seems that salinity was first elevated in the basin margin area and then in the basin center, which further clarifies our conclusion in the previous chapter (Boak et al., 2021) that high evaporation rate achieved relatively high salinity in the shallow basin margin and that denser saline water was then transported into the basin center through density current flow from the shallow shelf.

## Conclusion

HCA in the Piceance Basin has proven to be a very useful method in generating chemofacies across the basin and provides us a novel perspective to study sedimentary processes of this lacustrine system. The chemofacies derived from the high-resolution ICP- OES/MS geochemistry data indicate variations of sedimentary processes and constituents between the basin margin and the basin center. The differences in TOC, redox condition, siliciclastic sediments, carbonate and salinity features from the basin margin to the basin center are clearly identified and defined. High TOC facies are commonly found to show relatively elevated concentrations of trace metal proxies for redox conditions (As, Mo, U, Ni, Cu, Cr, Co, V, Zn), although in some zones these are not coherent. As, U and Mo are considered to be the most representative redox proxies in evaluating the reducing conditions in this lacustrine system. The two stratigraphic classifications in the basin margin provide us different perspectives to understand the evolutionary history of the margin area and more stratigraphic sections are needed in the future to confirm the stratigraphic interpretation. The timing of elevated salinity first occurring in the basin margin is further confirmed in this chapter. HCA helps us extract some hidden geological signals which cannot be observed from individual chemical logs in the previous chapter, i.e. the positive correlation between TOC and trace metal proxies, the coherent affinity of $P_{IV}$ transition metals and

the two different stratigraphic classifications in the basin margin that are characterized clearly by distinct chemofacies associations.

## Acknowledgements

We thank the U.S. Geological Survey Core Research Center for the access to core analysis and sampling. We are grateful for the funding support from Center for Oil Shale Technology and Research, funded by Shell, ExxonMobil, and Total Petroleum, and the funding support from Oklahoma Geological Survey for field work and conference. Special thanks go to Dr. Andrew Elwood Madden for helping in reviewing the manuscript. Any use of trade, product or firm names is for descriptive purposes only and does not imply endorsement by the U.S. Government.

## References

Birdwell, J.E., Johnson, R.C., and Brownfield, M. E., 2019, Distribution of mineral phases in the Eocene Green River Formation, Piceance Basin, Colorado-Implications for the evolution of Lake Uinta, The Mountain Geologist, vol.56, p.73-141.

Beard, T.N., Tait, D.B., and Smith, J.W., 1974, Nahcolite and dawsonite resources in the Green River Formation, Piceance Creek Basin, Colorado: *in* D. Keith Murray, ed., Guidebook to the Energy Resources of the Piceance Creek Basin Colorado: Rocky Mountain Association of Geologists Twenty-Fifth Field Conference Guidebook, p. 101-109.

Boak, J., and Poole, S., 2015, Mineralogy of the Green River Formation in the Piceance Creek Basin, Colorado, *in* Smith, M.E., Carroll, A.R., eds., Stratigraphy and paleolimnology of the Green River Formation, Western USA: Syntheses in Limnogeology, v. 1, p. 183-209.

Boak, J., Poole S., and Feng, J., 2016, Geochemistry of the Green River Formation, Piceance Creek Basin, Colorado: *in* Dolan, M.P., Higley, D.K., and Lillis, P.G., Hydrocarbon Source Rocks in Unconventional Plays, Rocky Mountain Region: Rocky Mountain Association of Geologists, p. 295-318.

Boak, J., Poole, S., Sarg, J.F., Tänavsuu-Milkeviciene, K., 2013. Evolution of Lake Uinta as Defined by Mineralogy and Geochemistry of the Green River Formation in Colorado,

Unconventional Resources Technology Conference. Society of Exploration Geophysicists, American Association of Petroleum Geologists, Society of Petroleum Engineers, pp. 1952-1961.

Boak, J., Wu, T.F., Birdwell, J., 2021. Geochemical studies of the Green River Formation in the Piceance Basin, Colorado: I. Major, minor, and trace elements. Submitted.

Bohacs, K.M., Carroll, A.R., Neal, J.E., Mankiewicz, P.J., 2000. Lake-basin type, source potential, and hydrocarbon character: an integrated sequence-stratigraphic-geochemical framework. Lake basins through space and time: AAPG Studies in Geology, 46: 3-34.

Bradley, W.H., 1928. Zeolite beds in the Green River formation. Science, 67(1725): 73-74.

Cashion, W.B., Donnell, J.R., 1972. Chart showing correlation of selected key units in the organic-rich sequence of the Green River Formation, Piceance Creek Basin, Colorado, and Uinta Basin, Utah: U.S. Geological Survey Oil and Gas Investigations Chart OC-65.

Cashion, W.B., Donnell, J.R., 1974. Revision of nomenclature of the upper part of the Green River Formation, Piceance Creek basin, Colorado, and eastern Uinta basin, Utah, U.S. Geological Survey Bulletin, 1394-G, 9 p.

Cloutier, V., Lefebvre, R., Therrien, R., Savard, M.M., 2008. Multivariate statistical analysis of geochemical data as indicative of the hydrogeochemical evolution of groundwater in a sedimentary rock aquifer system. J Hydrol 353:294–313.

Cole, R.D., Picard, M.D., 1978. Comparative mineralogy of nearshore and offshore lacustrine lithofacies, Parachute Creek Member of the Green River Formation, Piceance Creek basin, Colorado, and eastern Uinta basin, Utah. Geological Society of America Bulletin, 89(10): 1441-1454.

Davis, J.C.,1986. Statistics and data analysis in geology, Second Edition. John Wiley & Sons, New York. 646 p.

Dean, W.E., Pitman, J.K., Harrach, G.H., 1981. Geochemical and mineralogical analyses of US Geological Survey oil-shale core CR-2, Piceance Creek basin, Colorado: U.S. Geological Survey Open File Report 81-596, 93p.

Dong, T., Harris, N.B., Ayranci, K., Twemlow, C.E., Nassichuk, B.R., 2015. Porosity characteristics of the Devonian Horn River shale, Canada: Insights from lithofacies classification and shale composition. International Journal of Coal Geology, 141: 74-90.

Dyni, J.R., 1974, Stratigraphy and nahcolite resources of the saline facies of the Green River Formation, Rio Blanco County, Colorado: *in* Murray, D.K., ed., Energy Resources of the Piceance Creek Basin, Colorado, 25th Field Conference: Rocky Mountain Association of Geologists, p. 111–122.

Dyni, J.R., 1996. Sodium carbonate resources of the Green River Formation. U.S. Geological Survey Open- File Report, 96-729.

Dyni, J.R., 2006. Geology and Resources of Some World Oil-Shale Deposits. U. S. Geological Survey Scientific Investigations Report 2005-5294, p.42.

Dyni, J.R., 2008. Preliminary stratigraphic cross sections of oil shale in the Eocene Green River Formation, Uinta Basin, Utah: U.S. Geological Survey Open-File Report 2008–1220, p.11.

Feng, J., 2011. Source rock characterization of the Green River oil shale, Piceance Creek Basin, Colorado, M.S. Thesis, Colorado School of Mines, Golden, CO, 84p.

Galvis-Portilla, H., 2017. Detailed lithostratigraphic characterization and sequence stratigraphy of a complete Woodford shale outcrop section in southern Oklahoma, University of Oklahoma, Norman, OK, 156p.

Güler, C., Thyne, G.D., McCray, J.E., Turner, K.A., 2002. Evaluation of graphical and multivariate statistical methods for classification of water chemistry data. Hydrogeology journal, 10(4): 455-474.

Harris, N.B., Mnich, C.A., Selby, D., Korn, D., 2013. Minor and trace element and Re–Os chemistry of the Upper Devonian Woodford Shale, Permian Basin, west Texas: insights into metal abundance and basin processes. Chemical Geology, 356: 76-93.

Jagniecki, E.A., Lowenstein, T.K., 2015, Evaporites of the Green River Formation, Bridger and Piceance Creek Basins: Deposition, diagenesis, paleobrine chemistry, and Eocene atmospheric CO2: *in* M.E. Smith and A.R. Carroll, eds., Stratigraphy and Paleolimnology of the Green River Formation, Western USA, Springer, Dordrecht, pp. 277-312.

JARVIE, D.M., 1991, Total organic carbon (TOC) analysis, in Merrill, R.K., ed., Treatise of Petroleum Geology: Handbook of Petroleum Geology, Source and Migration Processes and Evaluation Techniques: Tulsa, American Association of Petroleum Geologists, p. 113–118.

Johnson, R., Mercier, T., Brownfield, M., Pantea, M., Self, J., 2010. An assessment of in-place oil shale resources in the Green River Formation, Piceance Basin, Colorado. US Geological Survey Oil Shale Assessment Team, oil shale and nahcolite resources of the Piceance Basin, Colorado: US Geological Survey Digital Data Series DDS-69-Y: 1-185.

Johnson, R.C., 1985, Early Cenozoic history of the Uinta and Piceance Creek Basins, Utah and Colorado, with special reference to the development of Eocene Lake Uinta, *in* Flores, R.M., and Kaplan, S.S., eds, Cenozoic Paleogeography of the West-Central United States, Rocky Mountain Paleography Symposium 3: The Rocky Mountain Section, Society of Economic Paleontologists and Mineralogists p. 247-276.

Ketchen, D. J., and C. L. Shook, 1996. The application of cluster analysis in strategic management research: An analysis and critique. Strategic Management Journal,17, 441–458.

Kodinariya, T.M., Makwana, P.R, 2013. Review on determining number of cluster in K-means clustering. International Journal of Advance Research in Computer Science and Management Studies, 1 (6), pp. 90-95.

Mason, G.M., 2007. Saline Minerals in the Green River Formation, Green River and Washakie Basins, Wyoming, 27th Oil Shale Symposium Colorado School of Mines.

Nance, H.S., Rowe, H., 2015. Eustatic controls on stratigraphy, chemostratigraphy, and water mass evolution preserved in a Lower Permian mudrock succession, Delaware Basin, west Texas, USA. Interpretation, 3(1): SH11-SH25.

Andrew Ng, Clustering with the K-Means Algorithm, Machine Learning, 2012.

Offurum, C.G., 2016. Integrated geochemical, mechanical, and lithological characterization of the Marcellus Shale, Pennsylvania, Texas Christian University, Fort Worth, TX, p125.

Phillips, N.D., 1991. Refined subsidence analysis as a means to constrain Late Cenozoic fault movement, Ventura Basin, California, University of Texas at Austin, Austin, TX, 545p.

Pitman, J.K., 1996. Origin of primary and diagenetic carbonates in the lacustrine Green River Formation (Eocene), Colorado and Utah, U.S. Geological Survey Bulletin 2157.

Poole, S., 2014. Quantitative mineralogy and distributions of minerals of the green river formation, Piceance Creek Basin, Western Colorado, Colorado School of Mines, Golden, Co, 151p.

Remy, R.R., Ferrell, R.E., 1989. Distribution and origin of analcime in marginal lacustrine mudstones of the Green River Formation, south-central Uinta Basin, Utah. Clays and Clay minerals, 37(5): 419-432.

Sarg, J.F., Tänavsuu-Milkeviciene, K., Humphrey, J.D., 2013. Lithofacies, stable isotopic composition, and stratigraphic evolution of microbial and associated carbonates, Green River Formation (Eocene), Piceance Basin, Colorado. AAPG bulletin, 97(11): 1937-1966.

Schot, P.P., van der Wal, J., 1992. Human impact on regional groundwater composition through intervention in natural flow patterns and changes in land use. J Hydrol 134:297–313.

Smith, J.W., 1983. The Chemistry which Created Green River Formation Oil Shale. Symposium on Geochemistry and Chemistry of Oil Shale and Petroleum Chemistry Inc. American Chemical Society, Seattle Meeting, March 20-25, 1983. p. 76-84.

Smith, J.W., Milton, C., 1966. Dawsonite in the Green River formation of Colorado. Economic Geology, 61(6): 1029-1042.

Smith, M.E., Carroll, A.R., Scott, J.J., Singer, B.S., 2014. Early Eocene carbon isotope excursions and landscape destabilization at eccentricity minima: Green River Formation of Wyoming. Earth and Planetary Science Letters, 403: 393-406.

Smith, M.E., Carroll, A.R., Singer, B.S., 2008. Synoptic reconstruction of a major ancient lake system: Eocene Green River Formation, western United States. GSA bulletin, 120(1-2): 54-84.

Smith, M.E., Chamberlain, K., Singer, B., Carroll, A., 2010. Eocene clocks agree: Coeval 40Ar/39Ar, U-Pb, and astronomical ages from the Green River Formation. Geology, 38(6): 527-530.

Steinhorst, R.K., Williams, R.E., 1985. Discrimination of groundwater sources using cluster analysis, MANOVA, canonical analysis and discriminant analysis. Water Resources Res 21:1149–1156.

Surdam, R.C., Parker, R.D., 1972. Authigenic aluminosilicate minerals in the tuffaceous rocks of the Green River Formation, Wyoming. Geological Society of America Bulletin, 83(3): 689-700.

Suriamin, 2010. Facies, diagenesis, and geochemistry of the Eocene Green River Formation carbonates in the Piceance Creek basin, Colorado, Colorado School of Mines, Golden, CO, 107p.

Tänavsuu-Milkeviciene, K., Sarg, J.F., 2012. Evolution of an organic-rich lake basin–stratigraphy, climate and tectonics: Piceance Creek basin, Eocene Green River Formation. Sedimentology, 59(6): 1735-1768.

Tänavsuu-Milkeviciene, K., Sarg, J.F., 2010. Rich and lean oil shale deposits, link to climate changes: Piceance Creek Basin, Eocene, Colorado, U.S.A, 30th Oil Shale Symposium, Golden, Colorado, U.S.A.

Tänavsuu-Milkeviciene, K., Sarg, J.F., Bartov, Y., 2017. Depositional Cycles and Sequences In An Organic-Rich Lake Basin: Eocene Green River Formation, Lake Uinta, Colorado and Utah, USA. Journal of Sedimentary Research, 87(3): 210-229.

Turner, B., 2016. Utilization of chemostratigraphic proxies for generating and refining sequence stratigraphic frameworks in mudrocks and shales, University of Oklahoma, Norman, OK, 135p.

Turner, A.K. & Closs, L.G. 2009. Cluster Analysis. *GEGN 532: Geological Data Analysis*. Colorado School of Mines Lecture, April 14, 2009.

Tuttle, M.L. 2009, A collection of chemical, mineralogical, and stable isotopic compositional data for Green River oil shale from depositional center cores in Colorado, Utah, and Wyoming: U.S. Geological Survey Open-File Report 2009–1274, 18 p.

USGS MRP, 2019a: 60 Elements by ICP-OES-MS, Na2OFusion Method, https://www.usgs.gov/media/files/60-elements-icp-oes-ms-na2o-fusion-method

USGS MRP, 2019b: Development of USGS Geochemical Reference Materials, https://www.usgs.gov/centers/gggsc/science/development-usgs-geochemical-reference-materials?qt-science_center_objects=0#qt-science_center_objects

Ward Jr, J.H., 1963. Hierarchical grouping to optimize an objective function. Journal of the American Statistical Association, 58(301): 236-244.

Zachos, J., Pagani, M., Sloan, L., Thomas, E., Billups, K., 2001. Trends, rhythms, and aberrations in global climate 65 Ma to present. Science, 292(5517): 686-693.

Zachos, J.C., Dickens, G.R., Zeebe, R.E., 2008. An early Cenozoic perspective on greenhouse warming and carbon-cycle dynamics. Nature, 451(7176): 279.

# Chapter 4: Variations in Water Chemistry of Eocene Lake Uinta derived from mineral assemblages in the Green River Formation, Piceance Basin, Colorado

Tengfei Wu[1], Jeremy Boak[2], Justin Birdwell[3]

1. School of Geosciences, University of Oklahoma

2. Hurricane Peak Geosciences, Littleton, CO

3. U.S. Geological Survey, Denver

## Abstract

The Green River Formation of Colorado was deposited in a large lake, Lake Uinta, during the Eocene Epoch. Mineral distributions show temporal and spatial variations throughout Lake Uinta's existence, and across the Piceance Basin, wherein the basin center was enriched in saline minerals, including nahcolite ($NaHCO_3$), dawsonite ($NaAl(CO_3)(OH)_2$), and halite (NaCl) and the basin margin was characterized by analcime ($NaAlSi_2O_6 \cdot H_2O$), and clay minerals, primarily illite, as defined by others (Poole, 2014; Boak and Poole, 2015; Birdwell et al., 2019).

Major changes in mineral assemblages and relative mineral proportions occur in the basin center, which help to divide the stratigraphic column into three distinct mineral units, bounded by two transitional zones. The lower mineralogic unit (LMU) of Poole (2014) and Boak and Poole (2015) contains illite with albite and potassium feldspar. The lower transition zone is characterized by sharp reduction in illite and increases in dawsonite and feldspars. The middle mineralogic unit (MMU) shows little or no illite, but greater amounts of feldspar and dawsonite, and, within the unit, the beginning of nahcolite precipitation. The upper transition zone is characterized by a sharp reduction in dawsonite, but with further increase in feldspar and recurrence of illite. The upper

mineralogic unit (UMU) is characterized by increased feldspar, the recurrence of illite and analcime, and continued deposition of nahcolite without dawsonite.

Calculation of indicator mineral stability diagrams were performed using estimated values and ranges of silica activity, pH, activity of sodium and potassium, and $CO_2$ content in the aqueous system. The estimated water conditions are:

1. *Douglas Pass (lowermost)*: pH = 7; $Na^+$ = 2,300 ppm; $[SiO_2]aq$ =9.5 ppm, $K^+/H^+$ = 4; at a $CO_2$ content of ~0.6 ppm , under P= 1 atm, and T=25°C;
2. *Douglas Pass (upper):* pH = 8; $Na^+$ = 46,000 ppm; $[SiO_2]aq$ =3.9 ppm, $K^+/H^+$ = 4, at $CO_{2,aq}$ ~ 0.6 ppm, under P= 1 atm, and T=25°C
3. *LMU*: pH=8, $Na^+$ = 7,200 ppm, $[SiO_2]aq$ =10.6 ppm, $K^+/H^+$ = 4, $CO_{2,aq}$ ~ 3ppm, given the condition P= 1 atm and T=25°C;
4. *MMU*: pH of ~9-10, $Na^+$ ~36,500 - ~58,000 ppm, $SiO_2$~ 7.5 ppm, at $CO_{2,aq}$ 5 ppm-10ppm, under P= 10 atm, and T=25°C;
5. *UMU*: pH=8, $Na^+$ = 51,000 ppm, $[SiO_2]aq$ = 4.8 ppm, at $CO_{2,aq}$ ~ 5 ppm, when P= 10 atm and T=25°C.

Silica activity, salinity, and $CO_2$ concentration are the key parameters to determine the stability of dawsonite, the appearance and disappearance of which act as indicators of shifts in the water chemistry of the deep basin center. Mineral stability diagrams are proven to be a feasible way to characterize the water chemistry more quantitatively in the lacustrine system.

In addition, inferred $CO_2$ concentrations may reflect levels above those expected for water equilibrated with the atmosphere and may reflect $CO_2$ released by organic degradation and closed-basin alkalinity that accumulates through hydrolysis and increased pH. Differences in the degree of organic matter production/oxidation might possibly explain the absence of nahcolite and the

presence of trona in Lake Gosiute. Our study indicates that dissolved $CO_2$ in the system is a combined effect of atmospheric input, biological metabolism and carbonate precipitation. In addition, the higher salinity in the basin margin when analcime is stable, at the intial stage, further support our finding in the previous chapter that elevated salinity occurs in the basin margin first and then high salinity was transported into the basin center by density flow.

## Introduction

The Green River Formation (GRF) of the Piceance Basin in northwestern Colorado contains the largest oil shale deposit in the world with 1.53 trillion barrels of total oil in-place, based on Fischer assay analyses (Johnson et al., 2010a, b). It has also has gained interest for associated saline mineral resources in the oil shale formation, like nahcolite ($NaHCO_3$) and dawsonite ($NaAl(CO_3)(OH)_2$) deposits, which are sources for soda ash (currently solution mined) and aluminum (potentially co-produced with shale oil), respectively (Hite and Dyni, 1967; Milton, 1971; Brobst and Tucker, 1973; Robb and Smith, 1974; Smith, 1983; Mason, 2007; Johnson et al., 2010a; Feng, 2011; Poole, 2014; Boak and Poole, 2015; Birdwell et al., 2018). The abundant mineral resources and rich organic matter in the Piceance basin make it a critical target for exploration and research into exploitation of oil shale resources (Brownfield et al., 2005; Dyni, 2006; Johnson et al., 2010a). Understanding the conditions under which such a rich and mineralogically unusual petroleum source rock was formed may assist in our knowledge of what Lake Uinta was like, and may also provide insight into this and other, more broadly distributed source rock formations, as well as into the Eocene environment.

The variations of mineral associations and organic content from the basin margin to basin center and through time reflect the water chemistry when those minerals and organic matter were

deposited and preserved (Smith and Robb, 1973; Eugster, 1980; Dyni, 1998; Last and Ginn, 2005; Poole, 2014; Birdwell et al., 2019). The distribution of major minerals in the GRF of the Piceance Basin provides valuable information about temporal changes in lake conditions in the Piceance Basin (Smith, 1974; Eugster and Hardie, 1978; Smith, 1983; Malicse, 2011; Boak et al., 2013; Poole, 2014; Boak and Poole, 2015; Boak et al., 2016), and potentially more broadly in the Eocene Epoch (Eugster, 1980; Last and Ginn, 2005). In addition, mineral occurrence maps in different oil shale zones generated from an extensive bulk X-ray diffraction (XRD) database in the GRF for Piceance Basin (Johnson et al., 2017; Johnson and Brownfield, 2013; Birdwell et al., 2019), extend the spatial component of mineral distribution and chemical conditions of the Piceance Basin paleolake.

Surdam and Parker (1972) inferred the water chemistry for the Green River Formation in Wyoming, which were deposited in Lake Gosiute over much the same time interval as in Lake Uinta (as summarized in Johnson, et al., 2018). They did so by modeling the stability of authigenic minerals formed in volcanic tuffs deposited in the lake, including montmorillonite, analcime, and potassium feldspar. Their calculations defined likely conditions at three stages of lake history in terms of pH, salinity ($Na^+$, $K^+$), and silica activity. These quantitative estimates of water conditions in Lake Gosiute form the model for this effort to identify likely conditions of deposition in the Piceance Basin portion of Lake Uinta, the richest part of the GRF.

However, volcanic tuffs are much more sparsely distributed in the Lake Uinta portion of the Green River Formation, as noted by Johnson et al. (2019). Thus, the approach of Surdam and Parker, using single indicator minerals in altered tuff, could not be applied. The saline minerals nahcolite and particularly dawsonite may be used to delineate conditions in certain stages of the evolution of Lake Uinta, as defined by Poole (2014) and Boak and Poole (2015). An additional

parameter, the concentration of $CO_2$ in the lake water, needed to be evaluated. With this additional parameter, it is also be possible to provide a preliminary evaluation of the differences between the saline minerals deposited in the two lakes (Gosiute and Uinta).

In addition, Jagniecki et al (2015) estimated the Eocene atmospheric $CO_2$ from the nahcolite stability diagram, based on the assumption that nahcolite in Lake Uinta formed in equilibrium with atmospheric $CO_2$. This condition places a constraint on the $CO_2$ partial pressure in the atmosphere from 680 ppm (below which trona or natron are the stable phases) to 1260 ppm (below which trona is stable at the maximum inferred temperature for Lake Uinta), although $CO_2$ partial pressure could have been still higher. They argued that the co-precipitation of halite and nahcolite took place at the air-water interface of a hypersaline lake, in contact with the atmosphere (Jagniecki et al., 2015).

Lake Gosiute is characterized by the presence of substantial deposits of trona ($Na_2CO_3 \bullet NaHCO_3 \bullet 2H_2O$), which forms under different chemical conditions, mainly a lower $CO_2$ concentration at a given temperature (Jagniecki and Lowenstein, 2015) than nahcolite. If equilibrium between the atmosphere and Lake Uinta was reached at that time, then regionally adjacent Lake Gosiute should also reach such a condition and similar saline minerals should also be observed or identified in Wyoming. Lake Uinta is interpreted as having been stratified for much of its history (Bradley and Eugster,1969; Desborough, 1978; Johnson, 1981, 1985; Tänavsuu-Milkeviciene et al., 2012), whereas Lake Gosiute is variously interpreted as a shallow or intermediate depth lake. If precipitation of the saline minerals might have occurred beneath a chemocline in the Piceance Basin, the $CO_2$ content might not be in equilibrium with the Eocene atmosphere, whatever its $CO_2$ content. The absence of any significant remnant of nahcolite in basin

margin sediment raises questions about the formation of nahcolite by evaporation at the air-water interface, which should have occurred in marginal areas as well.

The objective of this study was to simulate the water chemistry conditions based on the authigenic mineral assemblages in different lake stages and mineral units identified by Boak et al (2013), serving as a supplement to studies done by Poole (2014), Boak and Poole (2015) and Birdwell et al (2019). Based on the key minerals identified from previous studies, including analcime, illite, albite, K-feldspar, nahcolite, and dawsonite, we discuss how those minerals are related to water chemistry in Lake Uinta. Mineral stability diagrams were created using Geochemist's Workbench$^{TM}$ to provide quantitative estimates of the water compositions in terms of pH-a$CO_2$-a$SiO_2$-a$Na^+$-a$K^+$. The water chemistry inferred from those mineral assemblages is used to refine our understanding of lake evolution in the Eocene time.

## Geologic Setting

### History of Lake Uinta

The Piceance Basin is a typical asymmetric Rocky Mountain basin and started to subside approximately 65 Ma during the early part of the Laramide Orogeny (Fig. 4.1) (Gries, 1983; Young, 1995b). The Piceance Basin is bounded on the north by the Uinta uplift and the Axial Basin anticline, on the east by the White River uplift, and on the south by the Uncompahgre uplifts, and on the west by the Douglas Creek Arch (Johnson, 1985; Young, 1995b). Deposition of the GRF lacustrine sediments took place over a period of 5 Myr, between *ca* 53 and *ca* 48 Ma (Smith et al., 2008; 2010). Lake Uinta formed when two largely separate fresh-water lakes that continuously occupied the Uinta Basin and the Piceance Basin across the crest of the Douglas Creek arch merged into one large lake during the Long Point transgression (Surdam and Stanley,

1980; Smith et al., 2008). but for most of their history, these lacustrine systems developed and evolved differently as separate lakes, and were only connected periodically (Smith et al., 2008). Following the Long Point transgression, the newly enlarged lake had two deep depocenters inherited from earlier freshwater lakes, with one in the north-central part of the Piceance Basin and the other along the northern trough of the Uinta Basin, (Birdwell et al., 2019). These depocenters were continuously occupied by lakes throughout their histories until they were filled from the north by volcaniclastic sediments (Young,1995b; Birdwell et al., 2019).

The salinity in Lake Uinta increased after the transgression, which killed the freshwater mollusk population and ultimately reached hypersaline conditions, depositing large amounts of nahcolite and halite in the Piceance Basin (Johnson, 1985). Offshore lacustrine rocks deposited in the Piceance Basin after the Long Point transgression are composed of organic-rich mudstone that contain enough organic matter to be considered economically viable oil shale (Birdwell et al., 2019).

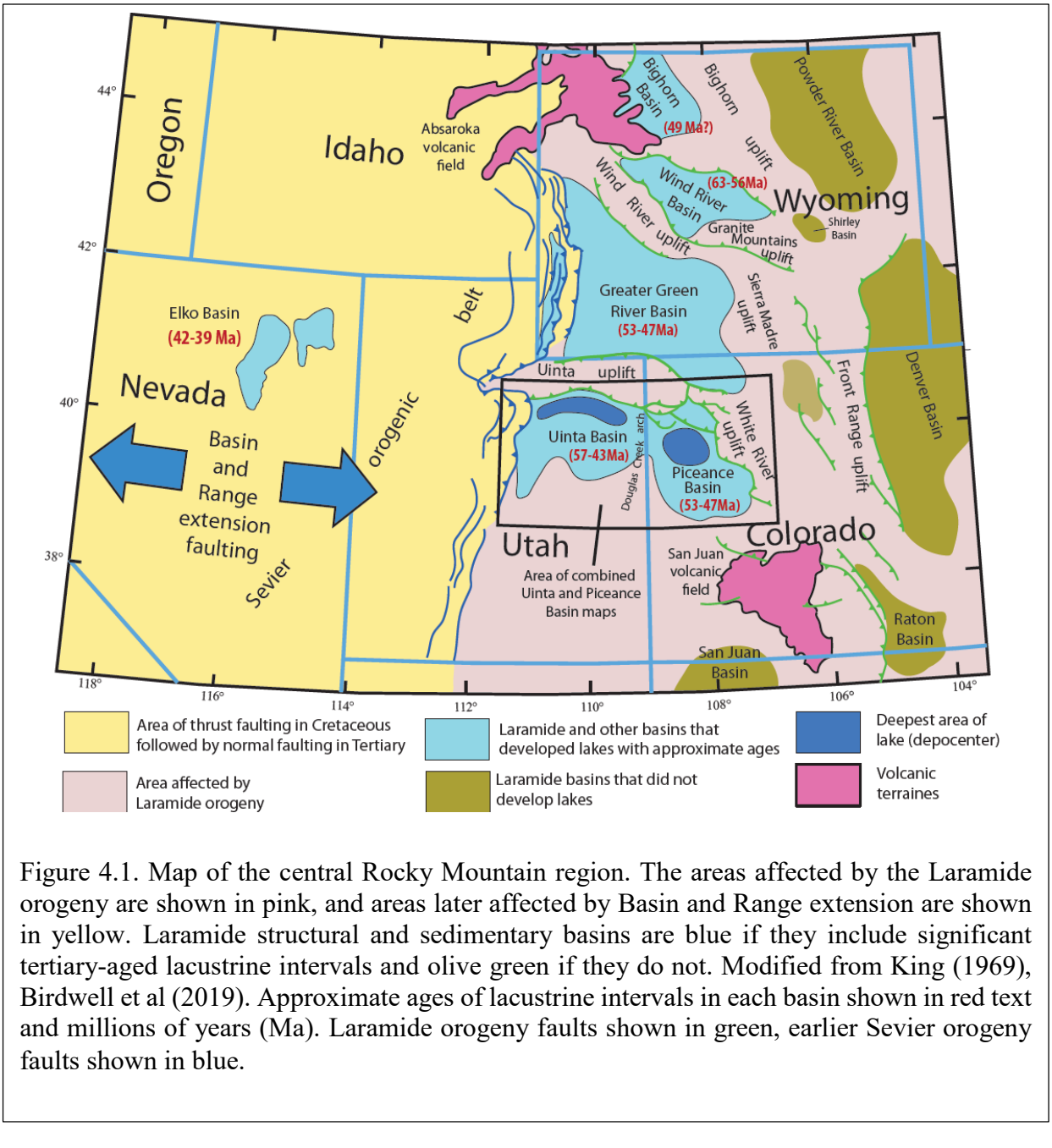



Figure 4.1. Map of the central Rocky Mountain region. The areas affected by the Laramide orogeny are shown in pink, and areas later affected by Basin and Range extension are shown in yellow. Laramide structural and sedimentary basins are blue if they include significant tertiary-aged lacustrine intervals and olive green if they do not. Modified from King (1969), Birdwell et al (2019). Approximate ages of lacustrine intervals in each basin shown in red text and millions of years (Ma). Laramide orogeny faults shown in green, earlier Sevier orogeny faults shown in blue.

Johnson (1981) concluded, on the basis of the height of a prograding delta deposited as the lake was filled from the north late in its history, that lake depth potentially reached 1000 feet, which is much deeper than some researchers suggest (Bradley and Eugster, 1969; Tänavsuu-

Milkeviciene and Sarg, 2012). Deposition of thousands of feet of fine-grained, organic-rich sediment with little sandstone and siltstone in the depocenter may further support this conclusion.

Stratigraphy of the GRF

The Green River Formation in the Piceance Basin has been subdivided into several members and smaller units, based on rock type and 17 rich and lean zones based on organic richness (Cashion and Donnell, 1970, 1972). The rich and lean oil shale zones mark time-stratigraphic units. The Garden Gulch Member forms the lower portion of the Green River Formation, consisting of alternating organic-rich and organic-poor illitic oil shale deposits. The thickest and most widespread part of the Green River Formation, the Parachute Creek Member, formed as deep-water, organic-rich and organic-poor feldspathic dolomitic mudstones, with bedded and disseminated evaporites (halite, nahcolite, dawsonite, shortite) (Bradley, 1931; Dyni, 1996, Boak et al. 2013). In the Piceance basin, most of the Parachute Creek Member contains various amounts of evaporite minerals, including dawsonite, nahcolite and halite (Dyni, 1981; Jagniecki and Lowenstein, 2015).

The Green River Formation in the Piceance Basin is subdivided into six lake stages by Tanavsuu-Milkeviciene and Sarg (2012), which reflect variations in facies association distribution, richness of oil shale, water chemistry, degrees of lake restriction and salinity, and siliciclastic sediment input. Johnson (1985) subdivided the history of the Piceance basin into five time-stratigraphic lake stages, based on rock type, and rich and lean oil shale zones, which are different from those of Tanavsuu-Milkeviciene and Sarg (2012), shown in Table 4.1. Boak et al.(2013) subdivided the Green River Formation into three mineralogical units in the basin center, based on changes of mineral assemblages in different stages.

**Table 4.1.** Stratigraphy of the Eocene Green River Formation, rich and lean oil shale zones (Cashion and Donnell, 1970, 1972), stages of Johnson (1985), Lake Stages of Tänavsuu-Milkeviciene and Sarg (2012), and mineralogic units defined in Boak et al. (2013).

| | Stratigraphic nomenclature for oil shale zones; stages of Johnson (1985) | | | Lake Stages of Tanavsuu-Milkeviciene and Sarg (2012) | | Mineralogic Units of Boak et al. (2013) |
|---|---|---|---|---|---|---|
| Green River Formation | Parachute Creek Member | Stage 5 | Top bed 76 - top Porcupine tuff | Stage 6 | Closing Lake | Upper Mineralogic Unit |
| | | | Porcupine Tuff | | | |
| | | | Base Porcupine tuff – top Bed 44 | | | |
| | | | Top Bed 44 – top A-groove | | | |
| | | | A-groove | | | |
| | | | Mahogany zone | Stage 5 | High Lake | |
| | | Stage 4 | B-groove | Stage 4 | Rising Lake | |
| | | | R-6 zone | | | |
| | | | L-5 zone | Stage 3 | Highly Fluctuating Lake | |
| | | | R-5 zone | | | Middle Mineralogic Unit |
| | | | L-4 zone | | | |
| | | Stage 3 | R-4 zone | | | |
| | | | L-3 zone | Stage 2 | Transitional Lake | |
| | | | R-3 zone | | | |
| | | | L-2 zone | | | |
| | | | R-2 zone | | | |
| | Garden Gulch Member | Stage 2 | L-1 zone | | | Lower Mineralogic unit |
| | | | R-1 zone | Stage 1 | Fresh to Brackish Lake | |
| | | Stage 1 | L-0 zone | | | |
| | | | R-0 zone | | | |

## Summary of Mineral Distributions

Birdwell et al. (2019) summarized the occurrences of key minerals by stratigraphic unit from six wells spanning a rough north-south cross section, from the depocenter to the basin margin (Fig.4.2). These cores included the key minerals and comprised large numbers of analyzed

samples so that they could represent the distributions and occurrences of those indicator minerals in the Piceance Basin (Birdwell et al., 2019). For the cores near the basin center, dawsonite occurs in the R2 zone and continues until R5; nahcolite occurs after dawsonite and also terminates at R5, probably due to leaching by groundwater in L5 and above (Birdwell et al., 2019). Moving away from the depocenter, the nahcolite and dawsonite occurrences become less frequent and illite, albite and analcime become more common (Fig.4.2), consistent with the observations from Poole (2014) and Boak and Poole (2015). These indicator mineral relative occurrence frequencies show stratigraphic shifts which are consistent with the three mineralogic units identified by Boak et al. (2013). The three mineralogic units are classified based on two transition zones: 1) the lower transition zone is characterized by sharp decrease of clay minerals and occurrence of dawsonite in the R2 zone; and 2) the upper transition zone is characterized by sharp reduction in dawsonite at or near the top of the R5 zone in the basin center.

In the Lower Mineral Unit (LMU), clay minerals, feldspar, quartz and dolomite are abundant without additional saline minerals. In the Middle Mineral Unit (MMU), the most distinct feature is that dawsonite and nahcolite are common and abundant, without clay minerals. In the Upper Mineral Unit (UMU), clay minerals, calcite and feldspar increase compared to MMU. Poole (2014) identified the authigenic minerals from the Green River Formation of the Piceance Basin, including nahcolite, precipitated from the water column or interstitial water layer, and dawsonite, analcime, albite, k-feldspar and illite, formed at and below the sediment-water interface. To determine constraints on water composition based on those authigenic mineral assemblages in the key stratigraphic zones is critical to our understanding of the paleolake water chemical evolution.

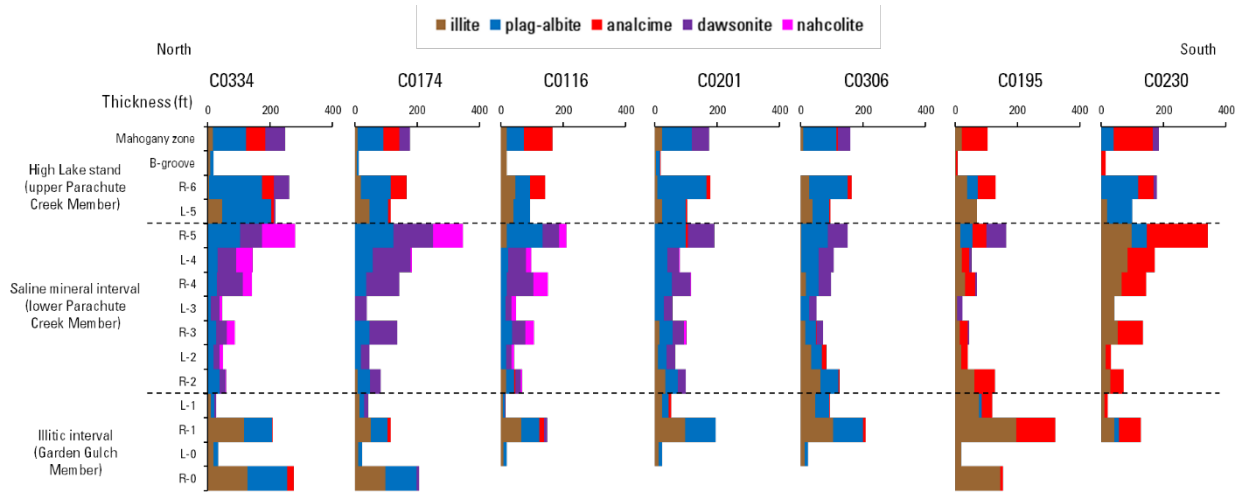



Fig. 4.2. North-South cross-section showing the transition in indicator mineral occurrences and oil shale thickness for the Green River Formation across the Piceance Basin for the oil shale strata between the base of the R-0 zone and the top of the Mahogany zone. Stacked, colored bars indicate the relative abundance of each mineral within each zone. Figure reproduced from Birdwell et al (2019).

## Methods

This study attempted to describe the water conditions in the Piceance Basin part of Lake Uinta in the three mineralogic units defined by Poole (2014) and Boak and Poole (2015). To do this, we depicted the equilibria among illite, K-feldspar, albite, analcime, dawsonite, and nahcolite in the system $Na_2O$-$K_2O$-$Al_2O_3$-$SiO_2$-$H_2O$-$CO_2$ in terms of log $K^+/H^+$, log $Na^+/H^+$, log $SiO_2$ and $CO_2$ fugacity, at 25°C and 1~10 atm. Geochemist's Workbench™ was the software used to create the mineral stability diagrams; detailed information about this software can be found at their website: https://gwb.com/. All the thermodynamic data for each species in the activity diagrams by the Geochemist's Workbench™ were from the thermo.tdat dataset.

To simplify the description of water chemistry through lake evolution, only the listed indicator minerals are discussed and evaluated. To create mineral stability diagrams that represent this multi-component system in two dimensional diagrams, certain assumptions about initial conditions need to be input into the software. We have to a large extent followed the lead of Surdam and Parker (1972) but depart from the values they used (for example, for $aK^+/aH^+$) where

those values do not accord with the mineral assemblages in the Piceance Basin. Based on the similar mineral assemblages in the initial stage of lake development between Lake Uinta and Lake Gosiute, we applied the water conditions of the fresh to brackish lake stage of Lake Gosiute in Surdam and Parker (1972) to Lake Uinta in terms of $SiO_2$, $K^+$, $Na^+$, and pH. Another assumption we have made here is that air-water $CO_2$ exchange in saline lakes is generally not at equilibrium, with an average ratio of the water to air $pCO_2$ ~5.07, derived from a compilation of published data for 196 saline lakes around the world (Duarte et al., 2008) and the ratio is only applied to the LMU and MMU of the basin center.

Throughout we have used muscovite as a surrogate for illite, whose composition varies substantially and for which we do not have a basin specific composition and relevant thermodynamic data. The mineral diagrams for the basin margin and Lower Mineralogic Unit in the basin center reflect the presence of illite, albite, and k-feldspar as potentially original detrital phases, but also as potential authigenic phases, and analcime as an authigenic phase. Birdwell et al. (2019) suggest that albite may be primarily authigenic. The mineral diagram for the Middle Mineralogic Unit reflects the presence of dawsonite, albite, and k-feldspar as authigenic phases, the disappearance of illite, and the addition of nahcolite partway through the deposition of this interval. The mineral diagrams for the Upper Mineralogic Unit reflect the disappearance of dawsonite, the continued presence of nahcolite, and the reappearance of analcime and illite.

## Results and Discussion

### The initial parameters in the system

Surdam and Parker (1972) carried out the study on authigenic aluminosilicate minerals altered from volcanic tuff in the GRF in Wyoming and depicted the water chemistry changes in Lake Gosiute based on the mineral assemblages in different lake stages. They concluded that lake

water ranged from fresh or brackish at a pH of 8.0 to hypersaline, with Na and $SiO_2$ reaching 100,000 ppm and 1,000 ppm, respectively, at a pH of 9.0 to 10.0 during the most saline and alkaline stage when trona was stable (Surdam and Parker, 1972). The work by Surdam and Parker (1972) lays a solid foundation for our research and provides a basic guide for us to follow: we make an assumption that similar mineral assemblages represent similar water chemistry during which those minerals were formed and stable in the Green River Formation deposited in both lakes, but with different mineral facies on their own.

Based on these assumptions, we are able to estimate water chemistry from our mineral dataset in different stratigraphic zones and the transition zones between them. During the fresh-brackish lake stage, especially when analcime was formed and stable, we assume the initial water chemistry from Lake Uinta is similar to Lake Gosiute, therefore, we apply the water chemistry variables in Lake Gosiute in our system: $SiO_2$ = 10 ppm, K= 50 ppm, Na=1,000 ppm and pH =8.0 as the fresh-water stage. When the salinity and alkalinity increased, analcime was formed and illite was abundant. The derived Na reached around 46,000 ppm, and the water is considered to be hypersaline. The saline condition at this period is similar to the water composition in Lake Gosiute when analcime was deposited during early Wilkins Peak time (Surdam and Parker, 1972).

However, later on, as the lake continued to evolve, the water chemistry in the two lakes diverged from each other, as indicated by the unique mineral assemblages in the two areas. The widespread dawsonite + nahcolite in the Piceance Basin is not found in Lake Gosiute, and trona is not found in Lake Uinta, indicating different water chemistry between the two lakes. As the water becomes more saline and alkaline, illite is not stable. In the lower transition zone of the basin center, illite is altered to feldspar, analcime was no longer stable, and dawsonite appears, indicating increasing $CO_2$ in the system. Based on the study of nahcolite stability by Jagniecki et al. (2015),

the estimated $CO_2$ content of the atmosphere when nahcolite is stable ranges from a lower limit of 680 ppm to an upper limit of 1260 ppm, and we are using these values as a control for nahcolite mineral stability, because the assumption that atmospheric air reaches an equilibrium with the lake in the Eocene time is made. However, in order to generate appropriate stability of dawsonite plus nahcolite, an average ratio (~5.07) of water to air partial pressure of $CO_2$ is assumed, suggesting lack of mixing and equilibrium in the stratified lake with atmospheric $CO_2$ and an overall lakewater enrichment in carbon dioxide, as is common for alkaline saline lakes (Duarte et al., 2008).

Origin of Analcime

Analcime is very common and widespread in the basin margin. It only occurs in the LMU and UMU at a very small proportion compared to other minerals in the basin center. Birdwell et al (2019) indicate that analcime occurs in the basin margin more frequently than in the basin center, and in the earliest stages of both regions.

Analcime was initially thought to be associated with the interaction with volcanic ash in saline lake water (Bradley, 1929; 1931; Surdam and Parker, 1972), which is not the case in our study area. Previous studies have suggested that analcime in the Green River Formation did not have to form from precursor zeolites derived from vitric material (Remy and Ferrell, 1989; Poole, 2014; Birdwell et al., 2019). Instead, analcime was considered to form as an alteration product of clays deposited in a saline, alkaline lake, based on clay mineral distributions across the Uinta and Piceance basins (Hay and Guldman, 1986; Remy and Ferrell, 1989; Poole, 2014; Birdwell et al., 2019). A possible reaction forming analcime from illite might take the form of:

$$KAl_3Si_3O_{10}(OH)_2 + 3SiO_2 + 3Na^+ \leftrightarrow 3NaAlSi_2O_6 \bullet H_2O + K^+ + 2H^+ \quad (1)$$

The equation indicates that formation of analcime is favored by increased salinity, pH and silica activity. Similar reactions may be written to create feldspar from illite.

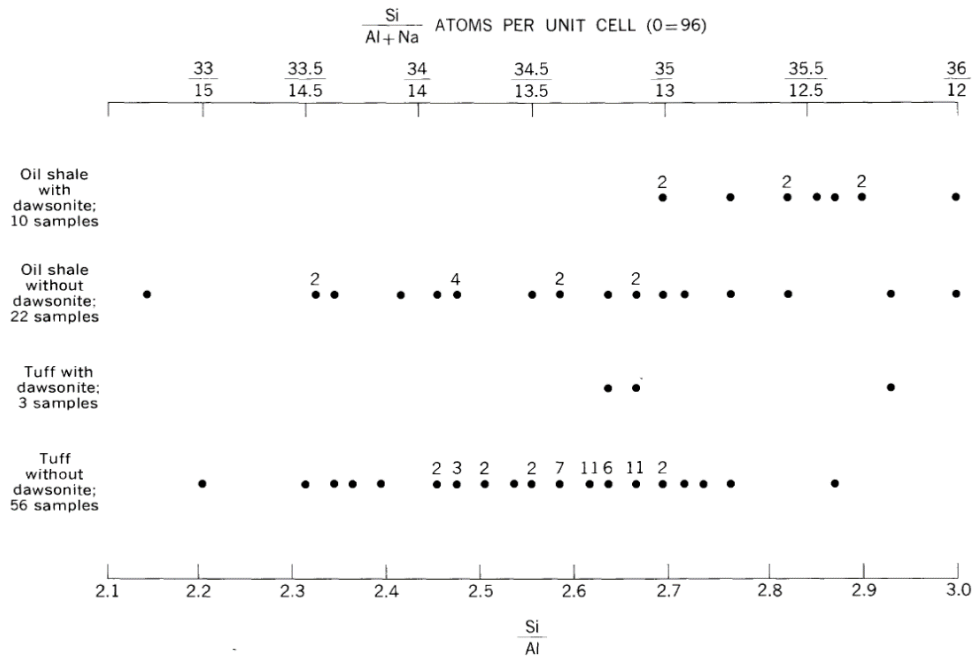



Fig. 4.3. Ratios of silicon to aluminum and silicon to aluminum plus sodium in analcime from 91 samples with and without dawsonite, Parachute Member. Numbers next to dots indicate number of samples plotted at that position. Figure reproduced from Brobst and Tucker (1973).

Brobst and Tucker (1973) stated dawsonite formed diagenetically from analcime based on the relations of analcime, dawsonite, and quartz in the exposed rocks. According to Brobst and Tucker (1973), analcime in rocks containing dawsonite has a higher silicon to aluminum ratio than analcime in rocks without dawsonite, shown in Fig.4.3. The Si/Al ratio of analcime is an important parameter, because it provides information on the conditions under which the analcime formed (Mariner and Surdam, 1970; Surdam, 1977; Remy and Ferrell, 1989). Analcime has an ideal structural formula of $NaAlSi_2O_6 \cdot H_2O$, with an ideal Si/Al ratio of 2.0. However, the structural formula and Si/Al ratio of natural analcime varies widely and analcime crystals from sediments in the Green River Formation of Piceance Basin, exhibiting a range of Si/Al ratios from 2.1 to 3.0 (Brobst and Tucker, 1973). The analcime samples from mudstones of the Green River Formation, Uinta Basin have a low Si/Al ratio (< 2.31) (Remy and Ferrell, 1989). These analcime samples reflects that detrital clays altered in a saline and alkaline environment, and thereby provide a source

of Si and Al for the formation of analcime, based on illite-illite/smectite clay mineral suite in the analcime-rich mudstones (Remy and Ferrell, 1989). In addition, evaporation in the basin margin concentrated the moderately saline and alkaline-lake water, which produced Na-rich brines that enhanced the formation of analcime by accelerating the alteration of detrital clays (Remy and Ferrell, 1989).

Boak et al. (2021) point out that, in the lowest part of the Douglas Pass Green River Formation section (corresponding to the basin margin), Na content is very low, and analcime is absent. Na content increases as analcime appears at the transition from Stage 1 to stage 2, according to Tänavsuu-Milkeviciene and Sarg (2012), or within Stage 1 of Johnson (1985). This change may also be accompanied by a decrease in clay mineral content, although the mineralogic dataset is sparse.

These changes may reflect a very substantial increase in salinity from 2,300 ppm to ~46,000 ppm $Na^+$ as shown in Figure 4.4. We raise $CO_2$ to the equivalent of 400ppm in atmosphere, about 0.6 ppm $[CO_2]$aq at least in the shallow lake. The ellipses show estimated water compositions below and above the increase in Na content and analcime in the section. They reflect the presence of clay minerals (mainly illite and illite/smectite) and feldspar in most samples from the area. Although these minerals are likely mainly detrital in origin, there is no indication that they are breaking down, as occurs with clay minerals later in the basin center. At pH of 7 below and 8 above the transition, with $K^+/H^+$ of 4, $CO_2$ (atm) of 400 ppm = $[CO_2]$ of ~0.6 ppm in the aqueous system. The silica activity in the system is also different when it includes analcime, with

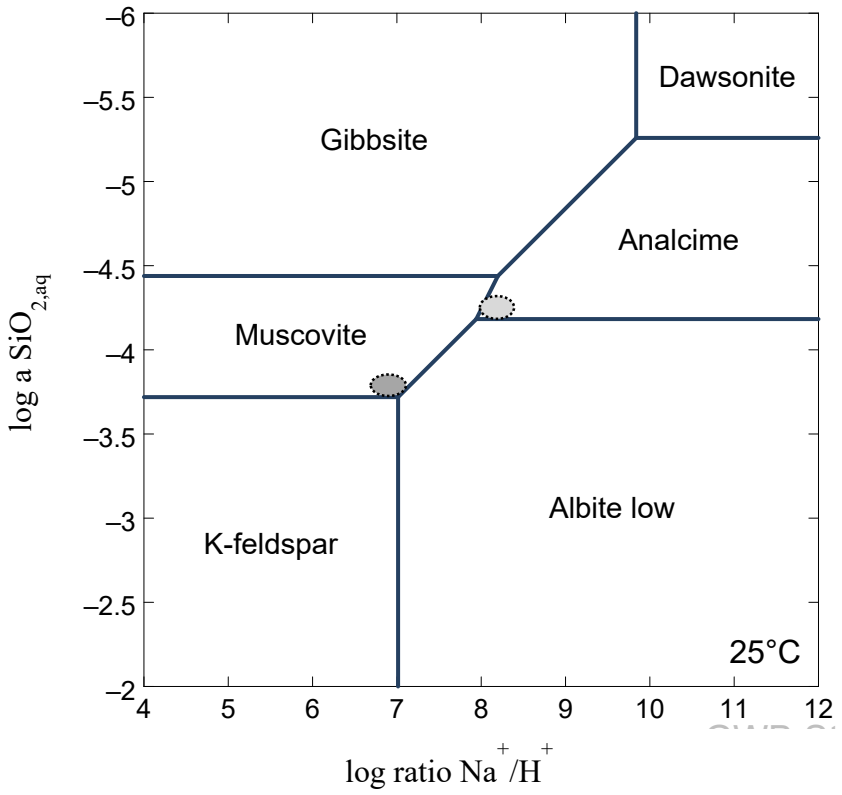



Fig. 4.4. Activity-activity diagram representing the mineral assemblage of the basin margin in the Douglas Pass area. The initial condition set at log $K^+/H^+$ =4, pH=8, T=25 ºC, P=1 bar and $CO_{2,aq}$ is 0.6 ppm; the dashed ellipses represent the water composition early in the basin margin history (darker gray), when analcime did not form, and later, when analcime is abundant (lighter gray). $Na^+$ and $SiO_2$, aq is 2,300 ppm, 9.5 ppm for the darker ellipse and 46,000 ppm, 3.9 ppm for the lighter ellipse, respectively.

$SiO_2$, $_{aq}$ higher (9.5 ppm) without analcime present. As shown in equation (1), elevated salinity and silica activity are required to form analcime from clay minerals (represented by muscovite in Fig. 4.4).

Lower Mineralogic Unit (LMU) water chemistry

Compositions in the lower mineralogic unit are similar to those in the basin margin, although analcime is rare in the wells sampled for this study. Birdwell et al. (2019) indicate that analcime is present in the basin center in the LMU with lesser frequency than in the margin. So, in this unit, the shaded area representing water composition shifts to the left towards the illite stability field. The only clay mineral identified in the LMU is illite, as shown in Fig. 4.5, implying conditions slightly more saline than the condition when analcime is not present, but less saline than the condition under which analcime formed in the basin margin, where a more diverse suite of clay minerals was reported by Poole (2014).

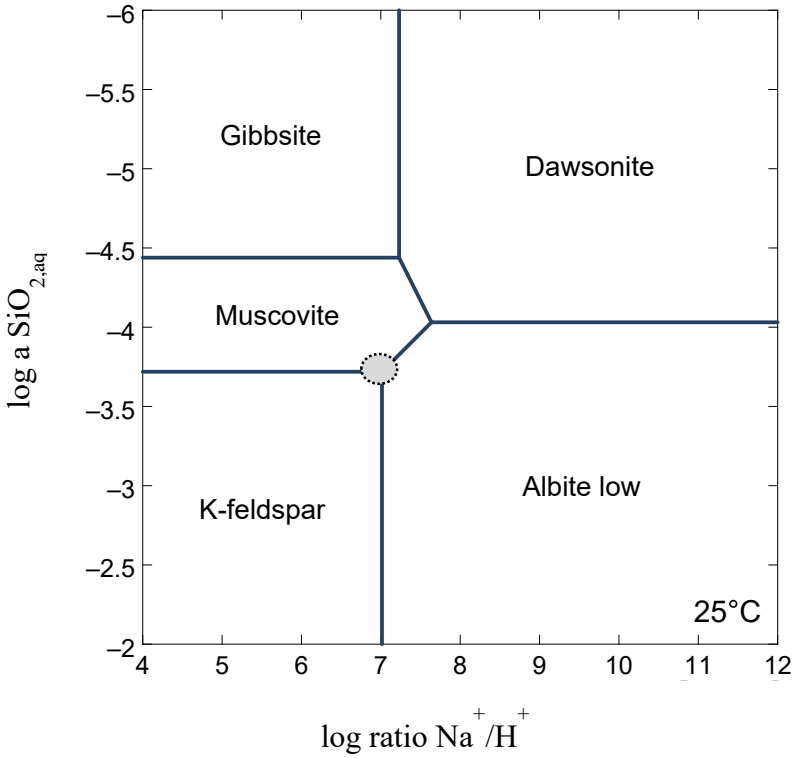


Fig. 4.5. Activity-activity diagram representing the mineral assemblage for the Lower Mineralogic Unit. The initial condition set at log $K^+/H^+$ =4, pH=8, T=25 $^oC$, P=1 bar and $CO_{2,aq}$ is 3 ppm; the dashed ellipses represent the water composition in this unit, shifting left towards the illite field compared to basin margin, with $Na^+$ = 7,200 ppm and $SiO_2$ = 10.6 ppm.

Middle Mineralogic Unit (MMU) water chemistry

Moving into the MMU, illite decreases sharply and dawsonite appears. The formation of dawsonite is favored by increased [$CO_2$]aq, increased salinity, increased pH, and decreased silica activity. The inferred composition is shown in Figure 4.6, where pH = 9, $Na^+$ =36,500 ppm and $SiO_{2,\ aq}$ = 7.5 ppm. The first occurrence of nahcolite is after the appearance of dawsonite, when $CO_2$ in the system reaches around 5.1 ppm, as shown in Fig.4.6.

It is known that silica activity tends to increase with elevated salinity and alkalinity (Surdam and Parker, 1972), and the alteration of illite to feldspar consumes large amounts of silica in the system, which corresponds to quartz decrease in the lower transition zone (Poole, 2014; Boak et al., 2013). Later on, nahcolite is deposited when the salinity, $CO_2$ concentration and alkalinity continues to increase; the dawsonite field will expand to the left at the cost of analcime and illite. As shown in Fig 4.6, when dawsonite is stable, and nahcolite is absent, the estimated Na is 36,500 ppm. The estimated water composition in the presence of dawsonite and nahcolite will be: pH=10, Na=58,000 ppm and $SiO_{2,\ aq}$ = 7.5 ppm. Still, the silica value remains low in the whole MMU, consistent with the mineral data from Poole (2014). The MMU is characterized by the presence of dawsonite and the absence of illite. In addition, both albite and k-feldspar may increase across the transition to this unit. Reactions characterizing this transition zone include:

$$KAl_3Si_3O_{10}(OH)_2 + 6SiO_2 + 2K^+ \leftrightarrow 3KAlSi_3O_8 + 2H^+ \quad (2)$$

$$KAl_3Si_3O_{10}(OH)_2 + 6SiO_2 + 3Na^+ \leftrightarrow 3NaAlSi_3O_8 + K^+ + 2H^+ \quad (3)$$

$$KAl_3Si_3O_{10}(OH)_2 + 2Na^+ + 2H_2O + 2CO_2 \leftrightarrow KAlSi_3O_8 + 2NaAlCO_3(OH)_2 + 2H^+ \quad (4)$$

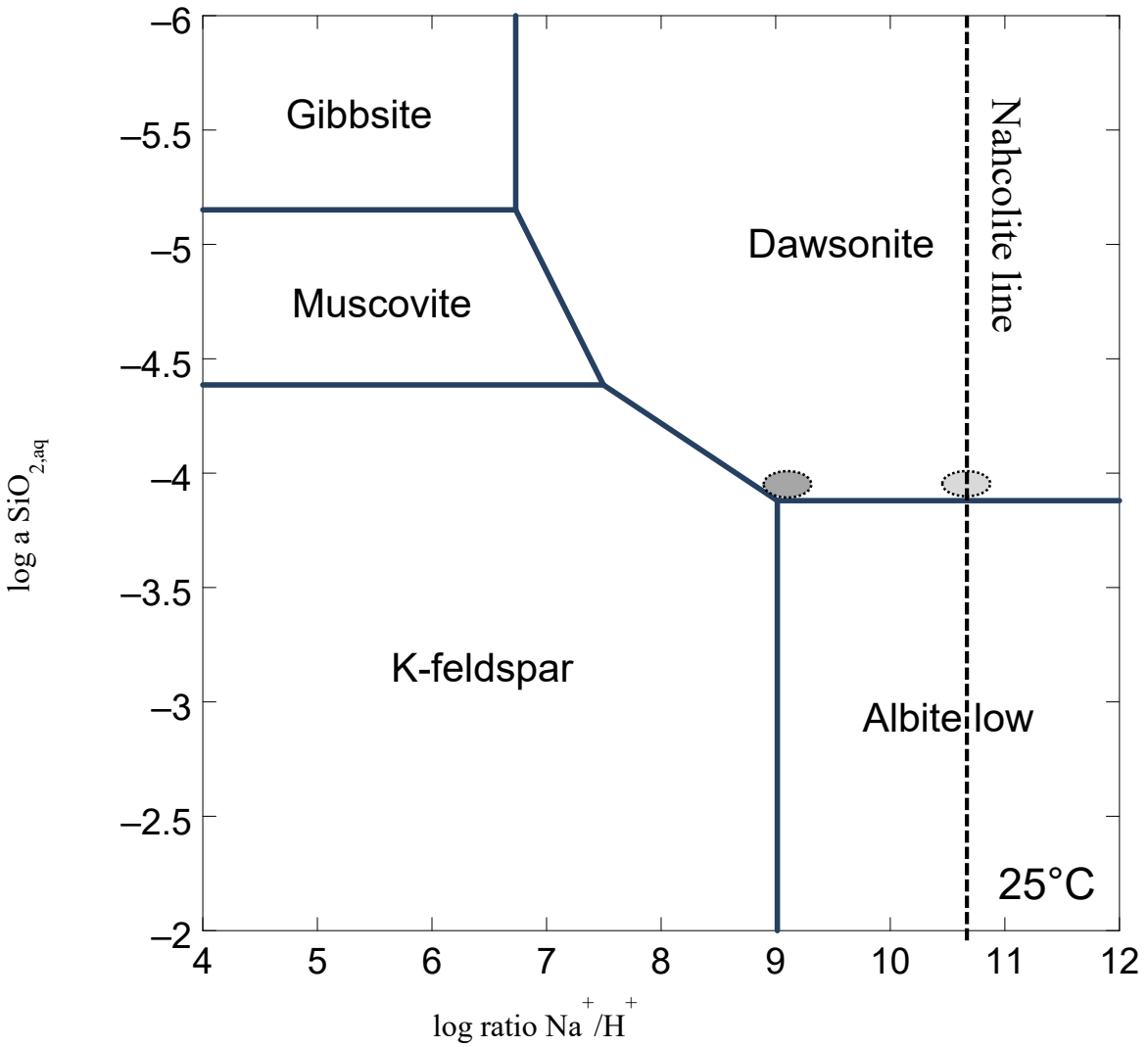



Fig. 4.6. Activity-activity diagram representing the mineral assemblage for the Middle Mineral Unit (MMU), when $CO_{2,\,air}$ is at 680 ppm - 1260 ppm. The diagram was generated in the presence of log $[K^+/H^+]$ =6, pH=10, $CO_{2,\,aq}$=10 ppm, $Na^+$ =58,000 ppm ppm, T =25ºC, P=10 bars. Ellipse (darker grey) represents the water composition when dawsonite occurs and ellipse (lighter grey) represents the water composition when dawsonite and nahcolite are both present. Nahcolite is stable to the right of the nahcolite line.

Upper Mineralogic Unit (UMU) water chemistry

When alkalinity, salinity and $CO_2$ decrease in the upper transition zone, dawsonite and nahcolite are not stable and greatly decrease, as shown in Fig. 4.7. In the UMU, the water composition is: pH=8, Na=51,000 ppm, $SiO_{2,aq}$= 4.8ppm, with most of mineral types similar to

those in the Lower Mineral Unit in the basin center, and the basin margin, except that nahcolite is present in the UMU.

The UMU is characterized by the disappearance (with a short recurrence in R-6) of dawsonite, the continued presence of nahcolite, and the recurrence of both illite and analcime. The disappearance of dawsonite in the UMU is mainly caused by the increase of silica activity in the lake system, as nahcolite continues to form in the lower part of the UMU, which indicates elevated aqueous $CO_2$ concentration persists at that time. The possible reaction defining this transition is as follows:

$$NaAlCO_3(OH)_2 + 2SiO_2 \leftrightarrow NaAlSi_2O_6 \bullet H_2O + CO_2 \quad (5)$$

In the transition to the UMU, quartz, k-feldspar and albite decreased along with dawsonite. This transition suggests that clay breakdown reactions listed above ceased to be as effective during this interval. Malicse (2011) suggests that a major overturn event occurred at this time. If so, conditions appear to have remained highly saline after this overturn, as nahcolite continues to be precipitated. The possible explanation is that, in this stage, silica activity increased, and the elevated silica led to the formation of analcime rather than dawsonite, while $CO_{2,\,aq}$ and salinity remained high, resulting in continued formation of nahcolite. The elevated silica activity will result in the formation of analcime rather than dawsonite with the consumption of $SiO_{2,}$ as the reaction (5) shows. The elevated silica content in analcime is likely to expand the stability field at the expense of albite, allowing analcime to form at higher $CO_2$ activity in the system.

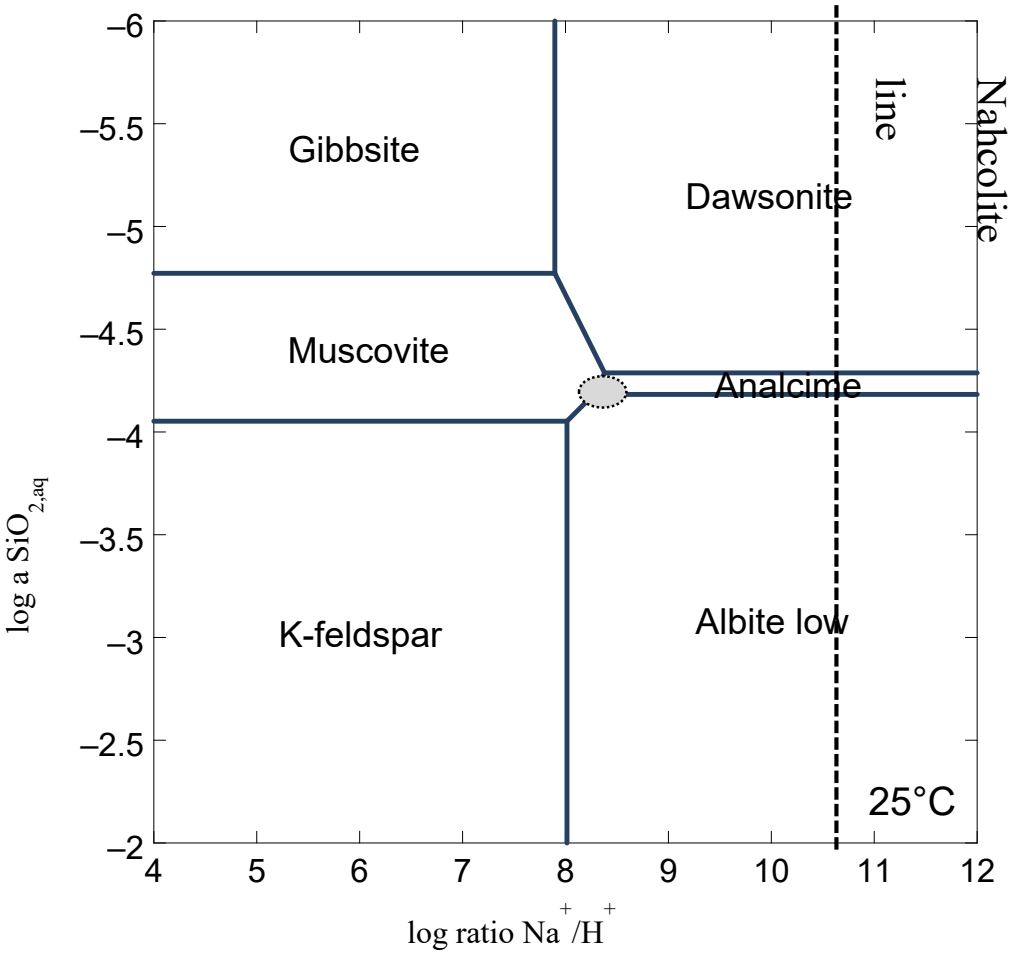



Fig. 4.7. Activity-activity diagram representing the mineral assemblage for the Upper Mineral Unit (UMU)when $CO_{2,\,aq}$ = 0.58 ppm. The diagram was generated in the presence of log $[K^+/H^+]$=5, pH=8, $[CO_2]_{aq}$ =0.58 ppm, $Na^+$ = 51,000 ppm, $SiO_{2,aq}$ = 4.8 ppm, T=25 ºC, P=10 bar. Dashed circle represents the water composition when dawsonite disappears and nahcolite is stable. Nahcolite is stable to the right of the nahcolite line.

The $CO_2$ concentration in the Eocene paleolake

To predict the $CO_2$ content in the paleolake when most saline minerals were precipitated and stable, studies have attempted to constrain aqueous $CO_2$ concentration based on the formation of nahcolite and then further estimate the Eocene $CO_2$ atmospheric concentration (Lowenstein and Demicco, 2006; Jagniecki et al., 2015; Demicco and Lowenstein, 2020). In those studies, the authors assumed that water and air has reached equilibrium and saline minerals are precipitated from waters in equilibrium with the atmosphere. By doing so, the estimated $CO_2$ concentration

was determined from the equilibrium assemblage of sodium carbonate minerals (mainly nahcolite, halite, trona and natron). However, the assumption of lake/atmosphere equilibrium may not be valid. For example, according to Duarte et al. (2008), the average surface water $pCO_2$ (partial pressure) in modern alkaline saline lakes exceeds atmospheric $pCO_2$ by a factor of 5-8 times, with average ratio ~5.07. In saline lakes, the flux of $CO_2$ to the atmosphere is governed by the surface water $pCO_2$, physical conditions at the air-water interface and chemical enhancement of the rage of gas exchange (Duarte et al., 2008). Based on their analysis, saline lakes with pH < 9 were generally higher net sources of $CO_2$ to the atmosphere whereas lakes at or above pH 9 were commonly weak $CO_2$ sinks. A negative relationship between pH and $pCO_2$ in saline lakes around the world was observed in the paper of Duarte et al. (2008), indicating $pCO_2$ in many saline lakes rarely equals the equilibrium with the atmosphere. Therefore, the estimated $CO_2$ in the atmosphere from mineral assemblages (Lowenstein and Demicco, 2006; Jagniecke et al., 2015; Demicco and Lowenstein, 2020), has to be used with caution.

The Significance of the Mineral Stability Diagrams for GRF water chemistry

Based on the changes of those mineral assemblages in different mineral units of the GRF, especially in the basin center, it is clear that the water chemistry in different lake stages, can be constrained quantitatively, in terms of silica activity, salinity, alkalinity and $CO_2$ concentration in the paleolake. As discussed above, the occurrences and changes of those key minerals in the GRF of the Piceance Basin provides insight into the water chemistry over time across the basin. Four major water chemistry zones in the Lake Uinta are summarized based on the mineral assemblages in the key stratigraphic boundaries:

1) analcime-illite zone (zone 1): in the basin margin and LMU, authigenic analcime is precipitated and stable when the water chemistry changes from fresh-brackish to mesosaline-hypersaline conditions of pH=8, $[Na^+]$ = 46,000 ppm, $SiO_{2,\,aq}$=3.9 ppm, $[CO_2]$aq = 0.6 ppm;

2) dawsonite-albite zone (zone 2): in the lower transition zone between the LMU and MMU in the basin center, illite and analcime decrease sharply, corresponding to the appearance and increase of dawsonite and increase in albite and k-feldspar, at pH=9, $[Na^+]$ = 36,500 ppm, $[SiO_{2,\,aq}]$ = 7.5 ppm, $[CO_2]$aq = 5 ppm;

3) dawsonite- nahcolite zone (zone 3): in the MMU, large quantities of dawsonite and nahcolite present in the basin center, at pH = 10, $[Na^+]$ = 58,000 ppm, $[SiO_{2,\,aq}]$ = 7.5 ppm, and $CO_{2,aq}$ = 10 ppm;

4) analcime-illite-nahcolite zone (zone 4): in the transition from the MMU to the UMU, dawsonite decreases significantly, nahcolite persisted, followed by an increase in albite and k-feldspar, and then analcime and illite re-appear in the basin center, equivalent to the mineral assemblages in the sodic units of the basin margin except nahcolite present in the UMU, indicating similar salinity and alkalinity across the basin in the UMU, at pH=8, $[Na^+]$ = 51,000 ppm, $[SiO_{2,\,aq}]$=4.8 ppm and $[CO_{2,\,aq}]$ = 5 ppm.

The differences in mineral assemblages between Lake Uinta and Lake Gosiute are mainly controlled by the internal water chemistry in the lake itself, as they both experienced similar Eocene climate change (Surdam and Stanley, 1979; 1980; Jagniecki et al., 2015; 2016; Lowenstein et al., 2017). Combined with the fact that distinct mineral assemblages occur in the two lakes, it seems difficult to contend that the $CO_2$ input in the paleolake is mainly driven by equilibrium with the Eocene atmosphere (Jagniecki et al., 2015), and suggests that biological metabolism, organic matter oxidation and carbonate precipitation may also play a significant role in determining the

$CO_2$ concentration in the lake system and the mineral assemblages resulting from that concentration. Otherwise, the calculated $CO_2$ contribution from the air-water equilibrium is much lower than the calculated dissolved inorganic carbon from the compiled data summary of the saline lakes around the world (Duarte et al., 2008). Our calculated results from the indicator mineral stability diagrams only assume $CO_2$ contribution from the atmosphere, which serves as a lower limit of the $CO_2$ in the lacustrine system. Therefore, the mineral study in the Piceance Basin could help us further understand the evolutionary history of the lacustrine system.

From the discussion above, it turns out that the quantitive analysis of the water chemistry of the Lake Uinta, based on the mineral stability in different mineral units, is feasible and an effective way for us to figure out the changes of the key parameters in the system. The mineral stability analysis allows better understanding of the water chemistry variations throughout the lake evolution in the Eocene time. The salinity estimate in the saline zones of the basin margin, when analcime is stable, is higher than in the basin center at the same intial stage, which further supports our finding in the previous chapter that elevated salinity occurs in the basin margin first and then saline brines were transported into the basin center by density flow.

## Conclusion

The spatial differences in mineral assemblages in different mineral units between the basin margin and the basin center reflect the variations of lake chemistry over time across the basin. The key parameters (salinity, alkalinity, silica activity and $CO_2$ concentration) to constrain water chemistry in the Lake Uinta provide us a new perspective to characterize the water conditions of the lacustrine system more quantitatively. The estimated salinity of the basin margin is higher than the basin center early in lake development (stage 1 according to Johnson (1985), and early

in stage 2 according to Tanavsuu-Milkeviciene and Sarg (2012), which further support our hypothesis that salinity in the basin margin rose earlier than in the basin center. The $CO_2$ calculated from the mineral assemblages based on the equilibrium between the atmosphere and water has to be used with caution, and is not strongly supported by our study, due to the limited stability of analcime at elevated aqueous $CO_2$ concentrations. The coexistence of nahcolite and analcime in the upper mineral unit reflects the elevated silica activity, which may stabilize analcime at higher $CO_2$. More research about the influence of analcime solid solution toward higher $SiO_2$ on thermodynamic models is needed in the future. The formation conditions of the index minerals in different lake stages further our understanding of the lake evolution, and may be a good analogue to study other lacustrine systems, given similar mineral assemblages and distributions.

## Acknowledgements

Many thanks go to Aqueous Solutions LLC for complementary student Geochemist's Workbench software. We also express our gratitude to core research lab at U.S Geological Survey for all the sampling cuts.

## References

Birdwell, J.E., Johnson, R.C., and Brownfield, M. E., 2019, Distribution of mineral phases in the Eocene Green River Formation, Piceance Basin, Colorado-Implications for the evolution of Lake Uinta, The Mountain Geologist, vol.56, p.73-141.

Boak, J., and Poole, S., 2015, Mineralogy of the Green River Formation in the Piceance Creek Basin, Colorado, *in* Smith, M.E., Carroll, A.R., eds., Stratigraphy and paleolimnology of the Green River Formation, Western USA: Syntheses in Limnogeology, v. 1, p. 183-209.

Boak, J., Poole S., and Feng, J., 2016, Geochemistry of the Green River Formation, Piceance Creek Basin, Colorado: *in* Dolan, M.P., Higley, D.K., and Lillis, P.G., Hydrocarbon Source Rocks in Unconventional Plays, Rocky Mountain Region: Rocky Mountain Association of Geologists, p. 295-318.

Boak, J., Poole, S., Sarg, J.F., and Tänavsuu-Milkeviciene, K., 2013, Evolution of Lake Uinta as defined by mineralogy and geochemistry of the Green River Formation in Colorado: Society of Exploration Geophysicists, American Association of Petroleum Geologists, Society of Petroleum Engineers, Unconventional Resources Technology Conference, URTEC-1578649-MS, Denver, Colorado, 12-14 August 2013, pp. 1952-1961.

Boak, J., Wu, T.F., Birdwell, J.E., 2021. Geochemical studies of the Green River Formation in the Piceance Basin, Colorado: I. Major, minor, and trace elements. Submitted.

Bradley, W.H., 1929, The occurrence and origin of analcite and meerschaum beds in the Green River Formation of Utah, Colorado, and Wyoming: U.S. Geological Survey Professional Paper 158-A, 8 p.

Bradley, W.H., 1931, Origin and microfossils of the oil shale of the Green River Formation of Colorado and Utah: U.S. Geological Survey Professional Paper 168, 58 p.

Bradley, W.H., and Eugster, H.P., 1969, Geochemistry and paleolimnology of the trona deposits and associated authigenic minerals of the Green River Formation of Wyoming: U.S. Geological Survey Professional Paper 496-B, 71 p.

Brobst, D.A., and Tucker, J.D., 1973, X-ray mineralogy of the Parachute Creek Member, Green River Formation, in the northern Piceance Creek Basin, Colorado: U.S. Geological Survey Professional Paper 803, 53 p.

Brownfield, M.E., Mercier, T.J., Johnson, R.C., and Self, J.G., 2010, Nahcolite resources in the Green River Formation, Piceance Basin, Colorado: U.S. Geological Survey Digital Data Series DDS–69–Y, Ch. 2, 51 p.

Cooper, J.E., and Evans, W.S., 1983, Ammonium-nitrogen in Green River Formation oil shale: Science, v. 219, p. 492-493.

Dean, W.E., Pitman, J.K., and Harrach, G.H., 1981. Geochemical and Mineralogical Analyses of US Geologic Survey Oil-Shale Core CR-2, Piceance Creek Basin, Colorado. USGS Open File Report 81-596.

Demicco, R.V. and Lowenstein, T.K. (2020) When "evaporites" are not formed by evaporation: the role of temperature and pCO2 on saline deposits of the Eocene Green River Formation, Colorado, USA. Geol. Soc. Am. Bull., 132, 1365–1380.

Duarte, C. M., Y. T. Prairie, C. Montes, J. J. Cole, R. Striegl, J. Melack, and J. A. Downing (2008), CO2 emissions from saline lakes: A global estimate of a surprisingly large flux, J. Geophys. Res., 113, G04041, doi:10.1029/2007JG000637.

Dyni, J.R., 1974, Stratigraphy and nahcolite resources of the saline facies of the Green River Formation in northwest Colorado, *in* Murray, D. Keith, ed., Guidebook to the Energy Resources of the Piceance Creek Basin, Colorado: Rocky Mountain Association of Geologists 25th Field Conference, p. 111–122.

Dyni, J.R., 1998. Prospecting for Green River-type sodium carbonate deposits. Wyoming State Geolgoical Survey Public Information Circular 40, p. 37- 47.

Dyni, John R., 1996. Sodium Carbonate Resources of the Green River Formation. U.S. Geological Survey Open-File Report 96-729.

Dyni, J.R., 2006, Geology and resources of some world oil-shale deposits: U.S.Geological Survey Scientific Investigations Report 2005–5294, p. 42.

Eugster, H.P., 1966, Sodium carbonate-bicarbonate minerals as indicators of *p*CO2: Journal of Geophysical Research, v. 71, p. 3369–3377.

Eugster, H.P., and Hardie, L.A., 1978, Saline Lakes, *in* A. Lerman, ed., Saline lakes: in Lakes Chemistry, Geology, Physics, Springer-Verlag, New York, p. 237- 293. DOI: 10.1007/978-1-4757-1152-3.

Eugster, Hans P., 1980. Geochemistry of Evaporitic Lacustrine Deposits. Annual Reviews of Earth and Planetary Science, 8, p. 35-63.

Feng, J.F., 2011. Source Rock Characteristics in the Green River Oil Shale, Piceance Creek Basin, Colorado – An Integrated Geochemical and Stratigraphic Analysis. Master Thesis Colorado School of Mines.

Gries, R.R., 1983, Oil and gas prospecting beneath Precambrian foreland thrust plates in the Rocky Mountains: American Association of Petroleum Geologists Bulletin, v. 67, p. 1-28.

Hay, R. L. and Guldman, S. G. (1986) Silicate diagenesis in sediments of Searles Lake, California: in Prog. and Abstracts,23rd Annual Meeting of the Clay Minerals Society, Jackson, Mississippi, 1986, p. 15.

Hite, R.J., and Dyni, J.R., 1967, Potential resources of dawsonite and nahcolite in the Piceance Creek Basin, northwest Colorado: Colorado School Mines Quarterly, v. 62, p. 25–38.

Iijima, A. and Hay, R. L. (1968) Analcime composition in tufts of the Green River Formation of Wyoming: *Amer.Mineral* 53, 184-200.

Jagniecki, E.A., Lowenstein, T.K., 2015, Evaporites of the Green River Formation, Bridger and Piceance Creek Basins: Deposition, diagenesis, paleobrine chemistry, and Eocene atmospheric CO2: *in* M.E. Smith and A.R. Carroll, eds., Stratigraphy and Paleolimnology of the Green River Formation, Western USA, Springer, Dordrecht, pp. 277-312.

Johnson, R.C., 1981, Stratigraphic evidence for a deep Eocene Lake Uinta, Piceance Creek Basin, Colorado: Geology, v. 9, p. 55–62.

Johnson, R.C., 1985, Early Cenozoic history of the Uinta and Piceance Creek Basins, Utah and Colorado, with special reference to the development of Eocene Lake Uinta, *in* Flores, R.M., and Kaplan, S.S., eds, Cenozoic Paleogeography of the West-Central United States, Rocky Mountain Paleography Symposium 3: The Rocky Mountain Section, Society of Economic Paleontologists and Mineralogists p. 247-276.

Johnson, R.C., Mercier, T.J., Brownfield, M.E., Pantea, M.P., and Self, J.G., 2010a, An assessment of in-place oil shale resources of the Green River Formation, Piceance Basin, Colorado: Oil Shale and Nahcolite Resources of the Piceance Basin, Colorado: U.S. Geological Survey Digital Data Series DDS-69-Y, Chapter 1, 187 p.

Johnson, R.C., Mercier, T.J., Brownfield, M.E., and Self, J.G., 2010b, Assessment of in-place oil shale resources of the Eocene Green River Formation, Uinta Basin, Utah and Colorado: Oil Shale Resources of the Uinta Basin, Utah and Colorado, U.S. Geological Survey Digital Data Series DDS-69-BB, Chapter 1, 153 p.

Johnson, R.C., and Brownfield, M.E., 2013, Development, evolution and destruction of the saline mineral area of Eocene Lake Uinta, Piceance Basin, western Colorado: U.S. Geological Survey Scientific Investigations Report 2013-5176.

Johnson, R.C, Birdwell, J.E., and Mercier T.J., 2017, Mineral occurrence data for the Eocene Green River Formation in the Piceance and Uinta Basins: USGS data release, https://doi. org/10.5066/F7XP7334.

King, P.B., 1969, The tectonics of North America; a discussion to accompany the tectonic map of North America, scale 1:5,000,000: U.S. Geological Survey Professional Paper 628, 94 p.

Last, W.M., and Ginn, F.M., 2005. Saline systems of the Great Plains of western Canada: an overview of the limnogeology and paleolimnology. In Saline Systems 1:10, p. 1-38.

Lowenstein, Tim, 2011. Deposition and Diagenesis of Basin-Center Evaporites, Green River Formation. Presentation at the 31st Oil Shale Symposium Proceedings. Golden, CO, October 17-21st, 2011.

Lowenstein, T.K. and Demicco, R.V., 2006. Elevated Eocene atmospheric $CO_2$ and its subsequent decline. Science **313**, 1928–1928.

Malicse, A., 2011, Mineralogy and geochemistry of the Parachute Creek Member of the Green River Formation, Piceance Basin, Colorado, U.S.A.: AAPG Datapages/Search and Discovery Article #50507, AAPG International Conference and Exhibition, Milan, Italy, October 23-26.

Mariner, R. H. and Surdam, R. C., 1970. Alkalinity and formation of zeolites in saline alkaline lakes: Science 170, 977-980.

Milton, C., 1971. Authigenic Minerals of the Green River Formation. Rocky Mountain Geology, Contributions to Geology, April, V. 10, No. 1, p. 57-63.

Milton, C., Axelrod, J.M., Grimaldi, F.S., 1955, New mineral garrelsite, $(Ba,Ca, Mg)_4H_4Si_{26}BO_{20}$) From the Green River Formation, Utah: Geological Society of America Bulletin, v. 66, p. 1597.

Mason, Glenn M., 2007. Saline Minerals in the Green River Formation, Green River and Washakie Basins, Wyoming. 27th Oil Shale Symposium Colorado School of Mines.

Milton, C., and Eugster, H.P., 1959, Mineral assemblages of the Green River Formation: *in* P.H. Abelson ed, Research in Geochemistry, John Wiley & Sons, Inc., New York, p. 118-150.

Poole, S., 2014, Quantitative mineralogy and distributions of minerals of the Green River Formation, Piceance Creek Basin, western Colorado: Colorado School of Mines MS Thesis, 151 p.

Pitman, Janet K., 1996. Origin of Primary and Diagenetic Carbonates in the Lacustrine Green River Formation (Eocene), Colorado and Utah. US Geological Survey Bulletin 2157.

Ramseyer, Karl, Diamond, Larryn W., Boles, James R., 1993. Authigenic K-NH4-feldspar in sandstones; a fingerprint of the diagenesis of organic matter. Journal of Sedimentary Petrology, Vol. 63. No. 6, p. 1092-1099.

Remy, Robert R. and Ferrell, Ray E., 1989. Distribution and Origin of Analcime in Marginal Lacustrine Mudstones of the Green River Formation, South-Central Uinta Basin, Utah. Clays and Clay Minerals, Vol. 37, No. 5, p. 419-432.

Robb, W.A., and Smith, J.W., 1974, Mineral profile of the oil shales in Colorado Core Hole No. 1, Piceance Creek Basin, Colorado: *in* D. Keith Murray, ed., Guidebook to the Energy Resources of the Piceance Creek Basin Colorado: Rocky Mountain Association of Geologists Twenty-Fifth Field Conference Guidebook, p. 91-100.

Slaughter, M., and Mathews, A., 1984, Mineralogy and geochemistry of the Green River Formation, Colorado Core Hole No. 1, Piceance Creek Basin, Colorado: U.S. Department of Energy, Report of Investigation no. 7234, 904 p.

Smith, J.W., 1974, Geochemistry of oil-shale genesis in Colorado's Piceance Creek Basin: *in* D. Keith Murray, ed., Guidebook to the Energy Resources of the Piceance Creek Basin Colorado: Rocky Mountain Association of Geologists Twenty-Fifth Field Conference Guidebook, p. 71-79.

Smith, J.W., 1983, The chemistry that formed the Green River Formation oil shale (Ch. 12): *in* F.P. Miknis and J.F. Mckay, eds., Geochemistry and Chemistry of Oil Shales, ACS Symposium Series, American Chemical Society, Washington, D.C., p. 225-248.

Smith, M.E., Carroll, A.R., and Singer, B.S., 2008, Synoptic reconstruction of a major ancient lake system–Eocene Green River Formation, western United States: Geological Society of America Bulletin, v. 120, p. 54-84.

Smith, M.E., Chamberlain, K.R., Singer, B.S., and Carroll, A.R., 2010. Eocene clocks agree: Coeval 40Ar/39Ar, U-Pb, and astronomical ages from the Green River Formation: Geology, v. 38, p. 527-530.

Smith, J.W., and Milton, C., 1966, Dawsonite in the Green River Formation of Colorado: Economic Geology, v. 61, p. 1029-1042.

Smith, J.W., and Robb, W.A., 1973. Aragonite and the Genesis of Carbonates in Mahogany Zone Oil Shales of Colorado's Green River Formation. Report of Investigations 7727, Bureau of Mines.

Surdam, R. C., 1977. Zeolites in closed hydrologic systems:in *Mineralogy and Geology of Natural Zeolites, F. A.*Mumpton, ed., Reviews in Mineralogy 4, Mineralogical Society of America, Washington, D.C., 65-79.

Surdam, Ronald, C., and Parker, Ronald D., 1972. Authigenic Aluminosilicate Minerals in the Tuffaceous Rocks of the Green River Formation, Wyoming. Geological Society of America Bulletin, v. 83, March, p. 689-700.

Surdam R.C., and Stanley K.O., (1980), Effects of changes in drainage- basin boundaries on sedimentation in Eocene Lakes Gosiute and Uinta of Wyoming, Utah, and Colorado. Geology 8:135–139.

Svensen H, Bebout G, Kronz A, Li L, Planke S, Chevallier L, Jamtveit B (2008) Nitrogen geochemistry as a tracer of fluid flow in a hydrothermal vent complex in the Karoo Basin, South Africa, Geochim Cosmochim Acta 72:4929–4947.

Tänavsuu-Milkeviciene, K., and Sarg, J.F., 2012, Evolution of an organic-rich lake basin – stratigraphy, climate and tectonics: Piceance Creek Basin, Eocene Green River Formation: Sedimentology, v. 59, p. 1735-1768.

Tuttle, Michele L., 2009. A Collection of chemical, mineralogical, and stable isotopic compositional data for Green River oil shale from depositional center cores in Colorado, Utah and Wyoming: US Geological Survey Open-File Report 2009-1274, p.18.

Young, R.G., 1995b, Structural controls of the Piceance Creek Basin, Colorado, *in* Averett, W.R., ed., The Green River Formation in Piceance Creek and Eastern Uinta Basin, Field Guidebook, p. 23-29.

# Chapter 5: Future Work

For the ICP-OES analysis, more stratigraphic sections from the basin margin need to be measured and analyzed, as these will help us better confirm the stratigraphic boundaries and define local environments in the basin margin. In addition, more sections from the basin center need to be collected on a more comprehensively representative basis, to minimize the effect of irregular sampling in the core sections. This approach will be particularly helpful to identify the most representative set of chemofacies. Moreover, in order to figure out the relationships of redox sensitive trace elements (Mo, As, U, $P_{IV}$ transition metals) identified in the lacustrine system, more data on organic matter composition may need to be collected on the same samples as the major and trace element analysis, which will make our conclusions more robust.

For the water chemistry analysis, the mineral stability diagrams are helpful, and can better constrain the water chemistry based on some key parameters, such as silica activity, sodium concentration, pH, $CO_2$ concentration in the lake. However, because of the limited data about the initial water condition in the Piceance Basin, the initial water condition was adopted from the adjacent Greater Green River basin, which might cause some uncertainties in evaluating the lake evolution of our study area. Therefore, if more water data in similar lake systems could be collected, the mineral stability diagram will be better defined and constrained. Additional thermodynamic data and experimental work will be needed to understand the coexistence of analcime and nahcolite in the Upper Mineralogic Unit. More research on solid solution in analcime (Si-rich) will be helpful to figure out stability relations in the saline and alkaline lacustrine system. Beyond these mentioned above, understanding the links between the precipitation of authigenic phases in various locations of the stratified lake system and equilibrium with the atmosphere is also essential. Additional quantitative mineralogic data, whether by X-Ray Diffraction or Fourier

Transform Infrared Spectroscopy, especially in the basin margin, would help relate geochemistry to mineralogy, and enhance interpretive quality.